The role of the HCN2 channel in the mouse septo-hippocampal circuit

Manuela Brümmer

Dissertation at the
Graduate School of Systemic Neuroscience at the
Ludwig-Maximilians-University Munich

21st of February, 2022

Supervisor:

Prof. Dr. Christian Wahl-Schott
Institute of Neurophysiology of Hannover Medical School (MHH)

I DON'T KNOW ANYTHING WITH CERTAINTY,
BUT SEEING THE STARS MAKES ME DREAM.

VINCENT VAN GOGH

Abstract

Hyperpolarization-activated cyclic nucleotide-gated (HCN) cation channels belong to the superfamily of voltage gated ion channels. They are activated by hyperpolarization and modulated by cyclic adenosine monophosphate (cAMP) and cyclic guanosine monophosphate (cGMP) binding to the cyclic nucleotide-binding domain (CNBD). There are four isoforms of HCN channels, HCN1-4, that convey a depolarizing inward current, termed I_h, which is essential for a variety of physiological processes in the brain, such as the stabilization of the resting membrane potential, the regulation of firing properties, and the generation of theta oscillations. In the central nervous system, HCN channels are expressed for example in the hippocampus and in the medial septum (MS). The hippocampus and the MS are interconnected via GABAergic (gamma-aminobutyric acid), cholinergic, and glutamatergic projection neurons and form the septo-hippocampal system. This system is crucial for the generation and modulation of the theta rhythm, which is one of the most prominent synchronous rhythms in the brain and is characterized by a frequency of 4-12 Hz. Functionally, the theta rhythm is critically involved in information processing, rapid-eye-movement sleep (REM), and organization of cognitive processes like learning and memory.

In this study, I knocked out HCN2 in distinct subsets of MS neurons by a lentiviral-based system with the help of a Cre-dependent approach. Investigating GABAergic neurons, electrophysiological recordings showed that in Cre-injected animals I_h and the theta power of REM sleep in electroencephalogram (EEG) recordings were reduced. Hippocampal spatial behavior was unaltered, while the object recognition memory was impaired. The examination of an HCN2 knockdown pan-neuronal of the MS resulted in a significantly reduction of I_h current and theta power of REM sleep. Additionally, HCN2 knockdown led to an impairment in hippocampal-dependent reversal learning in the Water Cross Maze (WCM). These findings implicate an important influence of HCN2 in the MS on septo-hippocampal neurons and the generation of theta oscillations in the hippocampus.
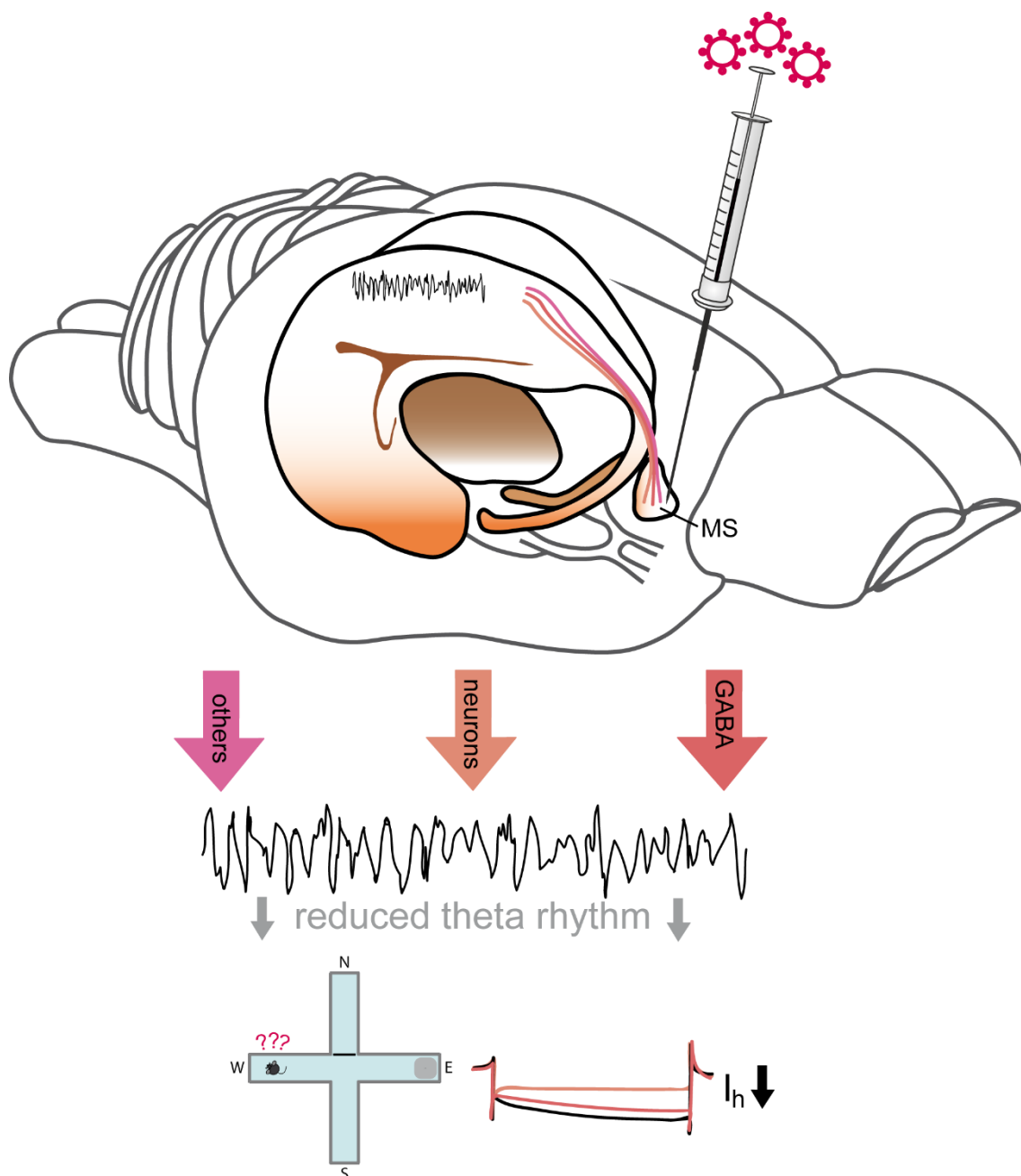
Figure 0.1: **Schematic illustration of the HCN-dependent projects**. Stereotactic injections of lentiviral particles delete HCN2 in specific neurons in the MS, which is connected to the hippocampus via GABAergic, glutamatergic, and cholinergic neurons. HCN2 knockdown in MS neurons and GABAergic neurons results in a decreased I_h, a reduced theta rhythm power during REM sleep, and partly in learning impairments in the Water Cross Maze (WCM).

Keywords: HCN channels, hippocampus CA1, medial septum, GABAergic neurons, cholinergic neurons, glutamatergic neurons, behavior, EEG, theta rhythm, REM sleep, Water Cross Maze, social recognition test, object recognition test.

Table of Contents

List of Figures

List of Tables

1 Introduction

The brain is the most complex organ in living beings, because of its function in receiving, processing, and interpreting information, as well as in executing actions in response to the received input. The brain consists of billions of neurons, which are highly interconnected and build up a sophisticated network. Ion channels are fundamentally required for such a network to generate and transmit electrical signals. Information processing is a process including complex interactions between electrical signals as well as the transformation of electrical signals into chemical signals and vice versa, thus enabling important physiological processes, cognitive functions, and complex behavior (M. F. Bear 2016).

1.1 Hyperpolarization-activated cyclic nucleotide-gated channels

Hyperpolarization-activated cyclic nucleotide-gated (HCN) channels belong to the voltage gated pore-loop channels family. Current caused by HCN channels is termed I_h. This current was discovered in the 1970s and 1980s in pacemaker cells of the sinoatrial node of the heart as well as in neurons (Noma and Irisawa 1976, Brown and Difrancesco 1980, Ludwig, Zong et al. 1998, Robinson and Siegelbaum 2003, Craven and Zagotta 2006, Biel, Wahl-Schott et al. 2009, M. F. Bear 2016). HCN channels are characterized by four major properties: Firstly, they are activated by membrane hyperpolarization (negative to -50 mV). The second property of HCN channels is their modulation by cyclic nucleotides like cAMP and cGMP, which facilitates the channel activation (Biel, Wahl-Schott et al. 2009). Thirdly, the non-domain swapped architecture distinguishes HCN channels from most other voltage-gated ion channels with swapped-domain interaction (Payandeh, Scheuer et al. 2011, Li, Zhou et al. 2017, Sun and MacKinnon 2017, Tao and MacKinnon 2019). At least, and comparable to canonical potassium channels, the pore domain of HCN channels contains a glycine-tyrosine-glycine motif (GYG motif) (see Figure 1.1), which is important for the potassium permeability. In contrast to potassium channels, HCN channels do not express the complete threonine-valine-GYG signature (TVGYG) sequence, which usually serves as selectivity filter in potassium channels. That might explain why HCN channels are only slightly more selective for potassium than for sodium ions (permeability ratio: 4:1) (Doyle, Morais Cabral et al. 1998, Ludwig, Zong et al. 1998, Biel, Wahl-Schott et al. 2009, Lee and MacKinnon 2017). Given the ion selectivity of HCN channels and the concentrations of potassium and sodium in the intracellular and extracellular compartments, the reversal potential of HCN channels is around -20

mV. Consequently, the reversal potential lies at the base of the activation curve, where HCN channels are closed. At normal resting membrane potentials (RMP) in neurons (approximately -70 mV), currents through HCN channels are depolarizing (thus drive the membrane potential towards the reversal potential of HCN channels). Furthermore, HCN channels regulate the membrane resistance (Moosmang, Biel et al. 1999) and consequently are stabilizing the RMP. They also have an influence on other basic neurophysiological processes such as synaptic transmission, dendritic integration, and long-term potentiation whereby complex processes are altered for example neuronal oscillations, learning, memory, and depression.

Further studies suggested that HCN channels are also expressed in other tissues such as pancreatic β-cells, kidney, testis, or bladder smooth muscle cells (Green, Edwards et al. 1996, Seifert, Scholten et al. 1999, El-Kholy, MacDonald et al. 2007, Biel, Wahl-Schott et al. 2009, Wahl-Schott, Fenske et al. 2014, Lopez-Gonzalez, Ayala-Aguilera et al. 2016). The I_h current is inwardly directed at rest and depolarizes the membrane while at the same time depolarization reduces the number of open HCN channels. I_h is therefore reduced, the tonic depolarizing current becomes smaller, and the membrane potential moves back towards resting potential. As a result of their hyperpolarization-dependent gating mechanism, HCN channels can counteract both depolarizing and hyperpolarizing influences by facilitating hyperpolarization (effect of deactivation of I_h) or production a depolarizing inward current (activation of I_h). This inductive property leads to the characteristic voltage sag which is caused by activation or deactivation of I_h. Therefore, these channels stabilize the RMP (Zagotta, Olivier et al. 2003, Biel, Wahl-Schott et al. 2009, Lee and MacKinnon 2017). Besides setting the RMP, I_h has a special role in regulating the firing properties of neurons and facilitating resonance and network oscillation which are crucially involved in information processing in neuronal circuits such as the hippocampus (Noma and Irisawa 1976, Halliwell and Adams 1982, Biel, Wahl-Schott et al. 2009, Muller and Remy 2018). In addition, HCN channels are involved in neuronal rhythmicity. These contributions are mainly ascribed to either HCN1, HCN2, and HCN4, while for HCN3 such functions have not been investigated (Biel, Wahl-Schott et al. 2009, Stieglitz, Fenske et al. 2017).

The four isoforms of HCN channels (HCN1-4) are 60% amino acid sequence homology. In the mouse brain, all HCN channel isoforms are expressed with different expression levels and distributions. The HCN1 channel is mainly expressed in brain stem, hippocampus, neocortex, olfactory bulb, and cerebellar Purkinje cells whilst HCN2 is expressed throughout the whole brain with highest levels in the brain stem, olfactory bulb, hippocampus, and thalamic nuclei. In the MS,

HCN2 is the major expressed isoform (Spahn 2015). On the other hand, HCN3 is expressed on a low level throughout the brain. HCN4 is expressed at a high level only in a few brain areas, such as the olfactory bulb and specific nuclei of the thalamus (Moosmang, Biel et al. 1999, Santoro, Chen et al. 2000, Notomi and Shigemoto 2004)

Like other pore-loop cation channels, HCN channels consist of four subunits and can exist as homo- or hetero-tetramers (Much, Wahl-Schott et al. 2003). Each subunit of these tetramers consists of six transmembrane α-helices (S1-S6) and a cytosolic N- and C-terminus (Zagotta, Olivier et al. 2003). The transmembrane domains S5 and S6 form the pore of the channel while the S4 segment is the voltage-sensing segment with 9 positively charged amino acids (e.g., arginine or lysine) at every third position (see Figure 1.1). When the cell is more depolarized, the S4 segment slides deeper into the cytoplasm and the S4-S5-linker forms a contact with the neighboring C-linker. The force exerted onto the C-linker and S6 segment stabilizes the closed state of the HCN channel. On the other hand, during hyperpolarization, the S4 segment moves towards the cytoplasm (inward), the force onto the C-linker and the S6 segments releases and the pore can switch into the open formation (Biel, Wahl-Schott et al. 2009). The S4 segment hereby moves in response to hyperpolarization in two steps and the second step has been shown to correlate with the opening of the channel (Wu, Ramentol et al. 2021).
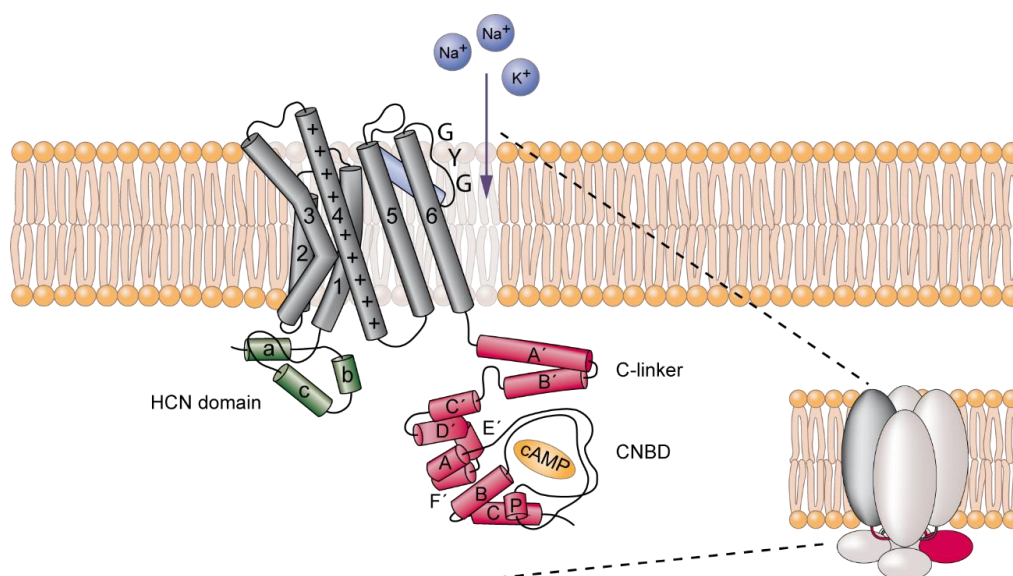
Figure 1.1: Schematic of the HCN channel subunit, interacting proteins, and low molecular factors. The tetrameric channel complex is formed by four subunits; here only one subunit is shown. Each subunit consists of six transmembrane domains (S1-S6) and the intracellularly located N- and C-terminus. The C-terminus contains the CNBD for binding of cAMP or cGMP. The pore is formed by S5 and S6 containing a GYG motif responsible for ion selectivity. The S4 domain is positively charged due to 9 positively charged amino acids and is therefore the voltage-sensing segment. Modified from Biel, Wahl-Schott et al. 2009.

HCN1 channels show the fastest kinetics and the native I_h of HCN1 is strongly voltage dependent. The HCN2 and HCN3 subtypes show an intermediate activation time, while HCN4 shows the slowest activation kinetics. Therefore, the following order of activation kinetics results: HCN1 >> HCN2 > HCN3 >> HCN4 (Biel, Wahl-Schott et al. 2009). As already mentioned above, the activation of I_h is voltage-dependent and the current-voltage relationship shows a typical sigmoidal shape. By fitting with Boltzmann functions, the half-maximal activation potentials ($V_{0.5}$) can be determined, which are around -70 to -100 mV in most cells.

The kinetics and voltage-dependence of HCN channels activation are also determined by the binding of cAMP. The C-terminus contains the CNBD for binding of the cyclic nucleotides cAMP and cGMP (Moosmang, Biel et al. 1999, Craven and Zagotta 2006). The CNBD is connected to the S6 domain via the C-linker (see Figure 1.1), which acts as an auto inhibitory domain that lowers the open probability in the absence of cAMP. Binding of cAMP induces conformational changes that facilitate the opening of HCN channels by removing tonic channel inhibition (conferred by this domain), leading to faster opening kinetics and a shift of the voltage-dependence towards more positive values. Importantly, cAMP facilitates channel opening, but it is not a general requirement for the activation of HCN channels (Luthi and McCormick 1998, Craven and Zagotta 2006, Lee and MacKinnon 2017). HCN1 is modulated by cAMP to a lesser extent compared to HCN2 and HCN4 while HCN3 is barely not modulated by cAMP (Ludwig, Zong et al. 1998, Santoro, Liu et al. 1998, Ishii, Takano et al. 1999, Ludwig, Zong et al. 1999, Stieber, Stockl et al. 2005, Biel, Wahl-Schott et al. 2009). Binding of cyclic nucleotides to HCN channels facilitates channel activation by shifting $V_{0.5}$ to more positive values and by accelerating the activation kinetics (Biel, Wahl-Schott et al. 2009).

HCN channels interact with different proteins, which substantially influence their cellular localization and function. For example, the tetratricopeptide repeat-containing Rab8b-interacting protein (Trip8b) is an auxiliary interacting subunit of HCN channels in the brain which significantly regulates the voltage-dependent gating and kinetics of I_h. It interacts with the CNBD and the end of the C-terminus with HCN1 channels (Lewis, Schwartz et al. 2009, Santoro, Piskorowski et al. 2009, Zolles, Wenzel et al. 2009). For correct localization and consequently correct function of HCN channels in general, Trip8b is an essential accessory protein. It determines the cell surface expression and dendritic localization of HCN channels (Lewis, Schwartz et al. 2009, Santoro, Piskorowski et al. 2009, Zolles, Wenzel et al. 2009).

Of particular interest for my thesis is the HCN2 subtype of the HCN channel family. HCN2-deficient mice (HCN2KO) exhibit spontaneous absence seizures

(Ludwig, Budde et al. 2003), depressive behavior (Cheng, Umschweif et al. 2019), reduced theta rhythm and learning behavior (Spahn 2015), and show changes in inflammation and neuropathic pain (Emery, Young et al. 2011). HCN2 channels are ubiquitously expressed in several brain areas and represent the dominant isoform in MS neurons (Varga, Hangya et al. 2008, Spahn 2015).

1.2 The medial septum and its influence on theta rhythm

Neurons of the MS are known to be involved in the generation of a prominent brain rhythm, the theta rhythm. Furthermore, it is generally suggested that I_h influences network oscillations that are involved in learning and memory (Kopell and LeMasson 1994, Hasselmo, Fransen et al. 2000, Rotstein, Pervouchine et al. 2005) and, in particular, in modulating the theta rhythm *in vivo* (Kocsis and Li 2004, Nolan, Malleret et al. 2004, Xu, Datta et al. 2004). Therefore, one major goal of my thesis was to investigate whether HCN2 channels also play an important role in generating the theta rhythm (Santoro, Chen et al. 2000, Notomi and Shigemoto 2004).

The main important brain circuit investigated in this thesis is the septo-hippocampal system, consisting of the MS, the diagonal band of Broca (DbB), and the hippocampus (see Figure 1.2).
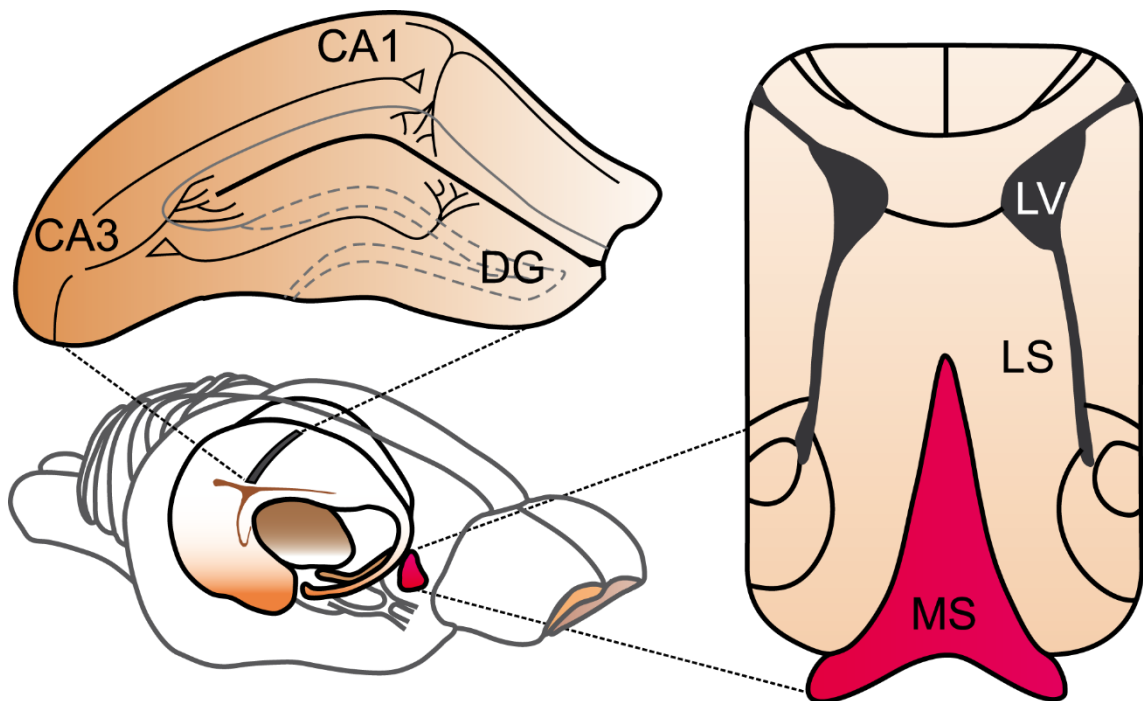
Figure 1.2: A schematic of the septo-hippocampal system in the mouse brain. The mouse brain (bottom left) and a magnification of the hippocampus (top left) and the MS (right). CA: Cornu ammonis, DG: Dentate gyrus, MS: Medial septum, LV: Lateral ventricle, LS: Lateral septum. Adapted from Amaral and Witter (Amaral and Witter 1989).

The MS is influenced by numerous pathways and brain areas (Takeuchi, Nagy et al. 2021). One of the most prominent projections of the MS is the hippocampal formation (Swanson and Cowan 1979, Vertes and Kocsis 1997, Vega-Flores, Gruart et al. 2014, Fuhrmann, Justus et al. 2015, Takeuchi, Nagy et al. 2021).

A disruption of the MS and DbB results in a loss of theta rhythm and neuronal activity in the hippocampus (Green and Arduini 1954, Petsche and Stumpf 1962, Buno, Garcia-Sanchez et al. 1978, Winson 1978, Mitchell, Rawlins et al. 1982, Freund and Antal 1988, Mizumori, Barnes et al. 1990, Pignatelli, Beyeler et al. 2012), as well as in impaired spatial learning (Winson 1978), or results in reduced anxiety behavior (Calandreau, Jaffard et al. 2007). On the other hand, previous studies showed induced theta rhythm by stimulating MS neurons (Colgin and Moser 2009). In the MS, different kinds of neurons are present, for example GABAergic, glutamatergic, and cholinergic neurons. GABAergic neurons can be identified by the presence of glutamate decarboxylase (GAD), glutamatergic neurons are immune-positive for Ca^{2+}/calmodulin-dependent protein kinase II (CamKII), and cholinergic neurons express choline acetyltransferase (ChAT) (Kohler, Chan-Palay et al. 1984, Frotscher and Leranth 1985, Freund and Antal 1988, Kiss, Patel et al. 1990, Hajszan, Alreja et al. 2004, Colom, Castaneda et al. 2005). These neurons project to the hippocampus and build a network to generate the theta rhythm (see Figure 1.3) (Macadar, Roig et al. 1970, Roig, Budelli et al. 1970, Freund and Antal 1988). They are highly interconnected in the MS and influence the hippocampal cornu ammonis 1 (CA1) region in part via DbB and the fornix fiber bundle (Monmaur and Thomson 1983, Freund and Antal 1988, Colom, Castaneda et al. 2005, Desikan, Koser et al. 2018, Unal, Crump et al. 2018). Thereby, these neurons regulate specific aspects of the hippocampal theta oscillation. Furthermore, GABAergic septal neurons inhibit CA1 and CA3 interneurons, which target pyramidal hippocampal neurons (Freund and Antal 1988, Sun, Nguyen et al. 2014, Joshi, Salib et al. 2017). The CA3 of the hippocampus is largely influencing the CA1 via the Schaffer collateral fibers (Witter 2007) and, together with the dentate gyrus (DG), is involved in spatial coding (Neunuebel and Knierim 2014).
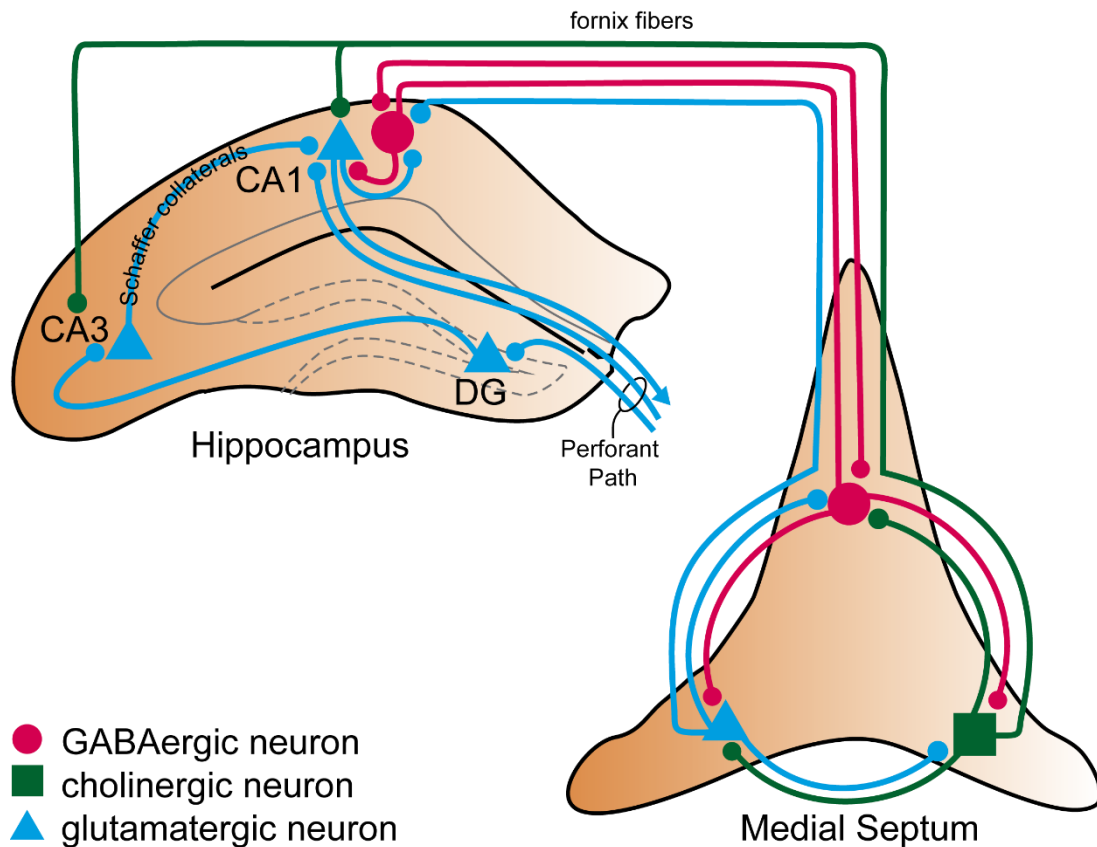
Figure 1.3: Schematic drawing of septo-hippocampal connectivity between MS and hippo-campus. GABAergic, glutamatergic, and cholinergic neurons from the MS project to the hippocampal CA1 and CA3 via the fornix fibers. CA1 is further influenced via the Schaffer collaterals and the perforant path. Modified from Mueller and Remy 2018.

In addition to the influence of the MS, CA1 is also innervated by the perforant path (see Figure 1.3), originating in the entorhinal cortex (M. F. Bear 2016). GABAergic neurons expressing HCN channels show a theta rhythmic firing frequency. For this reason, they are called pacemaker cells (Andersen and Eccles 1962, Freund 1989, Smythe, Colom et al. 1992, Toth, Freund et al. 1997, Knapp, Morris et al. 2000, Sotty, Danik et al. 2003, Varga, Hangya et al. 2008, Hangya, Borhegyi et al. 2009, Unal, Crump et al. 2018). Their activity leads to a strong rhythmic inhibition upon pyramidal neurons with direct consequences for the theta rhythm (Smythe, Colom et al. 1992, Hangya, Borhegyi et al. 2009, Unal, Crump et al. 2018). In particular, GABAergic neurons of the MS induce the theta rhythm within the hippocampus because of a disinhibitory signal to hippocampal pyramidal cells (Freund and Antal 1988). In contrast to GABAergic neurons, HCN channel expression in glutamatergic MS neurons has not yet been reported in literature. It is known that these neurons are an important source of synaptic excitation in the septo-hippocampal system (Manseau, Danik et al. 2005, Huh, Goutagny et al. 2010, Leao, Targino et al. 2015) and have an influence on theta oscillations

(Fuhrmann, Justus et al. 2015). The third group of neurons in the MS, the cholinergic neurons, fire at low frequencies below 4 Hz and show an I_h current with only a relatively small amplitude and slow activation kinetics (Sotty, Danik et al. 2003, Muller and Remy 2018). A diminished HCN channel expression might explain the absence of theta rhythmic burst-firing in this neuron type (Muller and Remy 2018). In addition to learning and memory formation, the theta rhythm also has a strong impact on sleep. Considering that human beings spend one third of their lives sleeping (Eric R. Kandel 2013) it is very likely that sleep per se is functionally relevant. In contrast to low overall physical activity during sleep, the "sleeping" human brain is highly active. This activity can be monitored using EEG recordings. Brain oscillations differ significantly in wake and sleep states (see Figure 1.4).
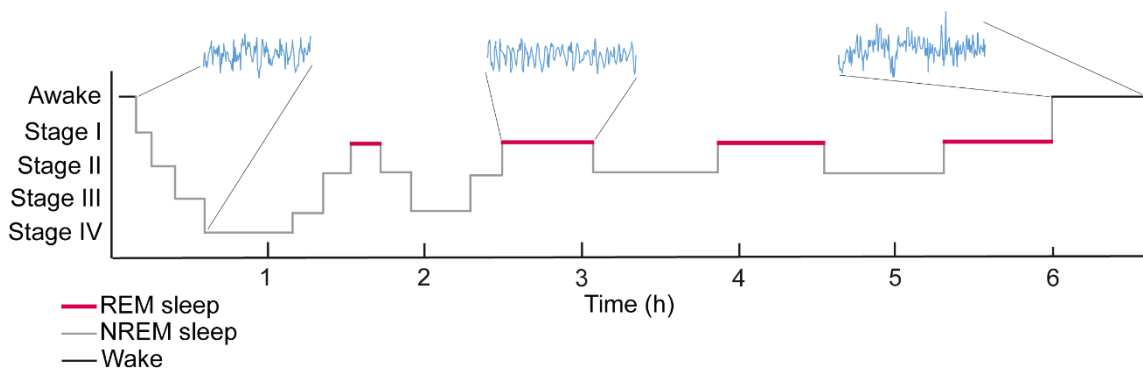
Figure 1.4: Human sleep cycles during a night. The ultradian rhythm with corresponding EEG recordings during NREM sleep (grey, left), REM sleep (red, middle), and wake (black, right). Modified from Bear et al. 2016.

During wakefulness, EEG recordings show low-voltage, high-frequency, and fast activity, whilst during sleep the electrical signals are more synchronous (Hobson and Pace-Schott 2002). During normal sleep, stages of rapid eye movement (REM) sleep alternate with episodes of non-REM (NREM) sleep. This cycle from NREM to REM and back to NREM sleep is called ultradian rhythm. Each cycle takes around 90 to 110 minutes. In humans, NREM sleep is subdivided in four stages: Stage 1 is the transition from wake to sleep. Stage 2 is slightly deeper and shows characteristic 8-14 Hertz (Hz) oscillations in the EEG, which are called sleep spindles. In stage 3, delta wave oscillations (0.5-4 Hz) occur and stage 4 is the deepest NREM sleep stage. These oscillations are assumed to be slow and regular. REM sleep is characterized by rapid eye movements while the rest of the body is immobilized (De Gennaro and Ferrara 2003, Dale Purves 2004, M. F. Bear 2016). During REM sleep, the prominent brain theta rhythm occurs (Pignatelli, Beyeler et al. 2012).

The theta rhythm was discovered in 1938 (Richard Jung 1938), characterized by a specific frequency of 4-8 Hz, and occurring in the hippocampus. It is measurable via EEG recordings and has been explored in many species such as rodents (Vanderwolf 1969, Landfield, McGaugh et al. 1972, Mitchell, Rawlins et al. 1982, Bland 1986, Liebe, Hoerzer et al. 2012). The theta rhythm is generated by the interconnection of brain areas like the brainstem, hippocampus, and the MS (Petsche and Stumpf 1962, Stumpf, Petsche et al. 1962, Bland 1986). The most important roles of the theta rhythm are mind formation, learning, memory, and information processing (Bland 1986, Lee and Kesner 2004, Lee and Kesner 2004, Colgin 2013, Colgin 2016). The theta rhythm also influences synaptic plasticity (Larson and Lynch 1986) and therefore long-term potentiation and long-term depression (LTP/LTD) (Jensen and Lisman 1996, Buzsaki 2002, Vertes 2005). The importance of the theta rhythm becomes visible when it is disturbed, because learning procedures and memory are impaired (Barbizet 1963, Winson 1978, Zola and Squire 2001). Theta rhythm occurs during wake, especially during active state like exploratory sniffing, and during REM sleep (Vanderwolf 1969, Bland 1986, Buzsaki 2002). The change of vigilance state from NREM to REM is visible in the change of characteristic waves: NREM sleep is determined by sharp ripple waves while in REM sleep the theta waves are starting and continue during the whole REM sleep period (see Figure 1.4) (Colgin and Moser 2009).

GABAergic neurons of the MS were strongly involved in the generation and entrainment of hippocampal field potential and additionally played a vital role in the generation of theta rhythm (Bender, Gorbati et al. 2015, Boyce, Glasgow et al. 2016, Gangadharan, Shin et al. 2016). This represents the fact, that GABAergic neurons regulate circuit activity by the rhythmic disinhibition of pyramidal neurons (Smythe, Colom et al. 1992, Toth, Freund et al. 1997, Buzsaki 2002, Unal, Crump et al. 2018). In addition, HCN channels in the MS, especially HCN2, are influencing the hippocampal learning and memory (Varga, Hangya et al. 2008, Spahn 2015). Finally, glutamatergic neurons of the MS and the DbB also have an impact on the theta rhythm generation, demonstrated in Robinson et al. mainly through local modulation of septal neurons (Robinson, Manseau et al. 2016). On electrophysiological levels, Huh et al. reported that glutamatergic neurons as well as GABAergic neurons show rhythmic spontaneous firing at theta frequency. The activation of the MS-DbB lead to fast AMPA (α-amino-3-hydroxy-5-methyl-4-isoxazolepropionic acid) receptor-mediated glutamatergic responses in CA3 hippocampal pyramidal neurons (Huh, Goutagny et al. 2010).

Although the circuits involved in theta rhythm generation are known (Hangya, Borhegyi et al. 2009, Huh, Goutagny et al. 2010, Robinson, Manseau et al. 2016), the involved ion channels and the detailed mechanisms are still largely elusive.

In particular, the role of HCN channels in theta rhythm generation needs to be investigated in more depth. There is evidence that HCN channels are critically involved in the generation of theta rhythm. For example, the HCN2 is expressed in different types of neurons in the MS (Varga, Hangya et al. 2008). In addition, these neurons fire rhythmically at theta frequencies and, in the hippocampus, are phase-locked to theta rhythms (Hangya, Borhegyi et al. 2009).

The examination of this local and neuron-specific knockdown of HCN2 in the MS was based on three lines of evidence, which are well knock in the field. At first, HCN2 is the predominant HCN channel isoform expressed in the MS (Notomi and Shigemoto 2004, Spahn 2015) and a MS HCN2-knockout (KO) did already indicate its influence on theta rhythm generation and its influence on learning behavior (Spahn 2015). Secondly, the MS had a well-known influence on the hippocampus and therefore on learning, memory, REM sleep, and especially theta rhythm generation (Kopell and LeMasson 1994, Hasselmo, Fransen et al. 2000, Kocsis and Li 2004, Nolan, Malleret et al. 2004, Xu, Datta et al. 2004, Rotstein, Pervouchine et al. 2005). Thirdly, literature showed numerous indications that GABAergic neurons played a predominant role by influencing the hippocampus: GABAergic neurons express the HCN2 channel (Varga, Hangya et al. 2008), influence the hippocampus (Freund and Antal 1988), and therefore influence hippocampal-dependent behavior and theta rhythm (Gangadharan, Shin et al. 2016). Varga et al. showed the rhythmic firing at theta frequency of GABAergic cells in the MS, although these data concern HCN channels in general (Varga, Hangya et al. 2008).

2   Aim of the thesis

The aim of the thesis was to study the role of HCN2 channels within the MS in the septo-hippocampal system and investigate its influence on neuronal oscillations. This was examined by a MS neuron-specific knockdown of HCN2 with the help of stereotactically injected lentiviral particles, specific promoters, and a Cre-dependent gene silencing approach in floxed HCN2 mice *in vivo*. HCN knockdown in MS neurons was then confirmed on protein level by immunohistochemical staining and on electrophysiological level via patch clamp recordings. Using patch clamp, I addressed the question how the loss of HCN2 channels lead to changes in firing pattern in the MS neurons *in vitro* on cellular level. The impact of HCN2 on neuronal rhythms was investigated *in vivo* with EEG measurements. In order to examine the behavioral phenotype of the neuron-specific HCN2 deletion in the MS the Water Cross Maze, object and social recognition tests were performed. Those experiments test for behavior in which the hippocampus is critically involved. Literature indicates GABAergic neurons to express HCN2, influencing the hippocampus and therefore theta rhythm.

3 Materials and methods

3.1 Chemicals and solutions

Unless stated otherwise, all chemical used were obtained from Akoya, Biorad, Merck, Roche, Roth, Sigma-Aldrich, Thermo Fisher, or VWR chemicals. The quality of the chemicals was either "pro analysis" or "for molecular biology". Working solutions were prepared with ultrapure and deionized water (Milli-Q water purification system, Merck Millipore) further named as H_2O or ISO3696 grade 3 analytical water (AnalaR Normapur, VWR chemicals.). Solutions were autoclaved for experiments in which high purity was needed. Long-term storage solutions were sterile-filtered or autoclaved. Experiments were performed at room temperature (RT) if not stated otherwise.

3.2 Experimental animals

For this thesis, wild type (WT) animals and the HCN2L2 genetically modified mouse strain were used. In HCN2L2, animals have two LoxP-sites flanking exons 2 and 3 of *HCN2*, encoding for the transmembrane segments 2 and 6 and the pore (Ludwig, Budde et al. 2003). The HCN2L2 mouse line allows the generation of a conditional HCN2 knockout upon stereotactic delivery of Cre-containing viral particles. The mouse lines were mated homozygous and HCN2L2 animals were bred on a C57-Bl6/N background. All experiments were performed on HCN2L2 and WT animals in accordance with legal regulations (ROB-55.2-2532.Vet-02-17-182) of the local committee of laboratory animal care (District Government of Upper Bavaria) and German Laws on animal welfare (Tierschutzgesetz).

3.3 Working with nucleic acids

To avoid contamination with nucleases, glassware, metal gear, and filter tips (VWR) were sterile, DNase, and RNase free. When working with RNA, material and surrounding were treated with RNase AWAY (Thermo Fisher).

3.3.1 Lentivirus plasmids

In general, plasmids are small, circular, double-stranded, and autonomously replicating deoxyribonucleic acid (DNA) molecules. Small DNA plasmids used in genetic engineering are called vectors. For amplification, bacteria such as *Escherichia coli (E. coli)* can be transformed using plasmid DNA leading to independent replication from chromosomal DNA. Therefore, these vectors need an origin of

replication. Other important components of vectors are selection markers like antibiotics resistance genes and a multiple cloning site (MCS). A polylinker or MCS is an artificially created DNA oligonucleotide of about 50 bp (base pairs), which is inserted into a plasmid and whose sequence contains various restriction sites for restriction endonucleases in direct succession. The purpose of the MCS is to allow insertion of DNA fragments into the plasmid with the help of restriction enzymes. Lentiviral (LV) vectors are powerful gene-transfer tools and have been used in many organs *in vivo* (e.g., eye, brain) or *in vitro* (e.g. in neurons) for heterologous expression of a gene of interest driven by specific promoters. For production of LV particles, the third generation of the human immunodeficiency virus-1 (HIV-1) derived delivery system was used. By reducing the number of viral sequences, the risk of homologous recombination has been reduced and the biosafety was consequently improved. Therefore, LV elements in the packaging helper constructs have been removed or replaced by additional heterologous sequences. More in detail, the structural genes *gag, pol,* and *env* are genes common to all retroviruses. The two regulatory genes *tat* and *rev* are important for viral replication. The *tat* trans-gene is not essential for the efficient production of LV particles, instead a strong heterologous promoter sequence was inserted. Additionally, there are four accessory genes: *vif, vpr, vplu* and *nef*. They are crucial for *in vivo* replication and pathogenesis which were therefore removed from the LV genome. Consequently, the risk of homologous recombination and the production of infectious particles was reduced (Delenda 2004). There are three helper plasmids used for LV particles production:

1. The pMD.2G plasmid is the vesicular stomatitis virus glycoprotein (VSV-G) envelope expressing plasmid (Verma and Weitzman 2005).
2. The second helper plasmid is the pMDL and contains the information of the *gag-pol* gene, which encodes a gag-pol precursor protein (probable ribonucleic acid (RNA)-directed RNA polymerase). It is processed to an integrase, a reverse transcriptase, and structural proteins essential for the LV particle production.
3. The third helper plasmid is pRSV-Rev and contains the *rev* gene. The *rev* gene in HIV-1 interacts with the rev response element and enhances the efficient nuclear export of the unspliced, full-length viral RNA genome transcripts of gag-pol RNA and genomic RNA of the transfer vector (Delenda 2004).

3.3.1.1   Cloning LV plasmids

The original plasmid contains several cloning sites to insert genes of interest and two long terminal repeats (LTR) encoding elements. LTRs are important for the efficient integration of retroviral DNA into the host chromosome via a specific integrase. Between the two LTRs, a polypurine tract, a cytomegalovirus (CMV) promoter, a WPRE (woodchuck hepatitis virus posttranscriptional regulatory element), and a nuclear localization site followed by the sequence for the Cre-recombinase exists. The Cre/loxP recombination system was first reported by Gu et al. and was subsequently used as a powerful and efficient tool for specific knockdowns (Gu, Marth et al. 1994). For selection of successfully transformed bacterial cells an ampicillin resistance gene was inserted into the vector. The gene of interest was cloned into the vector containing a specific promoter (human Synapsin (hSyn1.1), GAD67 or CamKIIα), the Cre-recombinase, and a fluorescent molecule (mCherry). The resulting vectors are illustrated in Figure 3.1.
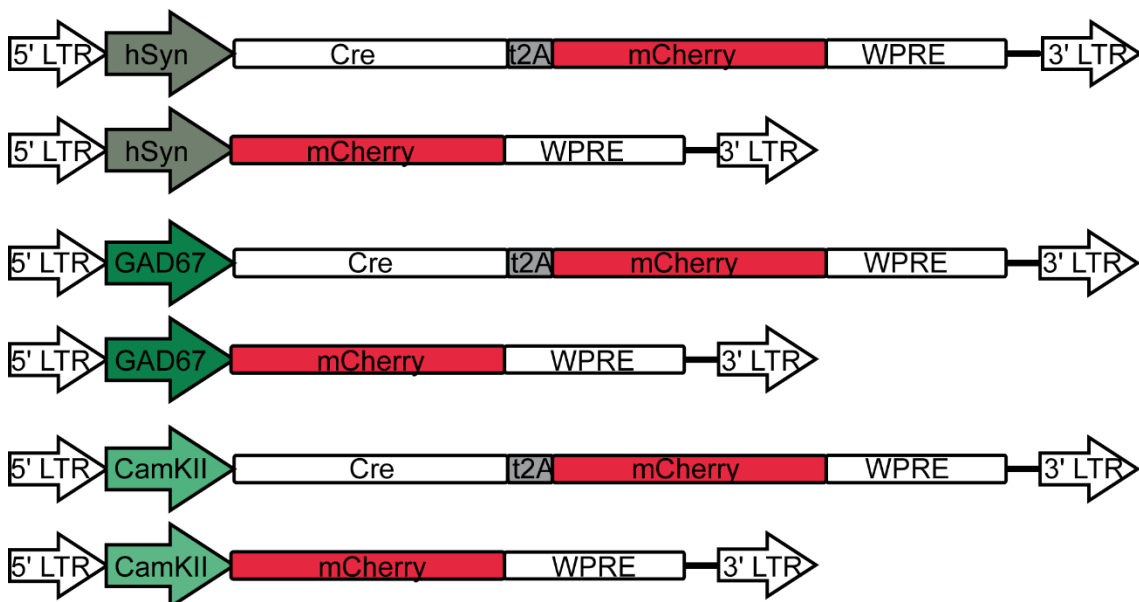
Figure 3.1: Schematic illustration of the produced LV particles. The promoters used are the hSyn1.1 promoter for pan-neuronal expression, the GAD67 promoter supports GABAergic neuron-specific expression, and the CAMKIIα promoter drives glutamatergic neuron-specific expression. As fluorescent protein mCherry was used. Control plasmids (ctrl) lack the Cre-t2A cassette.

The promoter hSyn1.1 allows neuron-specific expression (Dittgen, Nimmerjahn et al. 2004). Derived from its name, synapsin is a protein responsible for the neurotransmitter release and expressed in all types of neurons. The GAD67-promoter (Addgene, no: 25866) (Akama-Garren, Joshi et al. 2016) drives only expression in GABAergic neurons. The CAMKIIα promoter (Addgene, no: 34926) (Dittgen, Nimmerjahn et al. 2004) drives glutamatergic neuron-specific expres-

sion. The topoisomerase based Cre-t2A-GFP plasmid (Addgene, no: 68450) delivers the Cre-t2A cassette for expression of the Cre-recombinase, whereas the t2A element serves for separation of the Cre and mCherry protein. The control plasmids do not contain the Cre-t2A-casette with the information for the Cre recombinase.

3.3.2 Isolation of genomic DNA for genotyping

For extraction of genomic DNA for genotyping, the mouse tissues were incubated with 600 µl 50 mM NaOH for 10 minutes at 95°C. After adding 50 µl 1 M Tris-HCL (pH = 8) for neutralization, the samples were centrifuged for 6 minutes at 13,000 rpm. The DNA-containing supernatant was used as template in the polymerase chain reaction (PCR; see 3.3.3).

3.3.3 Polymerase chain reaction

The PCR is a common method for amplifying DNA fragments for genotyping animals and for amplifying DNA fragments to modify vectors (see 3.3.1.1). Depending on the experiment and therefore on the chosen DNA polymerase, the conditions of the PCR reaction had to be adjusted according to the manufacturer's instruction. The GoTaq polymerase (Promega) was used for genotyping, the Q5 polymerase (New England Biolabs) for all other PCR reactions.

Table 1: PCR conditions for polymerases GoTaq and Q5.

Polymerase	GoTaq		Q5	
Initial denaturation	95°C	2 min	98°C	30 sec
Denaturation	95°C	15 sec	98°C	10-15 sec
Annealing Time	61-67°C	15 sec 38 x	58-72°C	15-30 sec 35x
Elongation	72°C	1 min	72°C	0.5-2 min
Final elongation	72°C	5 min	72°C	5 min

Primers were custom designed and are listed in the appendix (see Appendix 8.1). The annealing temperature was calculated with the help of the Tm Calculator (NEB, version 1.9.8). The components of the PCR reaction mixture are listed in Table 2. The thoroughly mixing of the PCR reaction mix is essential.

Table 2: Standard PCR pipetting scheme for polymerase GoTaq and Q5.

PCR reaction mixture for polymerase			
GoTaq		**Q5**	
Primer 1 (10 µM)	1.25 µl	Primer 1 (10 µM)	1.25 µl
Primer 2 (10 µM)	1.25 µl	Primer 2 (10 µM)	1.25 µl
Primer 3 (10 µM)	1.25 µl	5x Q5 High Enhancer	10 µl
dNTP's	0.5 µl	dNTP's	0.5 µl
10x buffer	2.5 µl	Buffer	2.5 µl
Polymerase	0.125 µl	Polymerase	0.125 µl
DNA template	2 µl	DNA template	2 µl
H_2O, nuclease free	ad 25 µl	H_2O, nuclease free	ad 25 µl

For quantification of nucleic acids, the Nanodrop™2000c spectrophotometer and the associated software (Thermo Fisher) was used. The concentration of DNA and RNA was calculated by measuring the absorption at 260 nm wavelength. To verify the amplification a restriction enzyme digestion was performed after PCR protocol (see 3.3.7).

3.3.4   DNA precipitation

To separate the DNA from other proteins 0.1 volumes of sodium acetate (3M, pH = 5.2) and 3 volumes of ice cold ethanol were added to the DNA-containing solutions. After an incubation time of 10 minutes at -80°C the samples were centrifuged at 13,000 rpm and 4°C for 10 minutes and the DNA-pellets were washed with ethanol (70% in H_2O). After another centrifugation step (5 minutes, 13,000 rpm, 4°C) the pellets were resuspended in 50-100 µl H_2O.

3.3.5   Agarose gel electrophoresis

To separate DNA fragments according to their size agarose gel electrophoresis was used. Agarose (peqGOLD, VWR) was solved in TBE buffer (Tris/Borate/EDTA) at different concentrations between 0.7% and 3%, depending on the expected DNA fragment sizes. To visualize the DNA band via ultraviolet (UV) light, PegGreen (VWR) was added to the agarose solution. Bevor bringing the

DNA containing solution into the gel, a 6x loading-dye (Thermo Fisher) was added to the DNA samples to pursue the course of the separation process. To determine the DNA fragment size the 1 kb plus ladder (Thermo Fisher) was utilized. Then DNA was separated at 130-160 V in a TBE filled horizontal electrophoresis chamber (PEQBiotechnology GmbH). Afterwards, DNA band sizes were analyzed in a molecular imager (GelDoc 2000 or ChemiDoc Universal Hood III, Bio-Rad).

3.3.6 Purification of DNA fragments

The amplified PCR fragments need to be purified for further use. The DNA bands were excised under UV light with a scalpel (Braun) stored in 2 ml tubes and resolved from the gel. The QIAquick gel extraction kit (Qiagen) was used according to the manufacturer's instructions. First, threefold amount solubilization buffer of gel weight was added to the excised gel slices and the tubes were incubated in a Thermomixer (Thermomixer compact, Eppendorf) at 50°C and 500 rpm for 10 minutes, until the gels were completely dissolved. Then, one volume of Isopropanol (AnalaR NORMAPUR, VWR) was added and the tubes were inverted several times. The samples were loaded onto the provided column, washed with washing buffer, and eluted with 30 µl H2O or elution buffer into new tubes by centrifugation. The concentrations of DNA were measured with Nanodrop (see 3.3.3). The successful purification was verified by restriction enzyme digestion (see 3.3.7).

3.3.7 Restriction enzyme digestion

Palindromic sites in the DNA enable the cutting of linear or plasmid DNA with the help of restriction enzymes. All restriction enzymes were acquired from Thermo Fisher and were used according to the instructions. For cloning, usually 3-5 µg of DNA were digested at 37°C, separated via agarose gel electrophoresis (see 3.3.5), and purified via gel extraction (see 3.3.6) for further applications.

3.3.8 DNA fragment ligation

For inserting a DNA fragment into a linearized vector to produce a genetically modified plasmids, the T4 ligase (Thermo Scientific) was use according to the manufacturer's instructions. The used ligation mixture is shown in Table 3. Reactions were incubated over night at 16°C or at RT for 20-30 minutes. Processed reaction mixture was used for transformation (see 3.3.9) or stored at -20°C.

Table 3: Components and respective amounts of the ligation mixture.

Ligation mixture	
10x T4 DNA ligase buffer	1.5 µl
Linearized vector DNA	20-100 ng
Insert DNA fragment	2x to 5x molar ratio over vector
T4 DNA Ligase (5 U/µl)	0.2-1 µl
H$_2$O	ad 20 µl

3.3.9 Transformation

The ligated DNA plasmids (see 3.3.8) were transformed into a strain of chemically treated and competent β10 *E. coli*. Therefore, 100 µl β10 *E. coli* suspension were thawed on ice before 5-10 µl of ligation product or 5-10 ng of purified plasmid DNA samples were added to the cell suspension and mixed gently. After 10 minutes incubation on ice a heat shock at 42°C was applied for 45 seconds. Immediately after this, cells were subsequently incubated for 2 minutes on ice prior plating on a Luria-Bertani plus glucose (LB(+)) selection agar plate (Table 4) containing ampicillin and incubated overnight at 37°C.

Table 4: Components and respective amounts of the LB(+) medium and LB(+) agar.

LB(+) medium		LB(+) agar	
Peptone	10 g	agar	15 g
Yeast extract	5 g	Ampicillin	100 mg
NaCl	5 g		
Glucose	1 g		
H$_2$O, autoclave	ad 1 l	LB(+) medium	ad 1 l
adjust pH to 7.2 – 7.5		adjust pH to 7.2 – 7.5	

3.3.10 Inoculation of bacterial cells and isolation of plasmid DNA

Single bacterial clone colonies were picked from the agar plate and transferred into 13 ml tubes (Sarstedt) containing 5 ml of LB(+) medium (Table 4) and ampicillin (100 µg/ml). The suspensions were incubated at 37°C and 225 rpm in

a Thermomixer for approximately 24 hours. Afterwards, they were centrifuged at 3,500 rpm for 10 minutes and the supernatant was discarded. The bacterial cell pellets were resuspended in 250 μl resuspension buffer and transferred into a 1.5 ml tube. Then, 250 μl lysis buffer was added, the tubes were inverted two times, and incubated for 5 minutes at RT. After mixing 250 μl neutralization buffer to the suspensions they were allowed to incubate for 5 minutes at RT before being centrifuged at 13,000 rpm and 4°C for 15 minutes. The supernatants containing the plasmid DNA were transferred into a fresh tube and 250 μl ice-cold 100% isopropanol was added for precipitation. The samples were mixed thoroughly and spun at 13,000 rpm and 4°C for 15 minutes. The pellets were washed with 370 μl 70% ethanol and the solutions were centrifuged at 13,000 rpm at 4°C for 5 minutes. The supernatants were removed and the pellets were dried for approximately 15 minutes at 50°C. The pellets containing the DNA were resuspended in 30 μl H_2O.

For restriction analysis, 1 μl of the purified plasmid DNA solution was used (see 3.3.7). If the restriction analysis is correct, the samples were sent for sequencing (Eurofins Genomics) without further purification to verify the DNA sequences. The sequencing primers were designed in-house and ordered at Eurofins Genomics. Details of the primers can be found in the appendix (see Appendix 8.1).

To yield plasmid DNA in larger amounts and in higher purity, Plasmid-Midiprep- or Maxiprep kit (Invitrogen) was used. Therefore, colonies were inoculated in 100 or 200 ml LB(+) medium and the DNA isolation was performed following the manufacturer's instructions.

3.4   Cell culture

All work with mammalian cell lines (biosafety level 1 and 2) was performed in biological safety cabinets (HERAsafe, Thermo Fisher). The cells were maintained at 37°C and 5-10% CO_2 in incubators (HERAcell, Thermo Fisher).

3.4.1   Production of lentiviral particles

For generation of LV particles, human embryonal kidney 293 expressing SV40 large T antigene (HEK 293T) cells were used and maintained in Dulbecco's Mod- ified Eagle's Medium (DMEM) + GlutaMAX™-I medium containing 4.5 g/l glucose (Life technologies), pyruvate, 10% fetal bovine serum (FBS, Biochrom), and 1% penicillin/streptomycin (Biochrom). A calcium-phosphate transfection of HEK293T was used for preparation of lentiviral particles (Tiscornia, Singer et al. 2006). HEK293T cells were grown in cell culture plates (Cellstar 145 mm,

Greiner) to 60% confluence. For six culture plates (Ø 15 cm) a reaction mix was used as described in Table 5.

Table 5: Components and respective amounts of the transfection mix for LV production.

Transfection mix	
LV plasmid	108 µg
pMDL helper plasmid	70 µg
pREV helper plasmid	30.8 µg
pMD2G helper plasmid	29.2 µg
$CaCl_2$	700 µl
Polybrene (8 mg/ml)	7 µl
Dextran	700 µl
H_2O	ad 7 ml

While vortexing, 7 ml 2x BES-buffered solution (BBS) (see Table 6) was added dropwise. After inverting the transfection mixtures 6 times they were allowed to incubate 10-15 minutes at RT to facilitate the formation of homogenous DNA complexes. On each cell culture plate 2.3 ml of the transfection mixture was added dropwise. The HEK293T cells were incubated at 37°C and 5% CO_2 for at least 6 hours before the media was completely changed. Cells were placed back to 37°C and 10% CO_2 for 60 hours before harvest was performed on two subsequent days.

Table 6: Components of 2xBBS.

2xBBS	
BES	10.65 g
NaCl	16.35 g
Na_2HPO_4 x 2 H_2O	0.21 g
H_2O	ad 1000 ml
filtrate sterilely, adjust pH to 6.95 with NaOH	

For the first harvest, the media containing the lentiviral particles was collected and the cells were provided fresh media and were incubated at 37°C and 10% CO_2 for additional 24 hours. The media was collected and filtered using 0.45 µm pore filters (125ml Rapid-Flow, VWR) to remove cell debris. The flow-through was distributed to 30 ml centrifugation beakers (SW28 Beckman&Coulter), placed into swing-out buckets of the Beckman SW28 rotor, and centrifuged at 19,400 rpm at 17°C for 2 hours (Optima LE-50K ultracentrifuge, SW-28 rotor, Beckman&Coulter). The supernatants were removed, the cell pellets were resuspended in 100 µl HBSS (Hank's Buffered Salt Solution), and tubes were rinsed with additional 150 µl HBSS. The solution was vortexed and stored in screw cap tubes at 4°C until second harvest.

The second harvest was performed as indicated above. Both resuspended pellets were combined in 3 ml centrifugation beakers (SW55Ti Beckman&Coulter) with 2 ml of 20% sucrose solution in H_2O and centrifuged in swing-out buckets of the Beckman SW55 Ti rotor at 21,000 rpm at 17°C for 2 hours (Optima LE-50K ultracentrifuge, SW55 Ti rotor, Beckman&Coulter). The supernatant was removed, the pellet was resuspended in 50 µl HBSS and tubes were rinsed with 20 µl HBSS. The viral containing solution was vortexed for 45 minutes in a Thermomixer at RT at 1400 rpm. After a brief centrifugation step the supernatant was aliquoted and stored at -80°C.

3.4.2 LV titer determination

LV titer determination was performed using the ELISA-based HIV-1 p24/Capsid Protein p24 ELISA Pair Set (SEK11695, Sino Biological). Briefly, the plates were prepared by covering the wells with 100 µl capture antibody solution. The plate was sealed and incubated overnight at 4°C. After washing the wells thrice with

wash buffer, 300 µl blocking buffer was added and incubated for one hour before washing again thrice. For the assay procedure, 100 µl diluted sample (1:200) or standard solution was added, the plates were sealed and incubated for two hours at RT. After, washing thrice, 200 µl substrate solution was added and incubated for 20 minutes shielded from light. The reaction was stopped by adding 50 µl stop solution. The optical density of each well was measured using a microplate reader set to 450nm.

3.5 Histology and cytology

With histology it is possible to investigate the microscopic structure of organs, tissue, and cells. Most histological samples need preparations like fixing or coloring before an observation via microscope is possible. The preparation methods depend on the specimen and the observation method (M. F. Bear 2016).

3.5.1 Immunohistochemistry

With immunohistochemistry (IHC) it is possible to stain proteins by antibodies such as ion channels or other cell structures in native tissue sections and in addition to demonstrate co-localization of different proteins in cells and tissue. The principle of IHC is an antigen-antibody-reaction with a high specificity (M. F. Bear 2016).

3.5.1.1   Cryo-sectioning of mouse brains

Animals were anaesthetized and decapitated. The brains were carefully removed and for some minutes submerged in -30°C cold 2-methylbutane (AppliChem) for freezing and dehydration. For evaporation of 2-methylbutane the brains were maintained on dry ice for approximately 10 minutes and either were used immediately or were stored at -80°C until further usage. For cryo-sectioning, the brains were allowed to adopt to -20°C in the cryostat (CM3050 S, Leica and Epredia Cryostar NX70, Thermo Fisher). The brains were mounted onto a cutting plate with embedding medium (Tissue-Tek O.C.T.^{TM}, Sakura Finetek). Then they were sectioned with the cryostat into 12 µm thick coronal or sagittal sections and mounted on superfrost plus microscopic slide (Thermo Fisher). The sections were stored on -20°C until further usage.

3.5.1.2   Immunohistochemical staining of brain slices

All chemicals were diluted in ice-cold phosphate buffered saline (PBS, see Table 7). After thawing the slices (see chapter 3.5.1.1) to RT, the single brain slices were surrounded with a liquid blocker (PAP pen, Science Services) to build a

hydrophobic barrier. Brain slices were then rehydrated for 5 minutes with PBS and then post-fixed by 4% paraformaldehyde (PFA; Thomas Scientific) in PBS for 5 minutes. The slices were washed thrice with PBS and then permeabilized and blocked for one hour at RT with a solution of 10% ChemiBlocker (CB, Millipore) / 0.3% TritonX-100[1] (Roth) in PBS. Subsequently, the primary antibodies (see Appendix Table 15) were diluted in a solution of 5% CB / 0.2% TritonX-100 in PBS and applied on brain slices over night at 4°C. On one brain slice, the antibody dilution solution only was applied without primary antibody as negative control.

Table 7: Components of phosphate buffered saline.

Phosphate buffered saline (PBS)	
NaCl	137 mM
KCl	2.7 mM
$Na_2HPO_4 * 2 H_2O$	10 mM
KH_2PO_4	1.8 mM
in H_2O, pH = 7.4	

When using a horse radish peroxidase (HRP) conjugated secondary antibody the endogenous peroxidases were destroyed with a solution of 3% H_2O_2 in methanol for 10 minutes and then extensively washed with PBS before applying the secondary HRP conjugated antibody. The secondary antibody (see Appendix Table 16) was diluted in a solution of 2% CB in PBS and applied on brain slices for one hour at RT. Afterwards, brain slices were washed with PBS at least thrice for 5 minutes. If the primary antibody was an HRP, the brain slices were allowed to incubate for 5 minutes in amplification buffer (0.15M NaCl, 0.1M Tris-HCl, pH 8.0) followed by an incubation with PE-tyramide (Cy2 or Cy3, Perkin Elmer and Akoyabio) diluted in tyramine signal amplification buffer (Perkin Elmer and Akoyabio) for 8 minutes before washing the slices again twice with PBS for 5 minutes. If a double staining of antibodies raised in the same species was used, a second blocking step with a solution of 10% CB in PBS for one hour had to be performed. The primary antibody was diluted in a solution of 5% CB and 0.2% Triton-X100 in PBS and applied to the brain slices over night at 4°C. Brain slices were washed

---

1 TritonX-100 is a nonionic surfactant for increasing the permeability of membrane components under non-denaturing conditions; 4-(1,1,3,3-tetramethylbutyl)-phenyl-polyethyleneglycol

with PBS at least thrice for 5 minutes. The secondary antibody was incubated in a solution of 2% CB in PBS. After washing twice with PBS for 3 minutes a Hoechst staining (5 µg/ml; Hoechst 33342) was performed and again slices were washed with PBS for 5 minutes thrice. Slices were embedded in Fluoromount-G Slide mounting medium (Thermo Fisher), covered with cover slips (Menzel-Gläser), and let air dried. The slides were stored shielded from light at 4°C.

3.5.2 Microscopy

Images of IHC were captured and analyzed using the TCS SP8 confocal laser scanning microscope (Leica). The images were obtained using the LAX software (Leica). Figures were prepared using the Fiji ImageJ software (ImageJ), Photoshop (Adobe), and Illustrator (Adobe) whereby only threshold and brightness were adjusted and applied to the entire image series.

3.6 Electrophysiology

The preparation of acute brain slices containing the MS and their electrophysiological recordings were performed the same day. The relevant brain regions were identified using a standard mouse brain atlas (Paxinos 2004).

3.6.1 Experimental setup

Neurons were identified with a Zeiss Axioskop 2 equipped with a 5x objective, a 40x water-immersion objective and an infrared camera (VX55, Photonics). For electrophysiological recordings, an EPC 10 amplifier (HEKA Elektronic) in combination with PatchMaster software (Version v2x73.2, HEKA Electronic) was used. Voltage-clamp and current-clamp measurements were performed at RT. For pulling patch pipettes, borosilicate glass (1.5 OD x 0.086 x 100 L mm with filament, BM150F-10P, BioMedical Instruments) and a DMZ universal puller (Zeitz Instruments) were used. The pipettes were heat polished and had resistances of 2.5 – 5 MΩ when filled with intracellular solution (see Table 8).

Table 8: Chemical components of the intracellular solution.

Intracellular solution	
K-Gluconate	144 mM
$MgCl_2 * 6\ H_2O$	3 mM
EGTA	0.2 mM
HEPES	10 mM
ATP-Na	2 mM
GTP-Na	0.3 mM
In H_2O, pH = 7.2	

3.6.2 Brain slices

All solutions were with Millipore water and perfused with carbogen (95% O_2, 5% CO_2) before and during the whole experiment.

Brain slices were prepared as previously described (Ying and Goldstein 2005, Kuisle, Wanaverbecq et al. 2006, Ying, Tibbs et al. 2011). Injected female and male HCN2L2 mice used for electrophysiology were 70-90 days old. The animals were anaesthetized, decapitated, and the head was immediately dipped into ice-cold carbogen-perfused slicing solution (see Table 9).

Table 9: Chemical components of the slicing solution.

Slicing solution	
KCl	3 mM
NaHCO$_3$	24 mM
Na$_2$HPO$_4$	1.25 mM
Glucose * 1 H$_2$O	10 mM
CaCl$_2$ * 2 H$_2$O	1 mM
MgCl$_2$ * 6 H$_2$O	2 mM
Sucrose	252 mM
in H$_2$O, pH = 7.4	

After the brain was dissected, the cerebellum was removed using a scalpel. Subsequently, the cutting surface of the brain was glued onto the slicing platform of the microtome (Leica VTI200 S). Coronal slices with 225-300 µm thickness were slowly cut with the microtome in ice-cold carbonated slicing solution. Slices containing the MS-DbB were transferred to carbonated storage solution (extracellular solution, see Table 10) and incubated at 37°C for 40 minutes to enable metabolic regeneration. Before slices were used for patch clamp recordings, they were allowed to cool to RT for at least 20 minutes. Whole-cell voltage- and current-clamp recordings were implemented at RT and brain slices were constantly perfused with extracellular solution (see Table 10).

Table 10: Chemical components of the extracellular solution.

Extracellular solution	
NaCl	126 mM
KCl	3 mM
NaHCO$_3$	24 mM
Na$_2$HPO$_4$	1.25 mM
Glucose * 1 H$_2$O	1.8 mM
CaCl$_2$ * 2 H$_2$O	10 mM
MgCl$_2$ * 6 H$_2$O	2 mM
in H$_2$O, pH = 7.4	

3.6.3 Patch clamp protocols and analyses

For a standardized characterization of neurons similar to Sotty et al. and Huh et al., the following patch clamp protocols were used for current- and voltage-clamp experiments (Sotty, Danik et al. 2003, Huh, Goutagny et al. 2010). The analysis of the electrophysiological data was performed using PatchMaster, Clampfit10.5 (Molecular Devices) and GraphPadPrism 5 (GraphPad Software) as indicated in Huh et al. 2010 and Gangadharan et al. 2016 (Huh, Goutagny et al. 2010, Gangadharan, Shin et al. 2016).

For current-clamp measurements, the following protocols were used. To determine the RMP under nearly physiological conditions, a 100 or 500 ms measurement was performed without inducing action potentials during the recording. To investigate the spontaneous firing frequency a 60 seconds measurement was taken. The mean firing rate was calculated by dividing the number of spontaneous action potentials by the measurement duration. To determine the firing threshold and to distinguish between burst- and non-burst-firing cells, hyperpolarizing current was injected until a membrane potential of approximately -90 mV was set. In steps of 5 or 10 pA the cells were depolarized for one second until action potentials occurred, meaning that the threshold was reached (see Figure 3.2). With depolarization starting from -90 mV, burst-firing neurons show burst-firing characteristics, while depolarization from -80 mV does not induce the characteristic firing pattern in all burst-firing cells. The first occurring action potential was used

for analyzing the action potential characteristics. To determine the spike threshold, the occurring action potentials were further examined and the threshold of the first action potential was defined as the spike threshold.
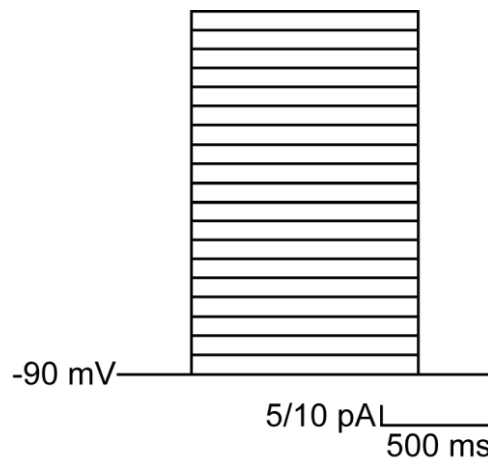
Figure 3.2: Graphic visualization of the threshold protocol used for neuron characterization. The cell was set to -90 mV and stepwise depolarized until the firs action potential occurred. Depending on the cellular response steps of 5 or 10 pA were used in the protocol.

Afterwards, the cell was depolarized for one second using the same current amplitude that was necessary to reach the threshold. This protocol was used for analyzing the firing frequency in order to categorize cells into fast (> 7 Hz) and slow (< 7 Hz) firing cells. For this purpose, the number of action potentials was counted and divided by the measurement duration. Depolarizing the cell for 5 seconds was necessary to determine cluster firing cells.

For analyzing the characteristic HCN channel-dependent depolarizing sag, the cells were hyperpolarized for 2.5 seconds starting from -60 mV using current injections in 5 or 10 pA steps, until the membrane potential was lower than -120 mV (see Figure 3.3). The sag amplitude was calculated as the difference in membrane potential between the lowest point of the depolarizing sag curve and the steady state at the end of hyperpolarization. Important characteristics arising from these experiments are the occurring rebound bursts.
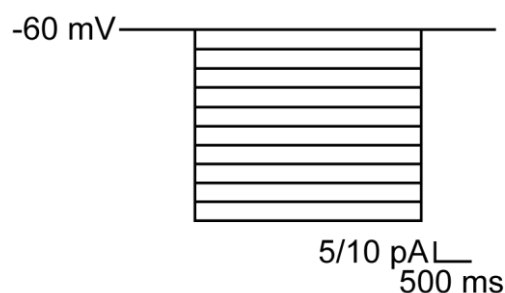
Figure 3.3: Graphic visualization of the depolarizing sag protocol used for neuron characterization. The cell was hyperpolarized from -60 mV to at least -95 mV for sag analysis.

For recordings of I_h, neurons were voltage-clamped at -70 mV, and a 3.5 second step pulse to -130 mV was applied (see Figure 3.4). From these measurements the amplitude of I_h was determined as the difference between the beginning of the I_h curve and the steady state current at the end of the hyperpolarizing voltage step.
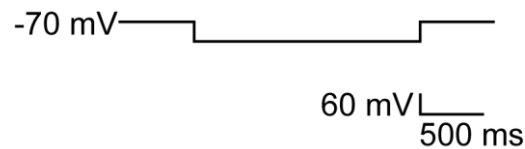
Figure 3.4: Graphic visualization of the I_h-protocol used for neuron characterization. The cell was hyperpolarized from -70 mV to -130 mV.

3.7   Stereotactic injections

To generate a MS specific HCN2 knockdown, 8 weeks old HCN2L2 mice were injected with control lentiviral particles LV-hSyn/GAD-mCherry or Cre-containing LV-hSyn/GAD-Cre-mCherry lentiviral particles.

Before starting the stereotactic injections, the surfaces and tools were disinfected thoroughly with 70% ethanol or Bacillol. The animal was anesthetized with an intraperitoneal injection of 10 mg/kg xylazine (Exuphar) / 80 mg/kg ketamine (Medistar) in 0.9% NaCl (Braun) and eye ointment was applied (Bepanthen, Bayer). After removing the fur from the skull and disinfecting the surgical area, 50 µl lidocaine was injected under the scalp for local anesthesia. The animals' head was fixed in the stereotactic apparatus (Robot Stereotactic, Neurostar) in sternal recumbence. The scalp was cut open along the dorsal midline and the subcutaneous tissue was removed. With a sterile applicator (Böttger) soaked in 3% H_2O_2 (Merck) bregma and lambda were visualized. The surgery area was washed thoroughly with isotonic 0.9% NaCl solution and kept moist throughout the surgery. For better vision of the small structures on the skull a magnifying glass was used. The software from Neurostar used Bregma and Lambda as reference for calibrating tilt and scaling. The coordinates of the points for bilateral injection of lentiviral particles in the MS (medial/lateral ± 0.09, anterior/posterior 0.74, dorsal/ventral 4.42). The angle of the syringe for injection (±10°) was set based on Paxinos (Paxinos 2004) which was necessary to avoid a damage of the sinus blood vessel and bleedings (see Figure 3.5).
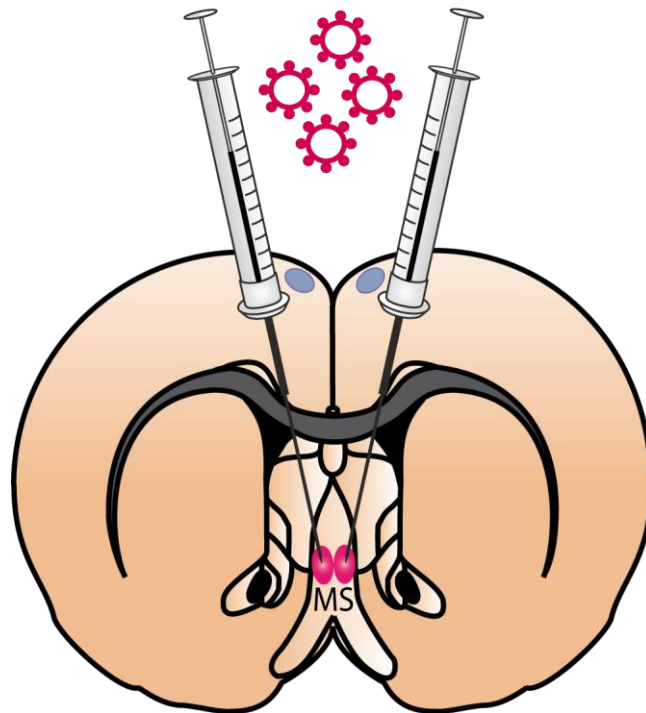
Figure 3.5: Stereotactic injection of lentiviral particles into the MS. Injection of lentiviral particles into the MS with an angle of ±10° was used for injection to avoid damaging the sinus blood vessel (blue).

With the help of a dentist's drill (K-control 4970 with K5 plus-tool holder, KaVo) a hole (< 1mm) was drilled into the skull at the appropriate coordinates. The micro syringe (Nanofill, WPI) with injection needle (NF34BL, WPI) was loaded with the appropriate lentiviral control particles (LV-hSyn/GAD-mCherry; Titer: 1.97×10^{10} to 7.73×10^{10} PFU/ml) or Cre-containing LV (LV-hSyn/GAD-Cre-mCherry; Titer: 7.77×10^{10} to 1.27×10^{12} PFU/ml). The syringe moved through the drilled holes and to the injection point with a speed of 1 mm per 12 seconds. To avoid a blockage of the syringe tip with tissue the syringe is moved 250 µm deeper into the brain and back to the injection point in 50 µm steps manually. The injector delivered 0.8 µl lentiviral particle solution at a flow-rate of 0.3 µl/minutes computer-driven into the MS. The syringe remained in place for two minutes after injection to ensure an efficient distribution of the LV in the tissue and to avoid backflow by capillary forces. Then the syringe was slowly pulled back. The animal was removed from the stereotactic frame and the scalp wound was sutured (4.0 silk HR 12, Resorba). A postoperative treatment consisting of povidone-iodine for disinfection of the wound, the application of isotonic 0.9% NaCl solution subcutaneously as rehydration, and intraperitoneal injection of analgesic at day of surgery and minimum 3 days thereafter (50 mg/ml Carprofen, cp pharma) was applied. The animals were monitored closely to ensure a return of normal posture and behavior. Mice were allowed to recover for two weeks before electrophysiological

or behavior experiments and to ensure lentiviral expression. Only animals with a verified mCherry expression in the MS were included for further analyses.

3.8 Electroencephalography

To record electrical activity of the mouse brain, EEG was performed. EEG and muscle electromyography (EMG) were recorded simultaneously during approximately 62h without disturbance.

3.8.1 EEG surgery

The implementation of the surgery for EEG transmitter was performed as previously described (Spahn 2015). Mice were allowed to recover for two weeks after surgery before EEG recordings, also to ensure lentiviral expression. Only animals with a verified MS mCherry expression were included for further analyses.

3.8.2 EEG recordings

In one session up to three animals were recorded simultaneously with the Dataquest A.R.T.™ system (Data Science International, USA). In parallel, EEG, EMG, activity, temperature, and video signals were recorded continuously for at least 64 hours. Before starting the recordings, transmitter properties had to be entered to configure with the Dataquest A.R.T. ™ system and the transmitters had to be turned on by a magnet (controlled by an AM radio tuned to 550 kHz).

3.8.3 EEG analyses

A 24 hours period (8 pm to 8 pm) is used for analyzing EEG of each animals. NeuroScore™ analysis software and Python™ were used to analyze the data recorded in Dataquest A.R.T.™. Analysis was focused on seizures and vigilance stages and therefore on brain oscillations like delta and theta rhythm. Seizures were detected by a software plugin and the vigilance states were scored by visual inspection of the traces manually. The 24 hours period was divided into 2 seconds epochs. Every epoch was scored as wake, NREM, or REM sleep using the EEG, EMG, and video data. The wake state was defined by movements visible in the video or in the EMG signals and includes a wide variety of behavior like eating, grooming, drowsiness, or exploratory behavior. Typically, in this vigilance state the EEG pattern showed various fast frequencies and a low amplitude. During wake state, lower frequencies (for example delta waves during drowsiness) but also higher frequencies (for example theta waves during grooming and exploratory behavior) occur. The EMG signal can be highly variable in wake state. NREM sleep is characterized by a lower EMG signal compared to wake state.

The EEG shows dominate high-amplitude slow waves in the delta frequency range (1-4 Hz). The REM sleep is characterized by a regular low-amplitude theta wave (4-8 Hz) in the EEG, muscle atonia, no activity, and therefore no signal in the EMG (see Figure 1.4). For more clear identification of REM sleep periods, the theta ratio (quotient of theta power to delta power) and the delta ratio (quotient of delta power to total power) were calculated. Periods are scored as REM sleep if the theta ratio was higher than a value of three for at least six seconds. Artifacts, unidentifiable epochs, or electric discharges were excluded from further analyses.

The EEG signal including time stamps and sleep stages in the frequency range of 0.5-25 Hz was exported to Excel (Microsoft) using a discrete Fourier transform and Damming window function. In Excel, artifacts and transitions were excluded and the epochs of the vigilance stages separated. For the power spectrum, the mean of all epochs for every 0.5 Hz frequency step (0 Hz, 0.5 Hz, 1 Hz until 25.5 Hz) was calculated and normalized to the mean of all values of each vigilance stage. The normalized spectral EEG power was plotted against the frequency (0-25.5 Hz) for each vigilance state. To investigate the time the animals spent in the three vigilance stages were summed up. To investigate the power change of each frequency over the time a heat plot and 3-dimenstional plot was created using Python. Time is plotted on the x-axis against the frequency on the y-axis. The power intensity was visualized by a color code.

3.9   Behavioral experiments

3.9.1   Water Cross Maze

The Water Cross Maze (WCM) specifically tests for CA1 hippocampal learning and was performed as previously described (Kleinknecht, Bedenk et al. 2012). It consisted of a cross while the four arms labeled North (N), East (E), South (S), and West (W) in a clockwise directon (see Figure 3.6). An escape platform was hidden 1 cm below the water surface in the West (learning week, week 1, d1-d5) or East arm (relearning week, week 2, d1r-d5r). A flexible barrier in the northern or southern arm transforms the cross into a T-shaped maze. Adult male animals were tested in cohorts of 3-12 animals. Each group consisted of 7 to 8 animals. Animals were trained in the place learning protocol because of the changing starting point but fixed platform position. As a result, the animals were able to find the constant position of the platform from both starting points (North and South). This learning type uses the hippocampal-dependent place learning.
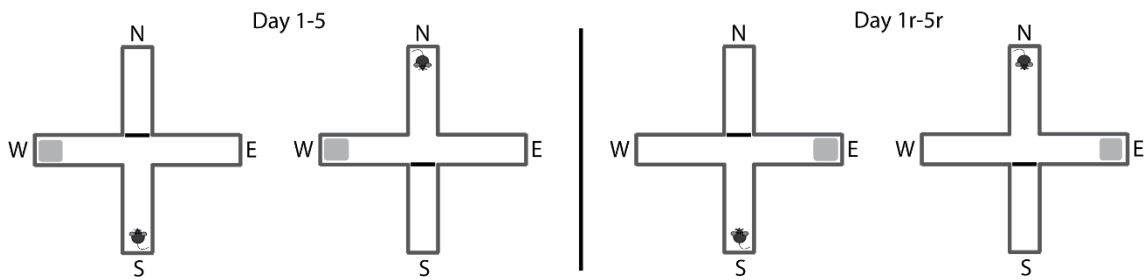
Figure 3.6: Water Cross Maze behavior experiment. The experimental setting consisted of a cross while the four arms labeled North (N), East (E), South (S), and West (W) in a clockwise direction. It was filled with water and a platform was hidden 1 cm below the water surface. A flexible barrier in the northern or southern arm transformed the cross into a T-shaped maze. Week 1 (day 1-5) was the learning week, and week 2 (day 1r-5r) was called the relearning week, in which the platform position was changed.

The learning efficiency was measured by four parameters: Latency, accuracy, wrong platform visits, and the accurate learner criterion. The latency was defined as the time the animal needed to find and climb on the platform. It was calculated as arithmetic mean of all six trials a day of each animal. If the animal was not able to locate the platform within 45 seconds, the value of 46 seconds was set into datasheet. The entrance of the animal into an arm was scored by the experimenter: It was assessed as entranced if the animal was within the arm with head and shoulders. Also, the latency was a parameter to reveal possible motor skill limitation, also possibly provoked by stereotactic injection. A trial was scored as accurate (value 1) if the animal immediately chose the arm with the platform and climbed on it. Different behavior such as turning around or swimming into the wrong arm was scored as non-accurate (value 0). The accuracy was defined as percentage of accurate trials on each day per animal. An accurate learner was defined as an animal with more than 83% accurate trials per day (i.e., ≥ 5 out of 6 trials). The wrong platform visits were counted when the animal entered the wrong arm with head and shoulder or made a turn in the start arm in the second half.

3.9.2 Object recognition test

The object recognition test (ORT) is based on the innate preference of rodents to explore an unfamiliar object rather than a familiar one. Therefore, a rodent with intact memory spends more time exploring the novel object (Leger, Quiedeville et al. 2013). The ORT performed was used to assess long-term memory (ltm) for objects (Clark and Martin 2005, Antunes and Biala 2012). The animals were between 10 and 14 weeks old.

The experiments were conducted in a clear plastic experimental chamber (22 cm x 38 cm x 15 cm) without embedding (see Figure 3.7A). The surrounding

was shielded with black curtain to avoid spatial cues and therefore avoid an influence of hippocampal spatial learning for the animal in this experiment (Mumby 2001). The objects used in this experiment have similar sizes and are produced of stainless steel (no odor, disinfectable) and the weight of the objects are such that mice cannot move them. Animals are able to climb on these objects (see in Figure 3.7B). For analyzing the time of object interaction for stereotactic injected animals the behavior experiment was performed at the beginning of the daily light cycle (8 am), so animals are still active. After minimum 30 minutes habituation time in the experimental room, the animal was allowed 5 minutes of habituation to the experimental chamber without any objects. The test consists of two phases, the familiarization phase and the test phase. The familiarization phase consists of 5 minutes exploration time, while the animal was explored two identical objects (cones) placed in the middle of the experimental chamber.
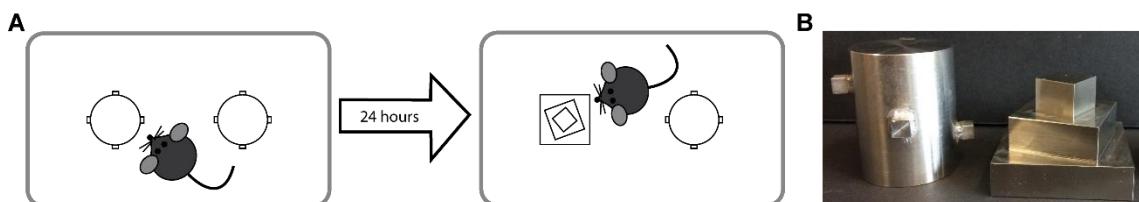
Figure 3.7: The object recognition test. (**A**) Experimental design of the object recognition test. After 5 minutes familiarization phase with two identical objects (cones) the test phase was performed with a familiar object (cone) and a new object (pyramid). **(B)** A photograph of the two objects for the object recognition test: cone (left) and pyramid (right). The objects were manufactured of stainless steel.

Afterwards, the animal was returned to its housing cage. The test phase was performed 24 hours later (long-term memory). After habituation periods similar to the day before, the test phase of 5 minutes starts. In this phase, one of the two familiar objects was exchanged with an unfamiliar object (pyramid). Each phase was video recorded and scored using an automated video-tracking system (TSE System) for time exploring and number of visits the objects in both phases.

In addition, the recordings from the object exploration test was reanalyzed by the TSA Software for a center-border-ratio. Here the percentage of time the animal was at the border of the cage compared to the center of the cage was calculated. Animals with anxiety spent more time at the border of the cage.

3.9.3 Social recognition test

For social interactions in rodent colonies social recognition is very important. The social recognition test (SRT) is similar to the ORT based on the innate preference of rodents to be more interested in unknown conspecifics than in familiar ones.

Therefore, a rodent with normal memory spends more time interacting with an unknown conspecific than with a familiar one.

The SRT performed was used to assess short- and long-term memory for juvenile conspecifics. The experiments were conducted in a clear plastic experimental chamber (22 cm x 38 cm x 15 cm) with usual amount of bedding. The social partners were juvenile male mice of 5 to 9 weeks of age. To prevent fighting between the animals a small wire enclosure was used to protect juvenile mice. For analyzing the time of social interaction for stereotactic injected animals the behavior experiment was performed at the beginning of the light cycle (8 am), so animals were still active. After minimum 30 minutes habituation time in the experimental room, the animals have 10-15 minutes of habituation to the experimental chamber (see Figure 3.8) (Stephanie A. Jacobs 2016).
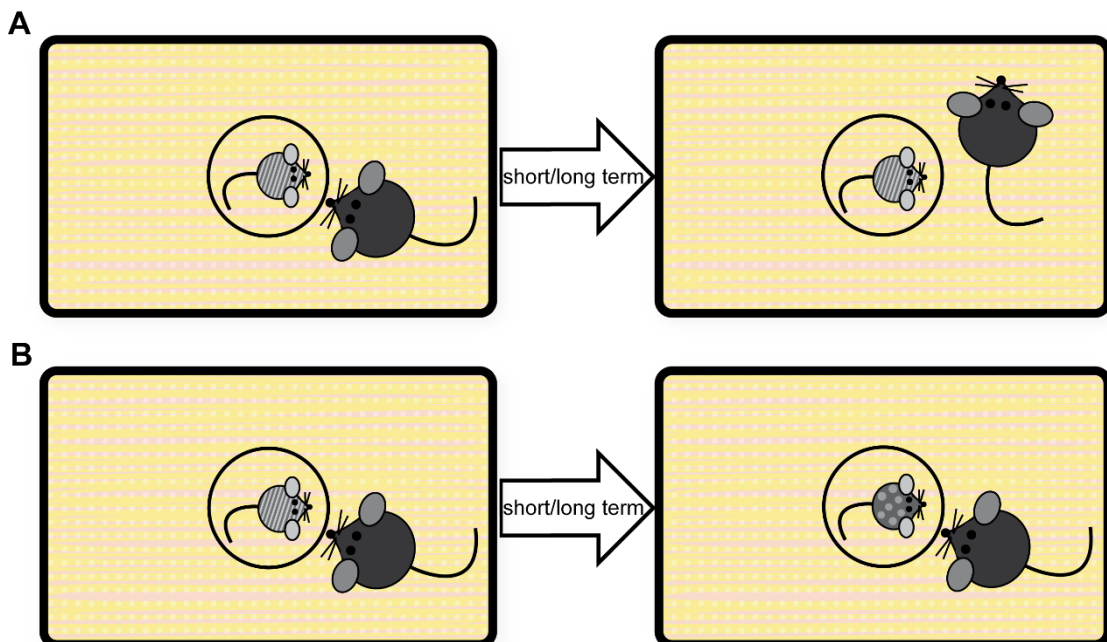
Figure 3.8: Experimental design of the social recognition test. After training phase with social partner (left) the recall phase was performed with the same (**A**) or unknown partner (**B**) after short- or long-term.

The test consists of three phases: the training phase, the recall phase for short-term memory (stm), and the recall phase for long-term memory. The training phase consists of 5 minutes of social interaction in the enclosure placed in the middle of the experimental chamber. Both animals were returned their home cages. The recall phase for short-term memory was performed 45-70 minutes after the training phase. Here the animals were habituated for 15 minutes to the experimental chamber followed by 5 minutes social interaction with the same social partner (see Figure 3.8A) or a new social partner (see Figure 3.8B). The recall

phase for long-term memory takes place 24 hours later. After 15 minutes habitu-ation, 5 minutes social interaction time with the known social partner or com-pletely unknown social partner starts. Afterwards, the animal was transferred to its home cage. Each phase was video recorded by TSE Systems and scored manually by the experimenter for the time of interactions with the social partner. Only the first 2.5 minutes were analyzed (Golden, Covington et al. 2011, Ayash, Schmitt et al. 2020) regarding percentage of total exploration time of the objects and the number of visits. To verify the experiment, the experimental group with different social partners (see Figure 3.8B) need to show a steady or increasing time of interaction.

3.10 Statistics

The calculations and statistical analyses of the results in this thesis were per-formed with Windows Excel (Windows), Origin 2018 (OriginLab) and Prism 5 (GraphPad). Depending on the issue the two-sample t-test, one-way or two-way ANOVA test were applied. For multiple comparisons *post hoc* tests (Bonferroni's, Tukey's Multiple Comparison Test) were applied. Data are presented as mean ± S.E.M. (n = number of cells or animals) and values of $p < 0.05$ were considered significant (*$p < 0.05$, **$p < 0.01$, ***$p < 0.001$).

4 Results

4.1 A GABAergic-specific knockdown of HCN2 in the MS

A GABAergic specific knockdown of HCN2 in the MS *in vivo* was designed by using an approach consisting of a floxed HCN2 mouse strain and stereotactic injection of Cre-dependent LV particles into the MS. Consequently Cre was expressed and a MS-specific HCN knockdown occurred. By inserting the specific promoter GAD67 into the lentiviral vectors, a GABAergic specific knockdown was created. Correct injections were verified via mCherry fluorescence.

4.1.1 GAD-Cre-injected animals showed a reduced HCN2 expression

In the first part of the thesis, the role of the HCN2 channel in GABAergic neurons of the MS in the septo-hippocampal system was investigated by IHC and patch clamp experiments. Thereby, changes in the protein expression and firing pattern was investigated. Afterwards, the influence of the HCN2 on brain oscillations and learning behavior was examined.

The expression of HCN2 channels specifically in GABAergic neurons was examined with IHC experiments by staining HCN2, along with markers for GAD67 and the mCherry protein.

The expression of HCN1 and HCN4 in GAD-injected animals is shown in the following IHC figures. The co-localization of mCherry and HCN2 in control-injected animals is visible in Figure 4.1 marked with arrow heads. In control-injected animals HCN2 channels were expressed ubiquitously in the MS, here in cells expressing mCherry fluorescence and cells not expressing mCherry. HCN4 was mainly expressed in the soma, while HCN2 was expressed in the dendrites.
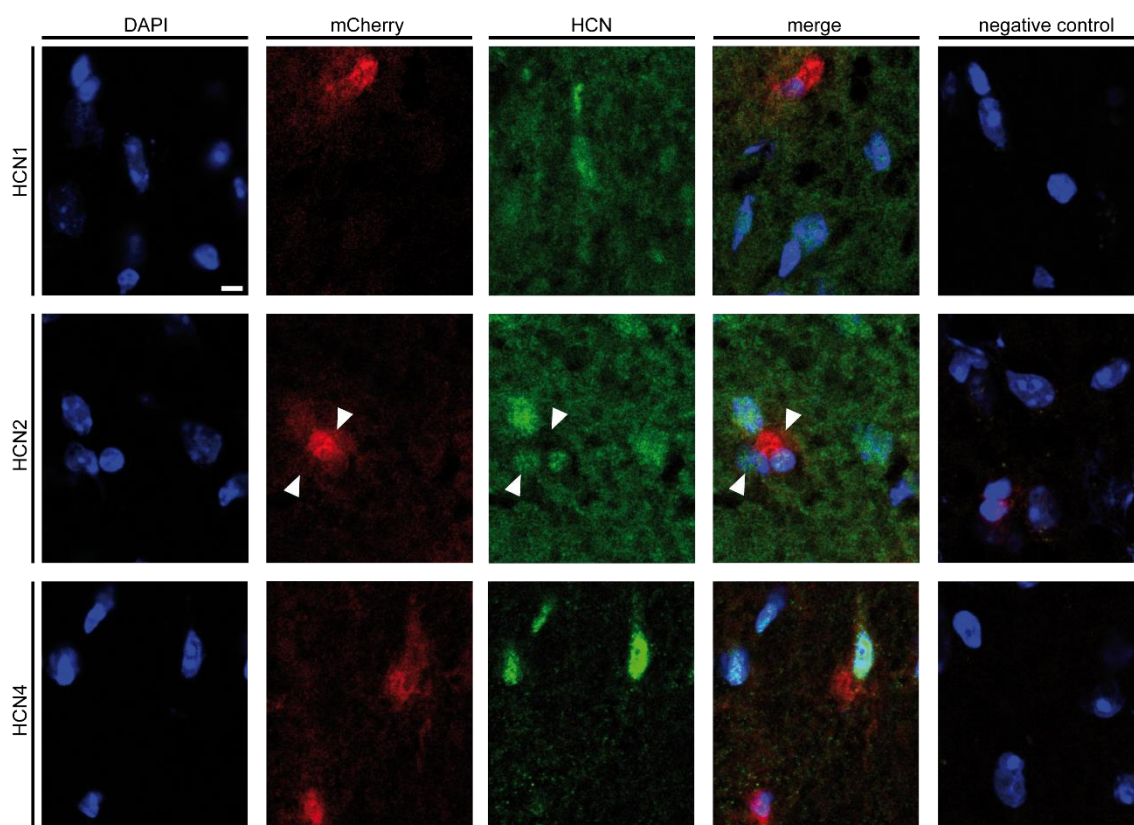
Figure 4.1: IHC of GAD-mCherry injected animals. The expression of HCN1, 2 and 4 (green) in the MS. Also stained was mCherry (red) and DAPI (blue). Arrow heads mark a mCherry and HCN2 expressing neuron. Scale bar 10 µm.

In Cre-injected animals, there was no HCN2 expression in cells expressing mCherry simultaneously (see Figure 4.2 middle row, marked with arrow heads). The cellular distribution of HCN1 and HCN4 was comparable with control-injected animals.
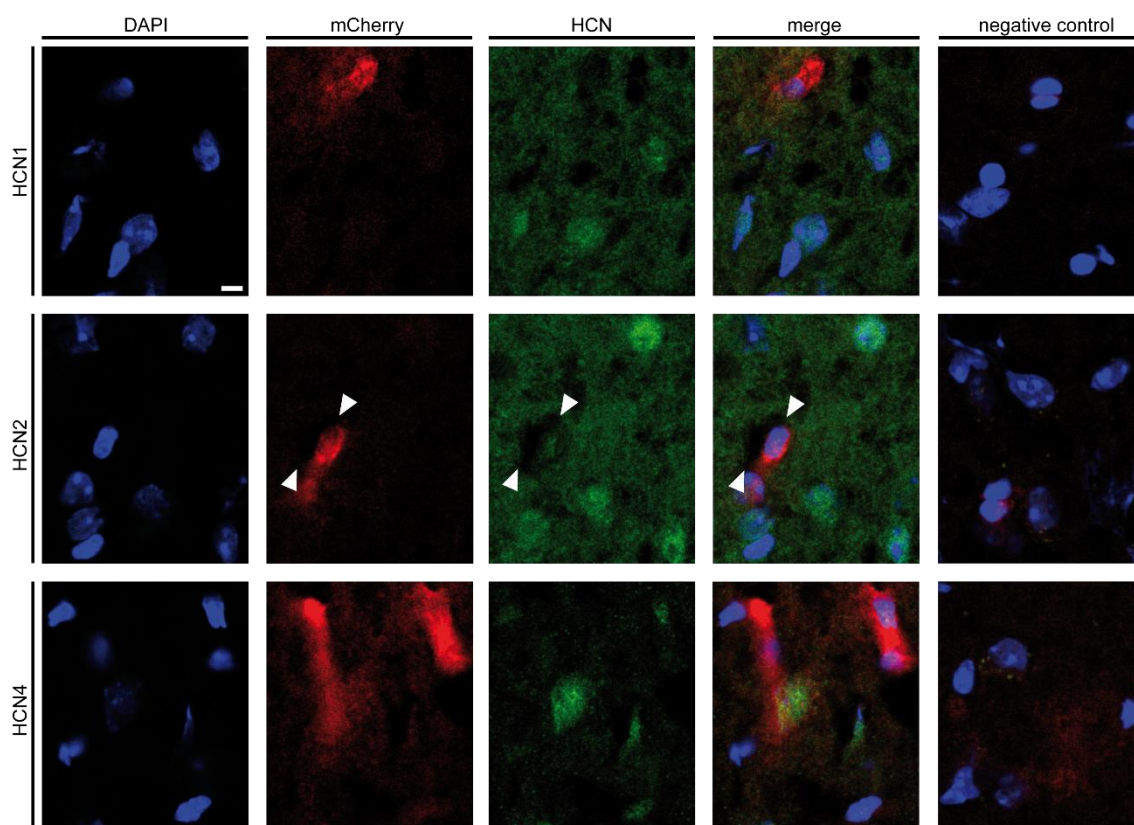
Figure 4.2: IHC of GAD-Cre-mCherry injected animals. The expression of HCN1, 2 and 4 (green) in the MS was stained in combination with mCherry (red) and DAPI (blue). Arrow heads mark a mCherry but no HCN2 expressing neuron. Scale bar 10 µm.

To check the specificity of the GAD67 promoter, the co-localization of GAD67 and mCherry was examined (see Figure 4.3). The co-localization of mCherry and GAD67 was visible by yellow color in the merged image.
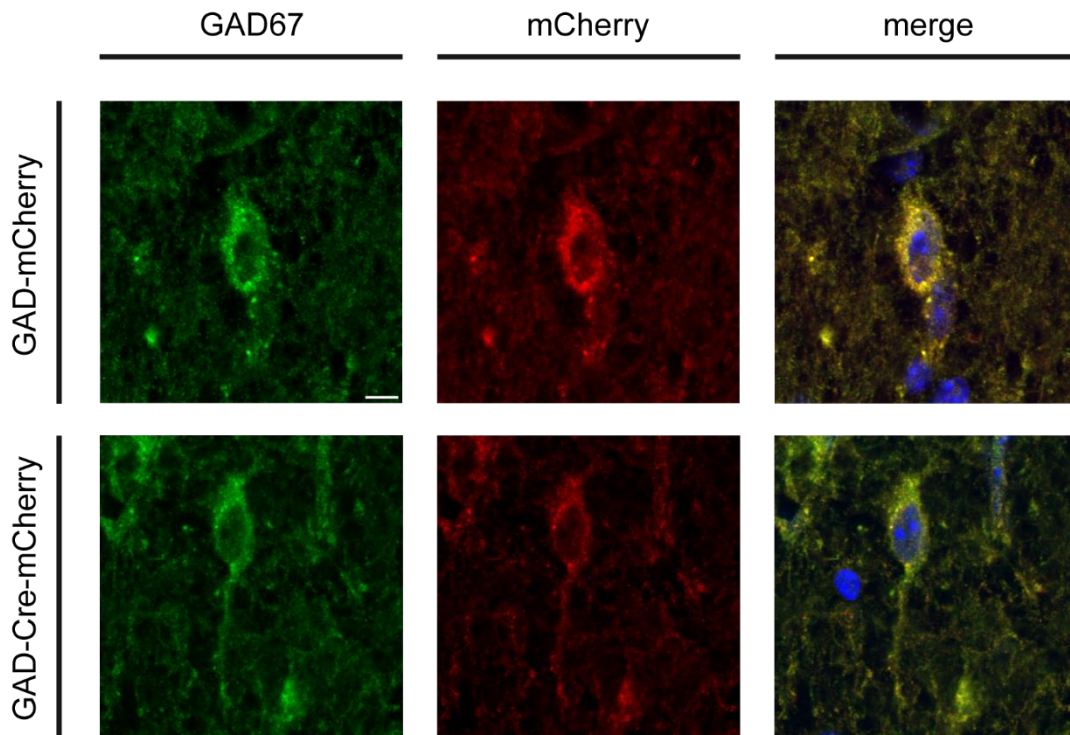
Figure 4.3: IHC of the co-localization of mCherry and GAD67. The co-localization of GAD67 signal (green) and mCherry signal (red) is shown in the merged image by yellow color. Scale bar 5 μm.

4.1.2   The I_h was reduced in GAD-Cre-injected animals in the MS

GAD-injected animals were used in patch clamp experiments to validate the successful deletion of HCN2 in the GABAergic neurons in the MS. Additionally, the influence of HCN2 deletion in GABAergic neurons of the MS on electrophysiological properties was examined. Specifically, the contribution of HCN2 in GABAergic neurons of the MS on the properties of I_h were examined. Therefore, whole-cell current and voltage-clamp measurements in GABAergic MS neurons of acute brain slices from control and Cre-injected animals were undertaken. Patch clamp protocols are described in section 3.6.3.

Neuronal cells of the MS showed three different firing modes, fast-, slow-, and burst-firing. Representing traces of the three different firing types were shown in Figure 4.4.
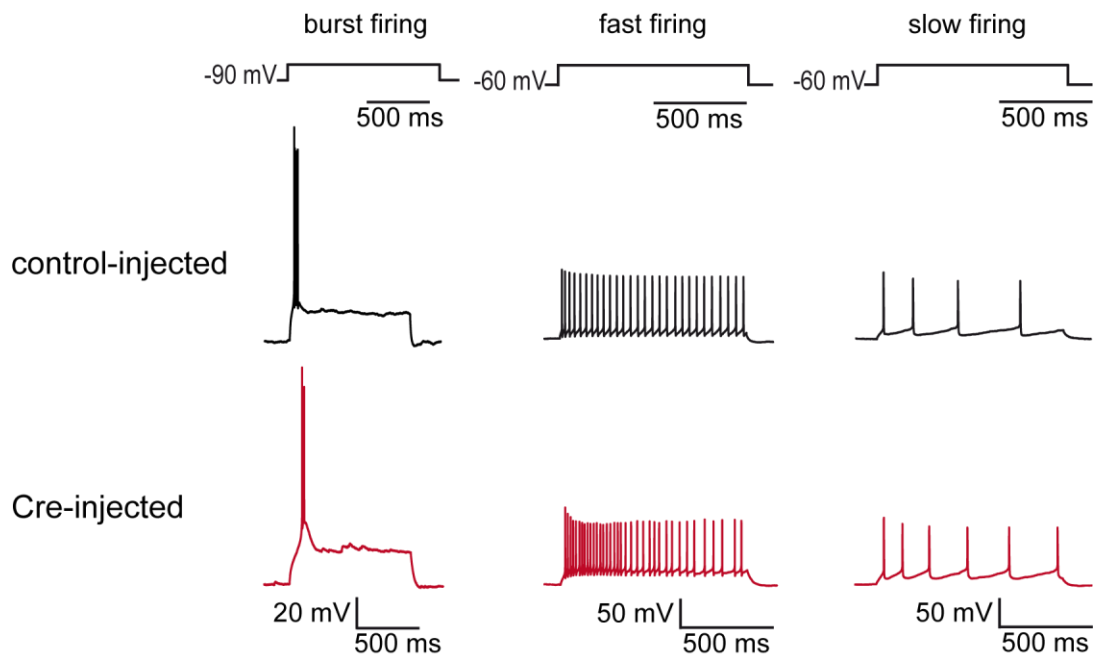
Figure 4.4: Representative traces of different firing types of MS neurons. Burst-, fast-, and slow-firing cells of control-injected (black) and Cre-injected (red) mice. These representative traces were recorded in neurons of Syn-injected mice.

The distribution of the three firing types of GABAergic neurons was different between control and Cre-injected animals (see Figure 4.5A). While in control-injected animals, most cells were fast-firing cells (63.16 %), in Cre-injected animals the prevalence of fast-firing was reduced (42.11 %) and burst-firing cells was increased (from 15.79 % to 36.84 %). In control neurons, burst-firing cells were quite rare, while in Cre-expressing burst-firing neurons were more frequent. In Cre-expressing neurons slow-firing cells were rarer than burst-firing cells. Representative I_h traces were shown in Figure 4.5B, here the I_h of Cre-expressing neurons (red) is abolished compared to control (black). The I_h current could be measured in 20 of 37 cells, thereby the number of cells exhibiting I_h was reduced in fast and burst-firing Cre-expressing neurons and was not altered in Cre-injected animals in slow-firing neurons (see Figure 4.5C).
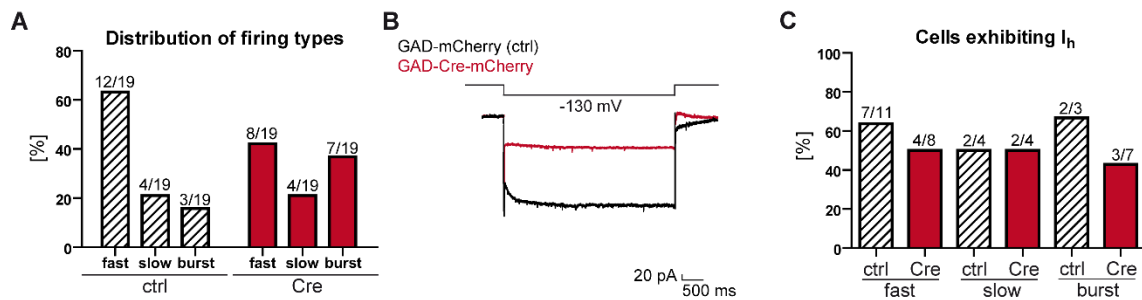
Figure 4.5: Patch clamp experiments in GAD-injected HCN2L2 mice showed changes in the distribution of firing types. (**A**) The distribution of firing types was different in control- and Cre-injected animals. Most of the cells of control-injected animals were fast-firing cells (63.16%), whereas only 42.11% of the cells of the Cre-injected animals were fast-firing cells. Slow-firing cells were unaltered by Cre-injection (21.05%). Burst-firing cells were more frequent in Cre-injected animals (36.84%) than in control animals (15.78%). (**B**) Representative I_h traces with protocol from neurons of the MS of GAD-mCherry injected mice (black) and GAD-Cre-mCherry injected mice (red). The representative Cre-expressing cells showed no I_h. (**C**) The number of cells exhibiting I_h was reduced in fast-firing and burst-firing cells but not altered in slow-firing cells. In collaboration with Dr. Hristo Varbanov (Hannover Medical School, Germany).

In Figure 4.6A representative traces of the sag and the corresponding protocol was shown. The black traces showed the control trace with a large sag, while the red trace (Cre) showed only a small or even no sag. The sag amplitude in fast-firing cells was significantly reduced in Cre-injected animals, but not in slow and burst-firing cells (Figure 4.6B). Cell properties like the RMP, did not show significant differences between control and Cre-injected animals in fast-, slow-, and burst-firing neurons (Figure 4.6C). The number of cells exhibiting rebound spikes are reduced in Cre-injected animals in fast- and burst-firing neurons and even abolished in slow-firing neurons (see Figure 4.6D).
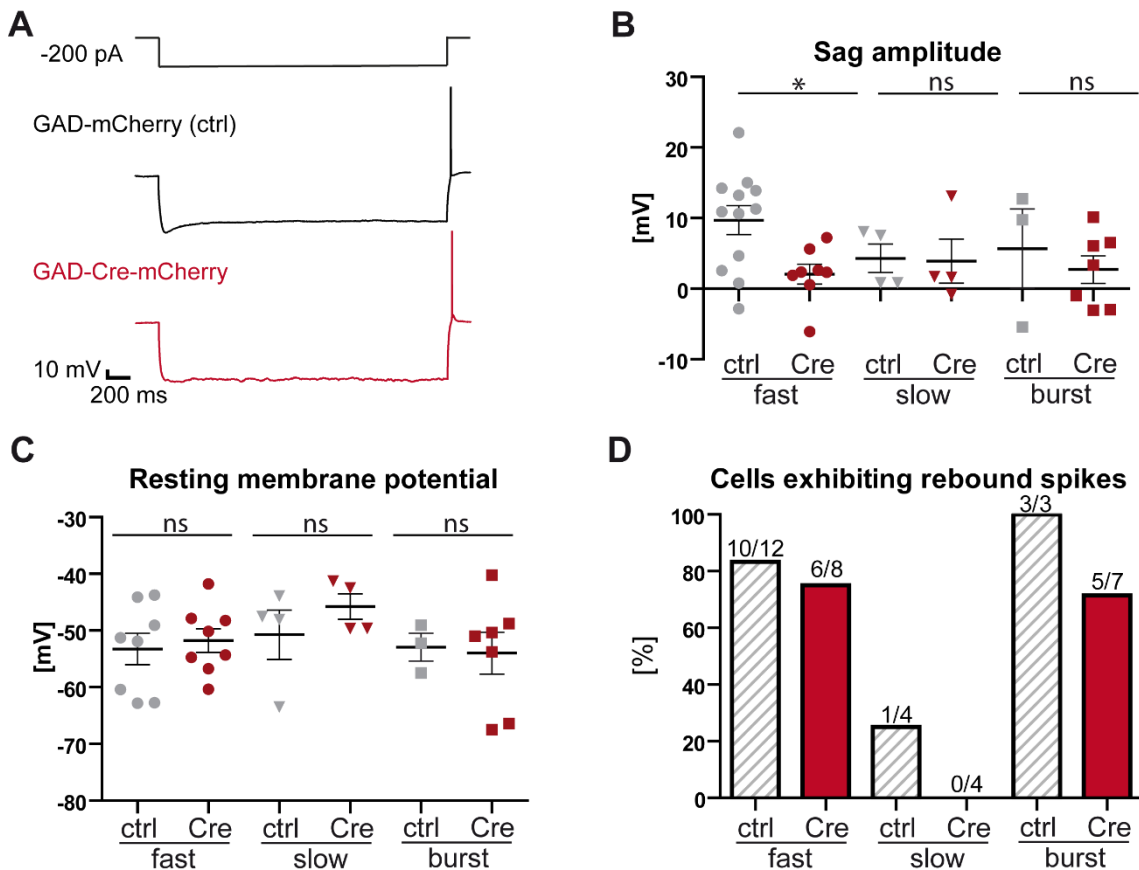
Figure 4.6: Patch clamp experiments in GAD-injected HCN2L2 mice showed a reduced number of cells exhibiting rebound spikes. (**A**) Representative sag traces with protocol from neurons of the MS of GAD-mCherry injected mice (black) and GAD-Cre-mCherry injected mice (red). The representative Cre-injected cell showed nearly no sag compared to control cells. (**B**) The sag amplitude in fast-firing cells was significantly reduced in Cre-injected animals ($p = 0.0128$), but not in slow and burst-firing cells. (**C**) The RMP was not significant different between GAD-Cre-mCherry and GAD-mCherry ($p > 0.05$). (**D**) Also the number of cells exhibiting rebound spikes and the cells exhibiting I_h was reduced in all firing types. Statistical analyses were done by unpaired t-test. In collaboration with Dr. Hristo Varbanov (Hannover Medical School, Germany).

4.1.3 The EEG of GAD-Cre-injected animals showed reduced theta rhythm

Analyzing the EEG recordings from GAD-Cre-mCherry, GAD-mCherry injected, and uninjected HCN2L2 animals served to investigate whether the knockdown of HCN2 in GABAergic neurons of the MS shows effects on EEG in mice. In Figure 4.7, representative EEG traces of the three vigilance states NREM sleep, wake, and REM sleep were shown from Cre- and control-injected animals. Raw EEG traces looked normal and did not show any signs of epileptiform activity in GAD-Cre- and control-injected animals.
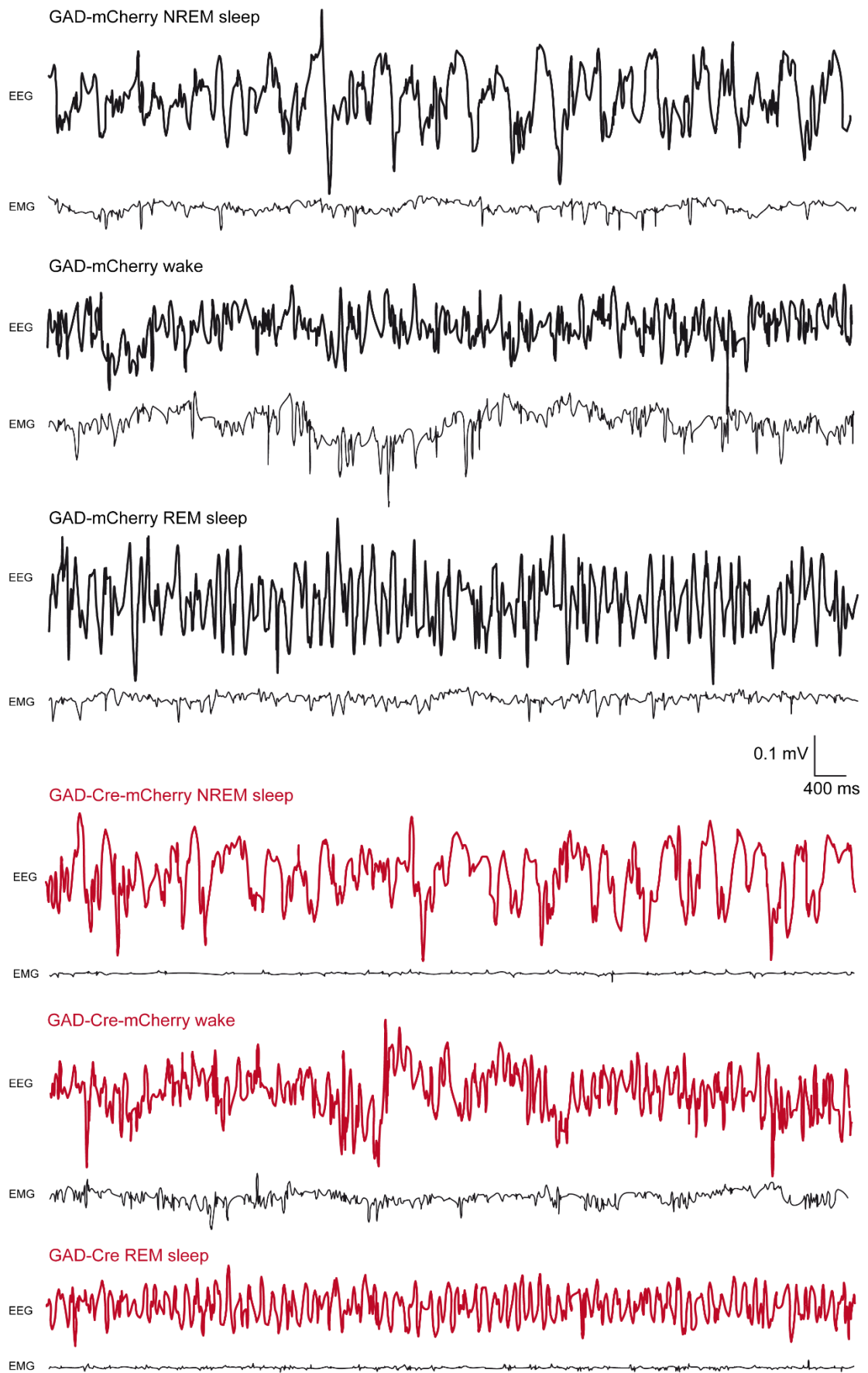
Figure 4.7: Representative EEG traces of GAD-mCherry and GAD-Cre-mCherry injected animals. Traces of GAD-mCherry (black) and GAD-Cre-mCherry (red) looked normal in NREM sleep, wake, and REM sleep.

In Figure 4.8 the EEG signal power of the frequency from 0 to 25 Hz was analyzed in the three vigilance stages. There was no significant differences in the power of NREM sleep analyses between Cre- and control-injected animals (see Figure 4.8A). Between Cre-injected animals and uninjected HCN2L2 there was a significant difference in the power of NREM sleep at frequency 1 Hz and 1.5 Hz (not indicated in data). Analysis of REM sleep power showed significant reduction in frequency values of 5 Hz, 7 Hz, and 7.5 Hz between Cre- and control-injected animals (see Figure 4.8B). Between Cre-injected animals and uninjected HCN2L2 there was also a significant difference in the power of REM sleep at frequency 5.5 Hz, 6 Hz, 7 Hz, and 7.5 Hz (data not shown). In the analysis of the wake state of mice showed a significant difference in general and more in detail at frequency values of 0 Hz and 0.5 Hz (data not shown) (see Figure 4.8C).
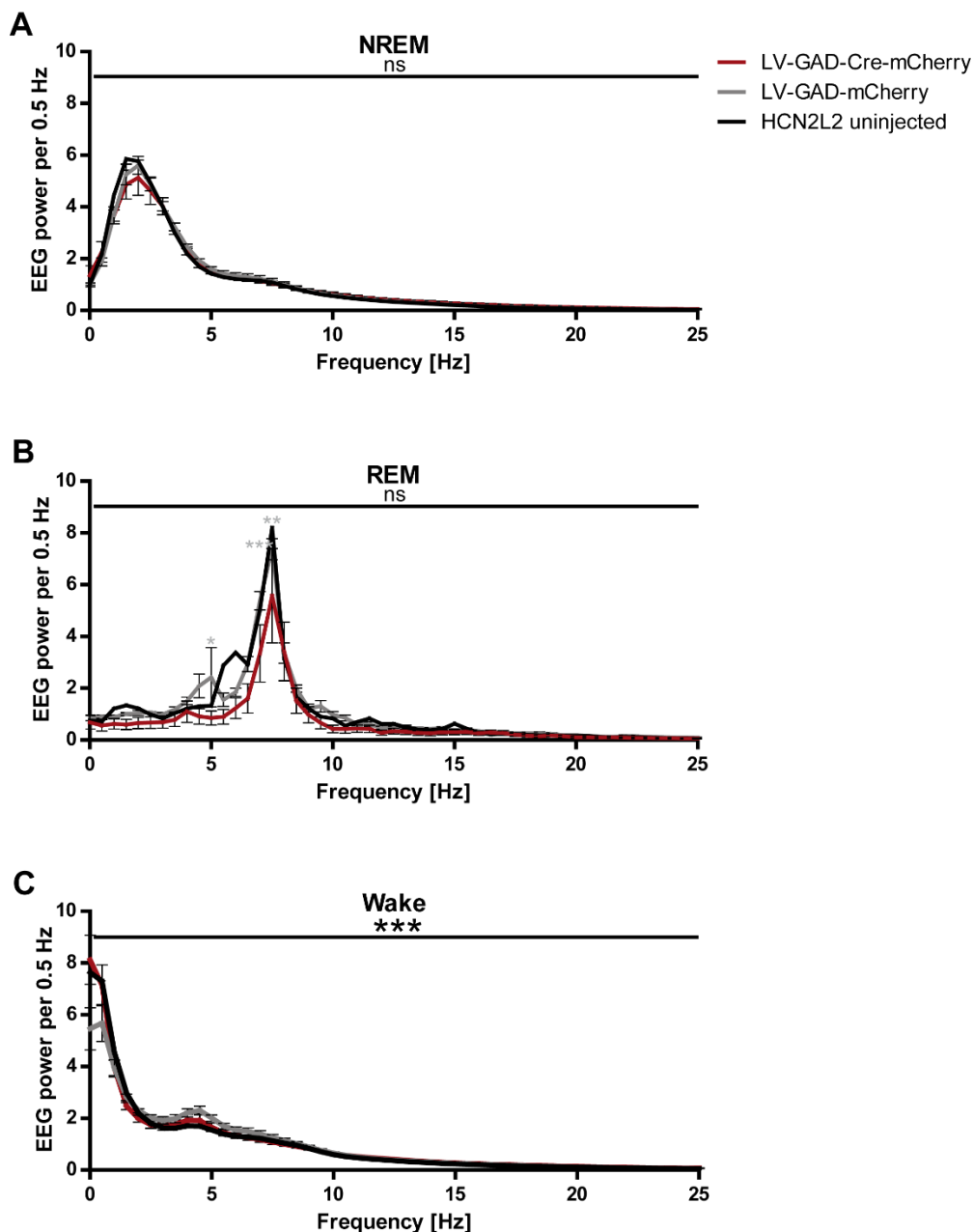
Figure 4.8: Hippocampal EEG measurements of GAD-Cre-mCherry and GAD-mCherry injected animals. (**A**) EEG power spectra of NREM sleep did not show significant differences between GAD-Cre-mCherry (red, n = 6), GAD-mCherry (grey, n = 6) injected, and uninjected (black, n = 5) HCN2L2 animals. Between Cre-injected animals and uninjected HCN2L2 a significant difference in NREM sleep in the Bonferroni's post hoc test (grey stars) at frequency 1 Hz (**p < 0.001) and 1.5 Hz (***p < 0.001) (not indicated in data) was calculated. (**B**) REM sleep EEG power spectrum was not significant in the two-way ANOVA, but Bonferroni's post hoc test (grey stars) showed significant differences at frequency values of 5 Hz (*p < 0.05), 7 Hz (***p < 0.001), and 7.5 Hz (**p < 0.01) between Cre- and control-injected animals. Between Cre- and uninjected HCN2L2 there is a significant difference in Bonferroni's post hoc test at frequency 5.5 Hz (**p < 0.01), 6 Hz (***p < 0.001), 7 Hz (*p < 0.05), and 7.5 Hz (***p < 0.001) (not indicated in data). (**C**) In wake state the two-way ANOVA showed a significant difference (***p < 0.001) and also the Bonferroni's post hoc test at frequency 0 Hz and 0.5 Hz (***p < 0.001) between the Cre- and control-injected animals (not indicated in data). Statistical analyses were done by two-way ANOVA test and Bonferroni's post hoc test.

Because of the differences in REM sleep shown in Figure 4.8B, analysis of REM sleep was done on the number of REM periods, the total time in sleep, the area under the curve (AUC), and the REM mean value (see Figure 4.9A-D). All parameters did not show significant differences GAD-Cre-mCherry and GAD-mCherry injected animals.
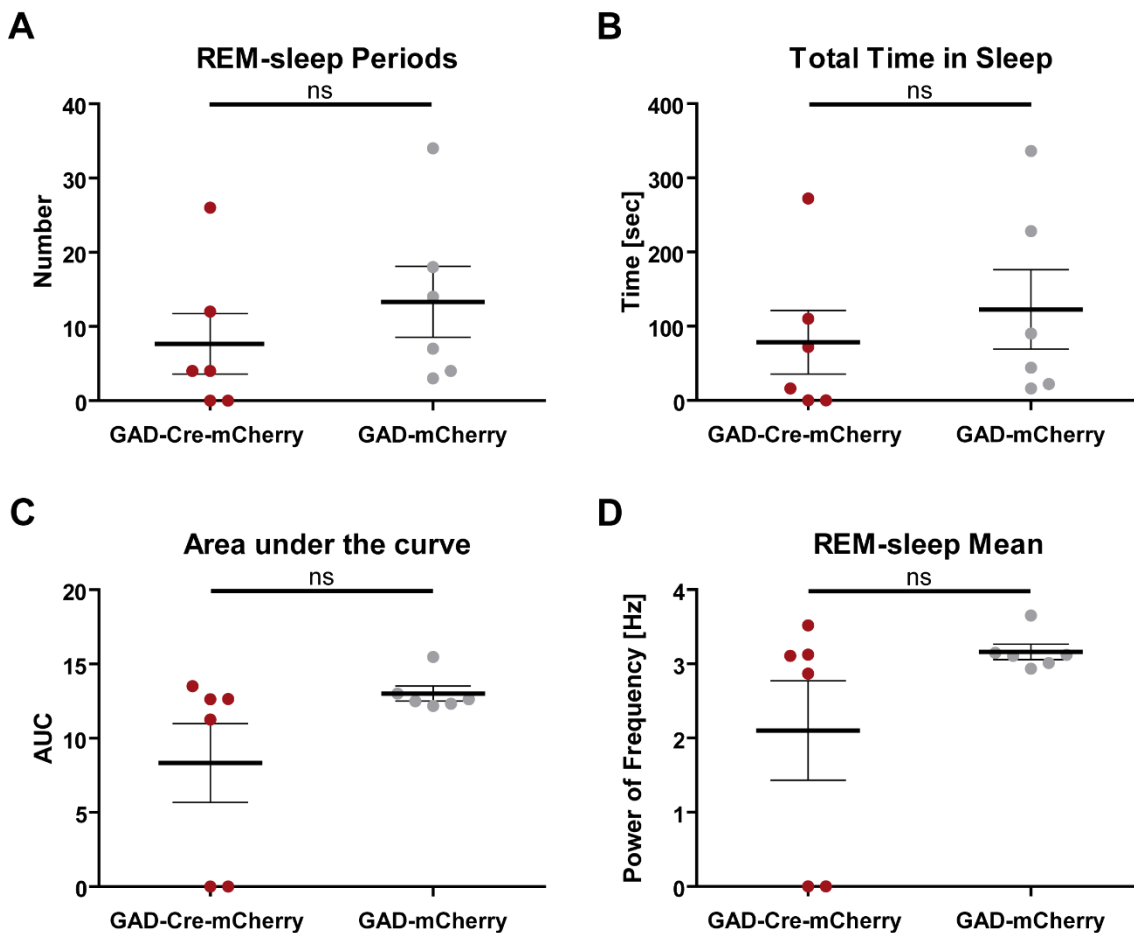
Figure 4.9: REM sleep analysis of GAD-Cre-mCherry and GAD-mCherry injected animals. (**A**) Sleep analysis of EEG measurements of Gad-mCherry (grey) and GAD-Cre-mCherry (red) showed no significant differences in the number of REM sleep periods (p = 0.3880). (**B**) Also the total time in sleep (p = 0.5311) was not significantly different between Cre and control group. (**C, D**) The area under the curve (AUC, p = 0.1136) and the REM mean (p = 0.1492) did also not show significant differences between the respective group in the unpaired two-tailed t-test.

Further analyses of a representative single REM sleep episode demonstrated the differences of GAD-mCherry and GAD-Cre-mCherry injected animals as already seen in Figure 4.8B. The power of theta frequency while REM sleep was reduced in Cre-injected animals compared to control-injected animals. This was shown in the heat map by different colors, while yellow indicates a high power of corresponding frequency. Yellow bars above indicated REM sleep episodes (see Figure 4.10A,B).
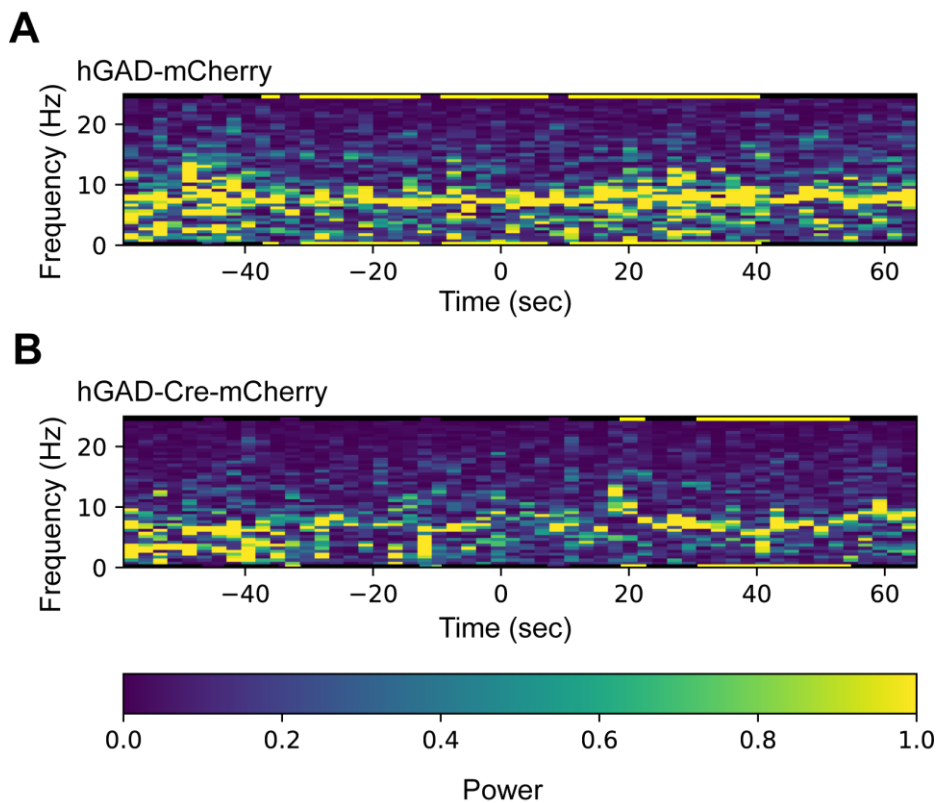
Figure 4.10: Representative REM sleep episodes in GAD-injected animals. A heat map was used to depict REM sleep episodes during NREM sleep. Yellow bars above indicate REM sleep episodes. (**A**) REM sleep in control-injected animals shows a high power at theta frequency (indicated by yellow color). (**B**) The power of theta frequency was not as prominent as in the control episode.

4.1.4 Hippocampal-dependent behavior was not impaired in GAD-Cre-injected animals

The WCM experiment was performed to clarify the effect if the deletion of HCN2 in GABAergic neurons in the MS had any effect on the hippocampus-dependent behavior. The animals used were uninjected HCN2L2 or injected with either LV-GAD-Cre-mCherry or LV-GAD-mCherry with an age between 10 and 11 weeks. The groups were compared in terms of four parameters: The latency [sec] indicates the time necessary for the animal to climb onto the platform. The accuracy [%] expresses the percentage of accurate trials per day. The number of wrong platform visits [#] was defined as the swimming into any direction, which is not straight to the platform. The accurate learners [%] were mice that accomplished ≥ 83% of accurate trials per day. The behavioral performance of week 1 (day 1-5) and week 2 (day 1r-5r) were analyzed separately.

Both groups showed no difference regarding the latency, accuracy, number of wrong platform visits, and the number of animals reaching the accurate learners criterion in the first and second week of the experiment (see Figure 4.11A-D).
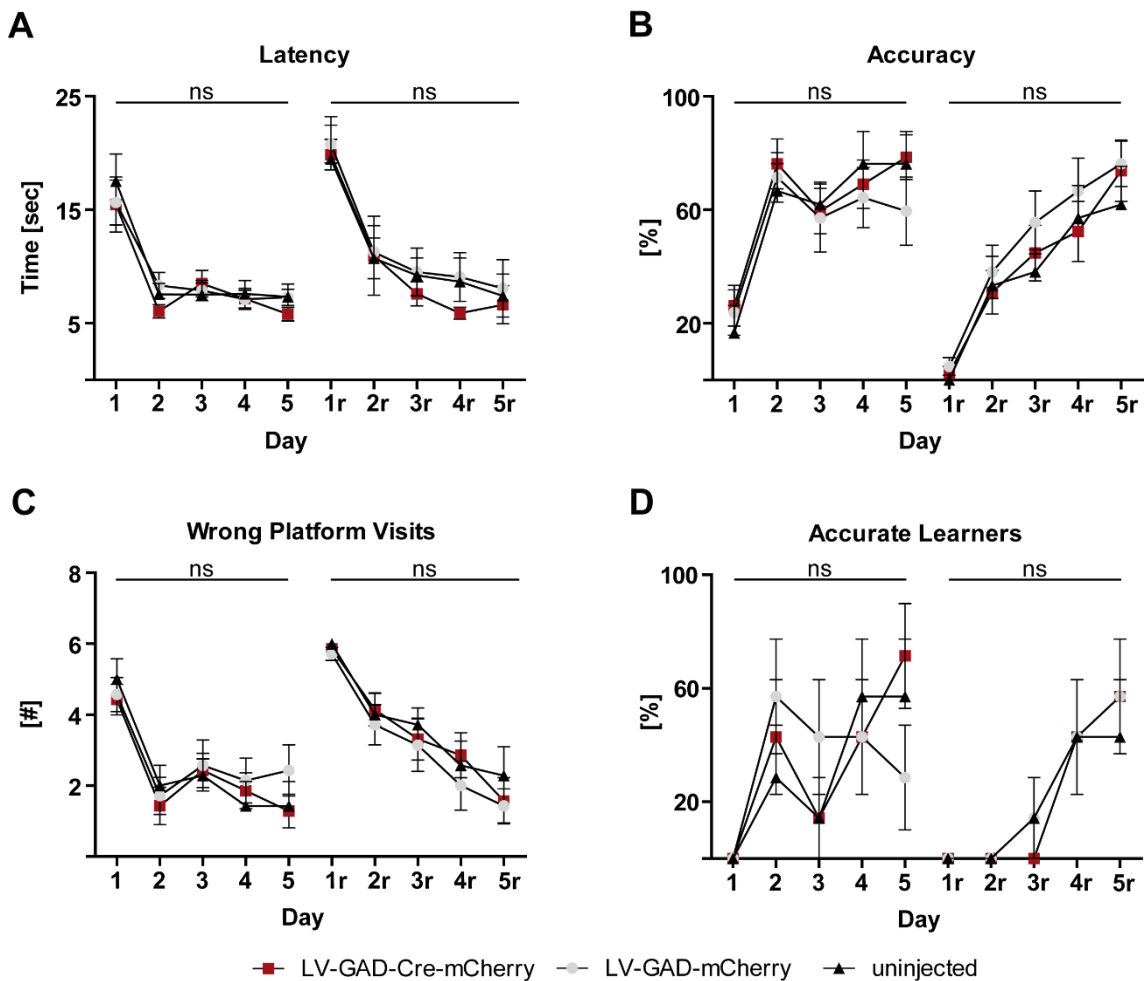
Figure 4.11: WCM of LV-GAD-injected mice showed no deficits in reversal learning in Cre-injected mice compared to control-injected mice. Learning curve of LV-GAD-mCherry (grey, n = 7), LV-GAD-Cre-mCherry (red, n = 7) injected mice and uninjected HCN2L2 mice (black, n = 7) did not show significant differences. (**A-D**) In the first week (learning week, day 1-5) all animals performed in the spatial learning equally in all four learning parameter. In the second week (relearning, day 1r-5r) the three groups underwent reversal learning with no significant differences in learning behavior. Statistical analyses were done by two-way ANOVA and Bonferroni's post hoc test.

4.1.5 Object and social recognition tests were influenced by GAD-Cre-injection

To examine a possible connection between the HCN2 expression in the MS GABAergic neurons and the object and social recognition, ORT and SRT behavioral experiments were performed.

For the ORT, the groups were compared in terms of number of visits of the novel object. The control group showed a significant higher number of visits of the novel object 2 compared to the already known object 1, indicating a correct test setup and implementation of the ORT. The GAD-Cre-mCherry injected animals did not

show a significant difference in number of visits between object 1 and object 2 (see Figure 4.12, red).
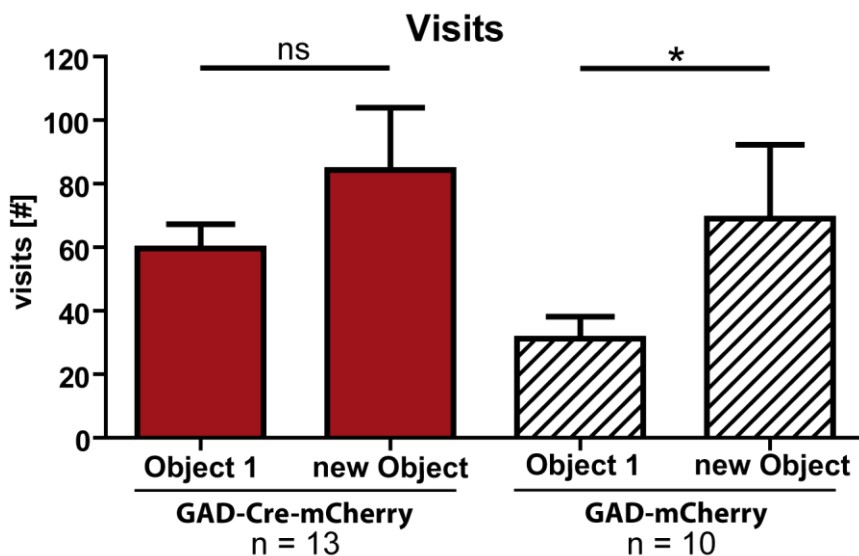
Figure 4.12: Object recognition was impaired by LV-GAD-Cre-injected mice. Control injected animals did show a significant higher number of visits of the novel object 2 compare to object 1 (*p = 0.0392). GAD-Cre-mCherry injected animals (red) did not show a significant difference in number of visits of the two objects (*p = 0.1618). Statistical analyses were done by unpaired t-test.

With the data of the object recognition test a reanalysis was possible with the TSE Software to investigate the fear condition of GAD-injected animals with a center-border-analysis. There was no significant difference calculated in speed while exploring time (see Figure 4.13A), the percentage of time spent at the border of the environment (see Figure 4.13B), and in the time spent in the center of the environment (see Figure 4.13C).
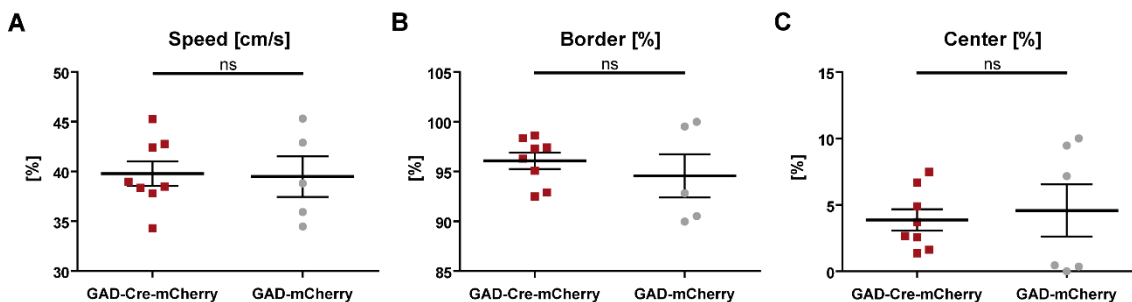
Figure 4.13: Center-border-ratio in GAD-injected animals.(**A**) The speed of GAD-Cre-injected animals while object recognition test was not significant different. (**B, C**) The percentage of time spent at the border or center area of the environment indicating the amount of fear is not significant different in GAD-injected animals. Statistical analyses were done by unpaired t-test.

The third behavior experiment performed was the social recognition test. The groups were compared in the time of contact between the two animals. The control group showed by interacting with different social partners (n = 5) no change of interaction time over all three trials, while Cre-injected animals (n = 5) decreased in the time of interaction in stm and stayed on this level in ltm (Figure 4.14A). By interacting with the same social partner, Cre-injected (n = 5) and control-injected animals (n = 4) spend less time in every trial with interacting with the social partner (see Figure 4.14B).
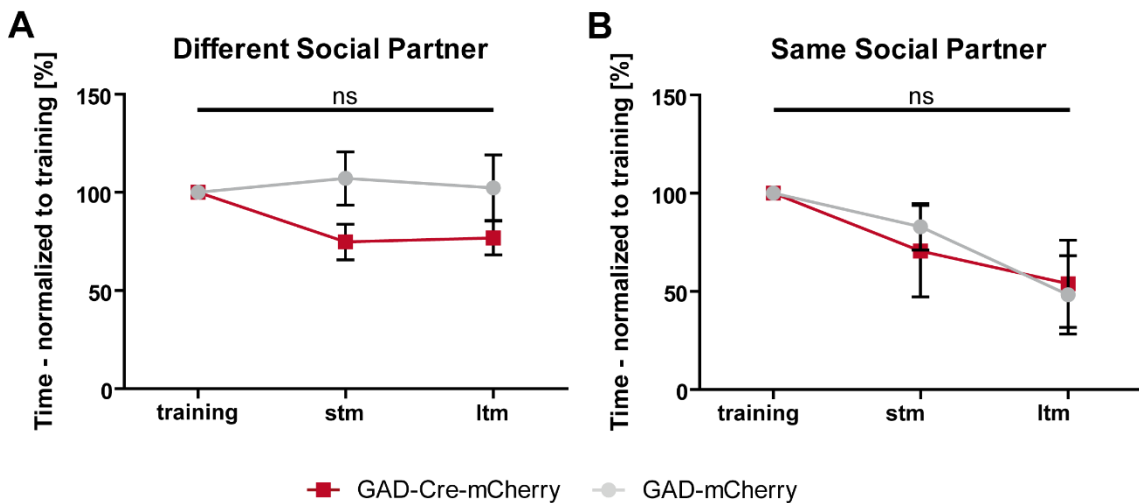
Figure 4.14: Social recognition test with LV-GAD injected mice showed no significant differences between Cre- and control-injected animals. (**A**) The normalized time of social contacts between the mouse of interest and the different social interaction partner was not significantly different between Cre- (red, n = 5) and control-injected animals (grey, n = 5). (**B**) The normalized time of social contacts between the mouse of interest and the same social interaction partner was not significant different between Cre- (red, n = 5) and control-injected (grey, n = 4). Statistical analyses were done by unpaired t-test.

4.2   A neuron-specific knockdown of HCN2 in the MS

To ensure a neuron-specific knockdown of HCN2 in the MS, lentiviral particles with the neuron-specific hSyn-promoter were produced and infused via stereotactic injection. Correct injections were verified via mCherry fluorescence.

In the second part of the thesis, the role of the HCN2 channel in all neuron types of the MS in the septo-hippocampal system was investigated in the same way as in GABAergic neurons by IHC, patch clamp experiments, EEG, and behavior experiments.

4.2.1   hSyn-Cre-injected animals showed a reduced HCN2 expression

IHC experiments revealed that HCN2 channels are broadly expressed across all neurons of the mouse MS without differentiating between different GABAergic, cholinergic, and glutamatergic neurons (see Figure 4.15 middle row). This finding nicely matched the fact that the hSyn-promoter is a pan-neuronal promoter which is activated in all neuron types. The mCherry expression indicated the transfection of the LV particle into the neuron including the successful activation of the promoter. This went in line with the expression of the Cre and mCherry proteins. Consequently, cells showing mCherry expression also expressed Cre and an HCN2 knockdown in this neuron was assumed. In Figure 4.15 a neuronal cell expressing mCherry and HCN2 was marked with arrow heads. HCN1 and HCN4 were not as ubiquitous expressed as HCN2 in the MS but rather showed a lower expression and less evenly (see Figure 4.15, upper and lower row). The HCN1 staining showed the typical expression in the soma of neurons, shown by the overlapping of the DAPI and HCN1 signal. HCN2 was more expressed in the dendrites.
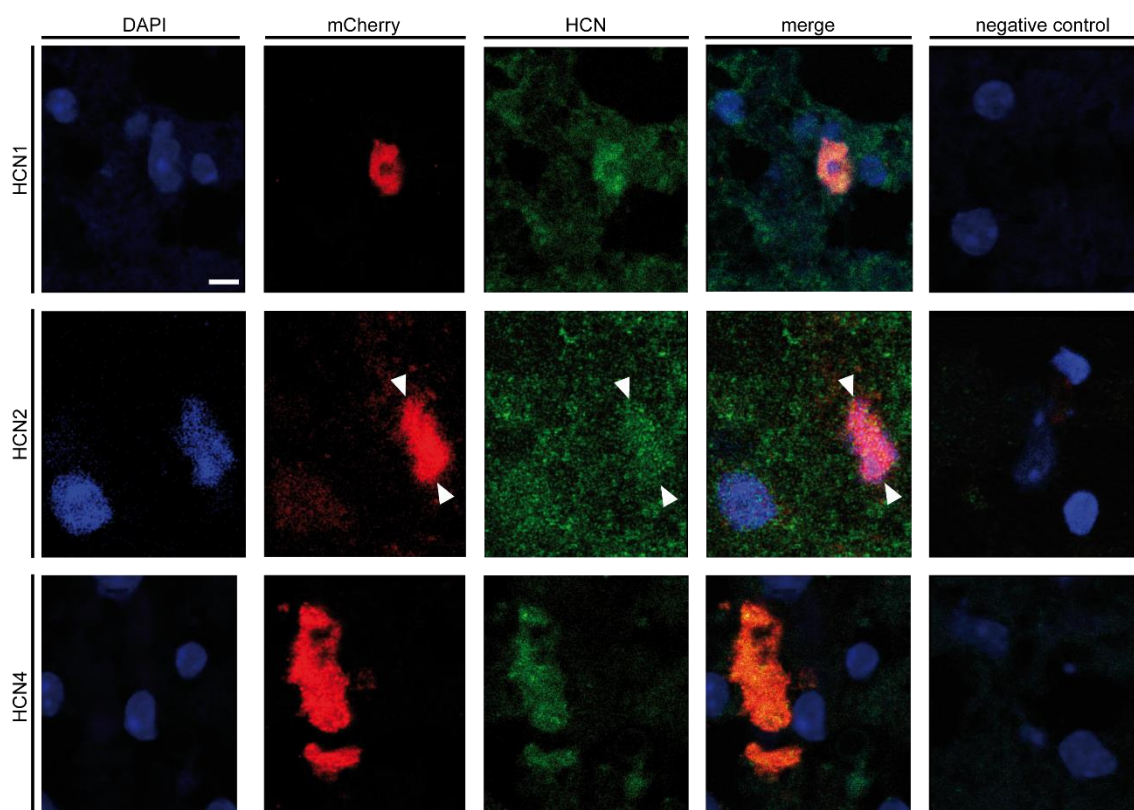
Figure 4.15: IHC of Syn-mCherry injected animals. The expression of HCN1, 2, and 4 (green) in the MS. Also stained was mCherry (red) and DAPI (blue). Arrow heads mark a mCherry and HCN2 expressing neuron. Scale bar 10 µm.

Syn-Cre-injected animals instead did not show HCN2 expression in cells expressing mCherry (see Figure 4.16, middle row marked with arrow heads). There was a little signal for HCN2 visible in cells expressing mCherry, but this was HCN2 signal from cells laying below or above the mCherry expressing cell. The distribution of HCN1 and HCN4 was not altered in Cre-injected neurons compared to control-injection.
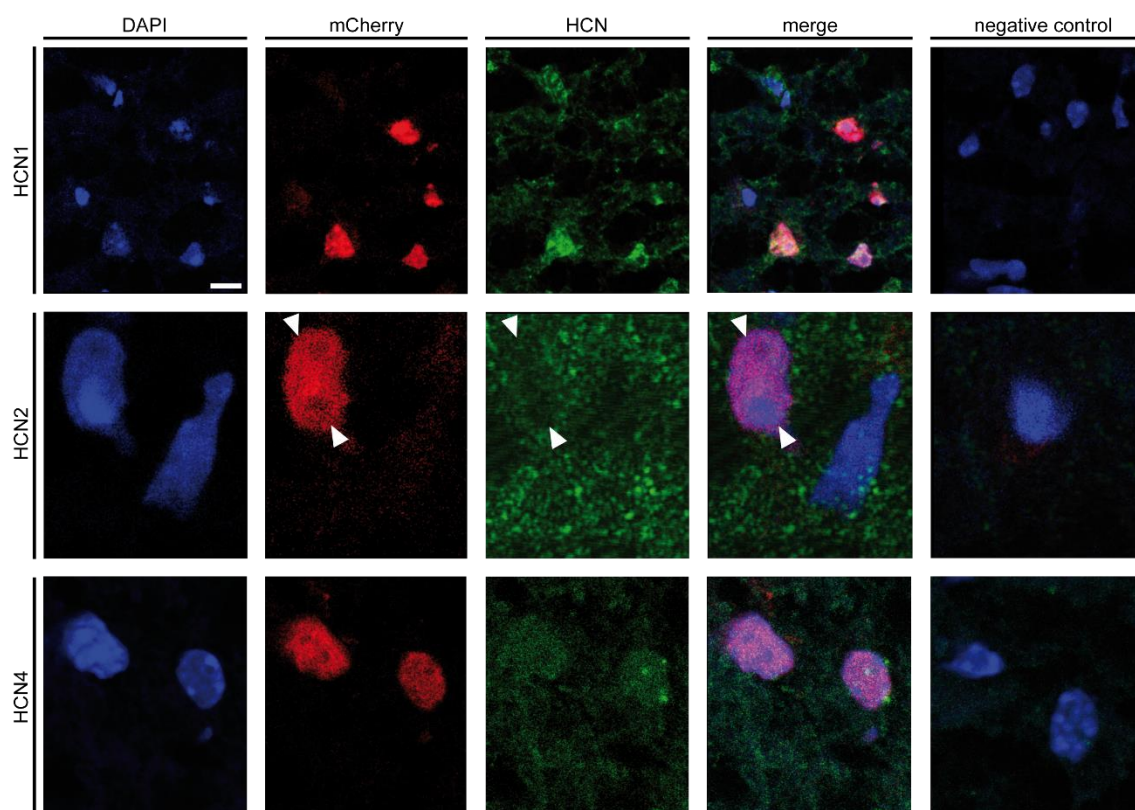
Figure 4.16: IHC of Syn-Cre-mCherry injected animals. The expression of HCN1, 2, and 4 (green) in the MS. Also stained was mCherry (red) and DAPI (blue). Arrow heads mark a mCherry, but not HCN2 expressing neuron. Scale bar 10 μm.

4.2.2 The I_h was reduced in hSyn-Cre-injected animals in the MS

As already mentioned, neurons were classified into three groups, fast-, slow-, and burst-firing MS neurons. Representing traces of the different firing types in hSyn-mCherry and hSyn-Cre-mCherry injected mice were shown in Figure 4.4.

In Figure 4.17A the distribution of these groups in control- and Cre-injected animals was shown. Fast-firing cells were occurring most in control-injected animals (57.58%) and in Cre-injected animals (66.67%). In control-injected animals, 27.28% cells were slow-firing cells, while in Cre-injected animals, 13.33% showed slow-firing characteristics. In control neurons, the burst-firing cells were rare (15.15%), while in Cre-expressing neurons occurred more burst-firing cells (20.00%) after Cre expression. Representative I_h traces were shown in Figure 4.17B of control neuron (black) and HCN2 knockdown neurons (red). I_h was totally absence (upper red trace) or the kinetic mainly driven by HCN4 resulting in slower activation kinetic (lower red trace). In MS control neurons the I_h current could be measured in 19 of 33 cells and only in 4 of 17 Cre-expressing neurons. Thereby the number of cells exhibiting I_h was reduced in fast (from 57.89% to 16.67%) and burst-firing neurons (60.00% to 40.00%) in Cre-injected animals. In slow-firing Cre-expressing cells no I_h current was measurable (see Figure 4.17C).
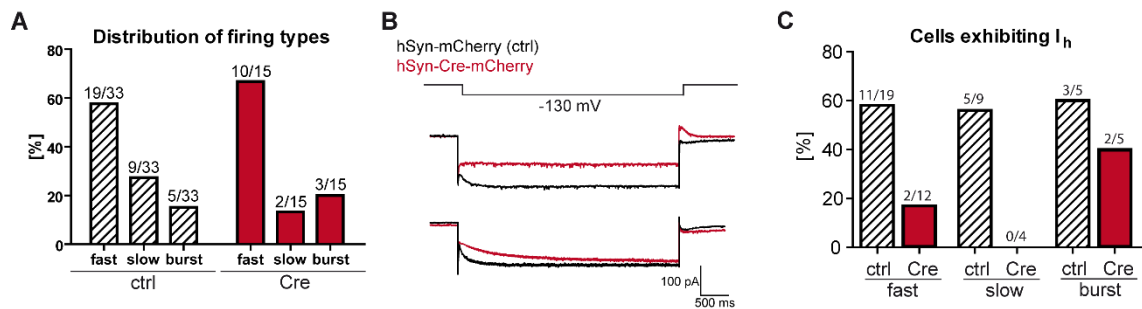
Figure 4.17: Patch clamp experiments in hSyn-injected HCN2L2 mice showed changes in firing and I$_h$ properties. (**A**) The distribution of firing types was different in control- and Cre-injected animals, while fast-firing cells occur most (control: 57.85%, Cre: 66.67%). Slow-firing cells were 27.27% in control coup and 13.33% Cre-injected. Burst-firing cells were rare in the control group (15.15%) and in the Cre-group (20.00%). (**B**) Representative I$_h$ traces from neurons of the MS of hSyn-mCherry (black, control injected mice) and hSyn-Cre-mCherry injected mice (red) showing a different kinetic. (**C**) The number of fast-, slow-, and burst-firing neurons exhibiting I$_h$ was reduced in Cre-expressing neurons compared to control neurons (16.67% vs. 57.89%, missing I$_h$ vs. 55.55%, and 40.00% vs. 60.00% respectively). Data was gathered in cooperation with Dr. Marc Stieglitz (LMU Munich).

In Figure 4.18A representative traces of voltage-clamp sag traces were shown, indicating a reduction or even loss of sag in Cre-injected neurons (red) compared to control (black). There was no difference in sag amplitude between Cre- and control-injected animals (see Figure 4.18B). Basic cell properties like the RMP did not show significant differences between control and Cre-injected animals in fast, slow, and burst-firing neurons. The number of cells exhibiting rebound spikes are reduced or even abolished in Cre-injected animals in fast and slow-firing neurons but not altered in burst-firing cells. The half-maximal activation voltage V$_{0.5}$ was calculated in Syn-mCherry injected animals with -90.71 mV (± SEM 1.78, n = 4), in Cre-injected animals a calculation was not possible, because neurons did not show I$_h$.
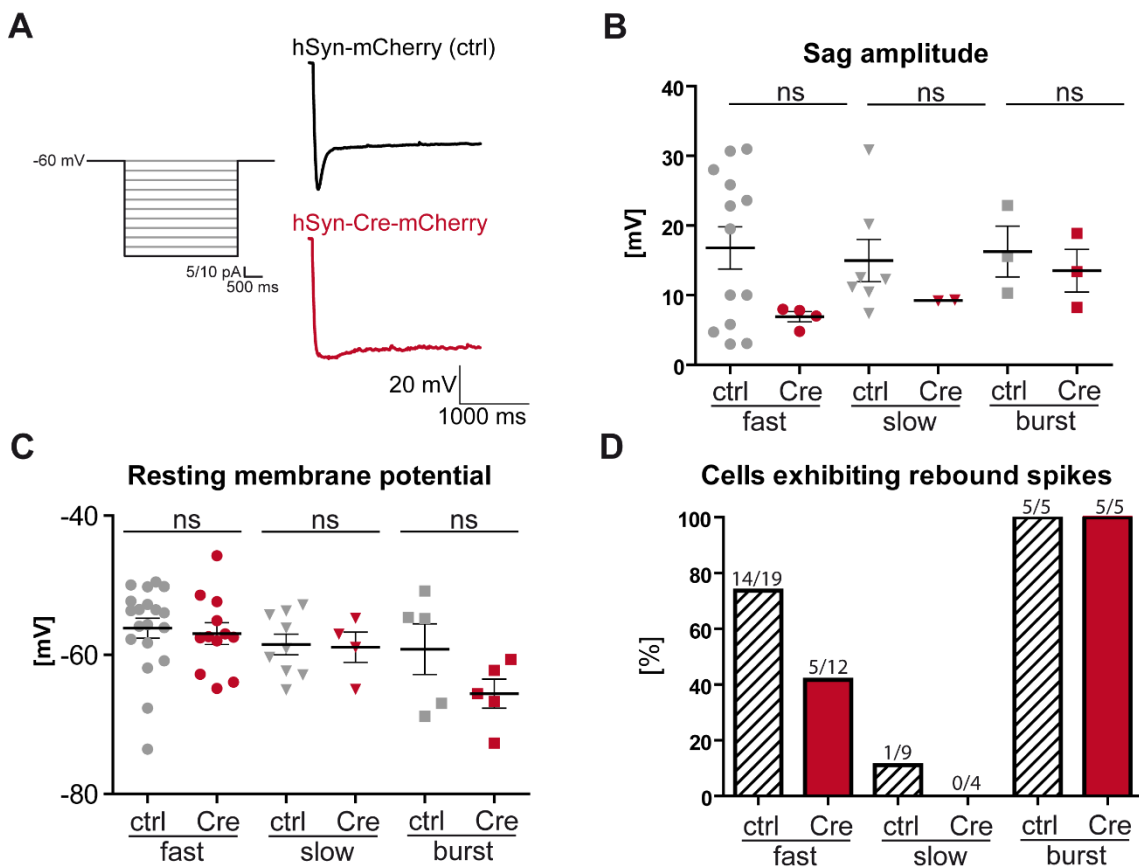
Figure 4.18: Patch clamp experiments in hSyn-injected HCN2L2 mice showed a reduced number of cells exhibiting rebound spikes. (**A**) Representative sag traces with protocol from neurons of the MS of hSyn-mCherry injected mice (black) and hSyn-Cre-mCherry injected mice (red). Cre-injected cells showed nearly no sag compared to control cells. (**B**) The sag amplitude was not significantly different between control and Cre-injected animals. (**C**) The RMP of fast, slow and burst-firing cells of Syn-mCherry (ctrl) and Cre-injected animals (Cre) did not show significant differences ($p > 0.05$). (**D**) The number of fast cells exhibiting rebound spikes was reduced in Cre-expressing neurons (41.67%) compared to the control (73.68%). Slow Cre-neurons did not show rebound spikes and burst neurons showed the same amount of rebound spikes in Cre- and control-neurons. Statistical analyses were done by unpaired t-test. Data was gathered in cooperation with Dr. Marc Stieglitz (LMU Munich).

4.2.3 The EEG of hSyn-Cre-injected animals showed reduced theta rhythm

Analyses of EEG recordings from Syn-Cre-mCherry, Syn-mCherry injected, and uninjected HCN2L2 animals served to investigate whether the knockdown of HCN2 in the neurons of the MS affects brain oscillations shown in EEG recordings. Raw EEG traces looked normal in all three vigilance stages and did not show any signs of epileptiform activity (Figure 4.19).
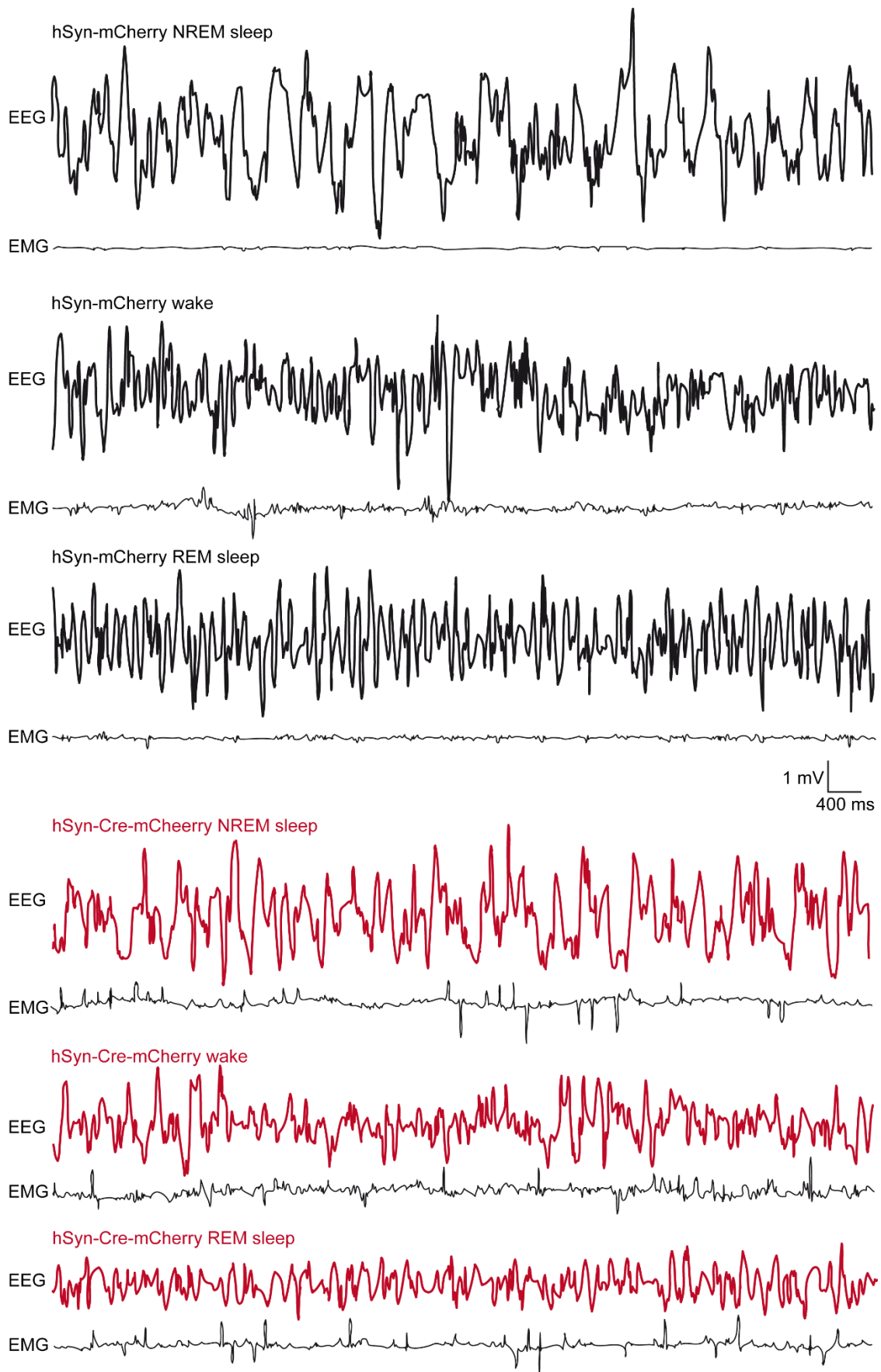
Figure 4.19: Representative EEG traces of hSyn-mCherry and hSyn-Cre-mCherry injected animals. Traces of hSyn-mCherry (black) and hSyn-Cre-mCherry (red) looked normal in NREM sleep, wake, and REM sleep.

In Figure 4.20 the EEG power of the frequency between 0 and 25 Hz was analyzed. The power of the NREM sleep vigilance state (see Figure 4.20A) did show significant differences between Cre-injected animals and uninjected HCN2L2 at frequencies between 1 Hz and 1.5 Hz. However, REM sleep power analysis (see Figure 4.20B) showed a significant difference, especially at frequency values of 7.5 Hz with and 8 Hz between the Syn-injected groups, which was similar to GAD-analysis. Therefore, also Syn-Cre-injected animals showed a reduction in EEG power during REM sleep, especially in the range of theta oscillation. Moreover, the analysis of the wake state showed a significant difference at frequency values of 0 Hz and 1 Hz (see Figure 4.20C, not indicated in data).
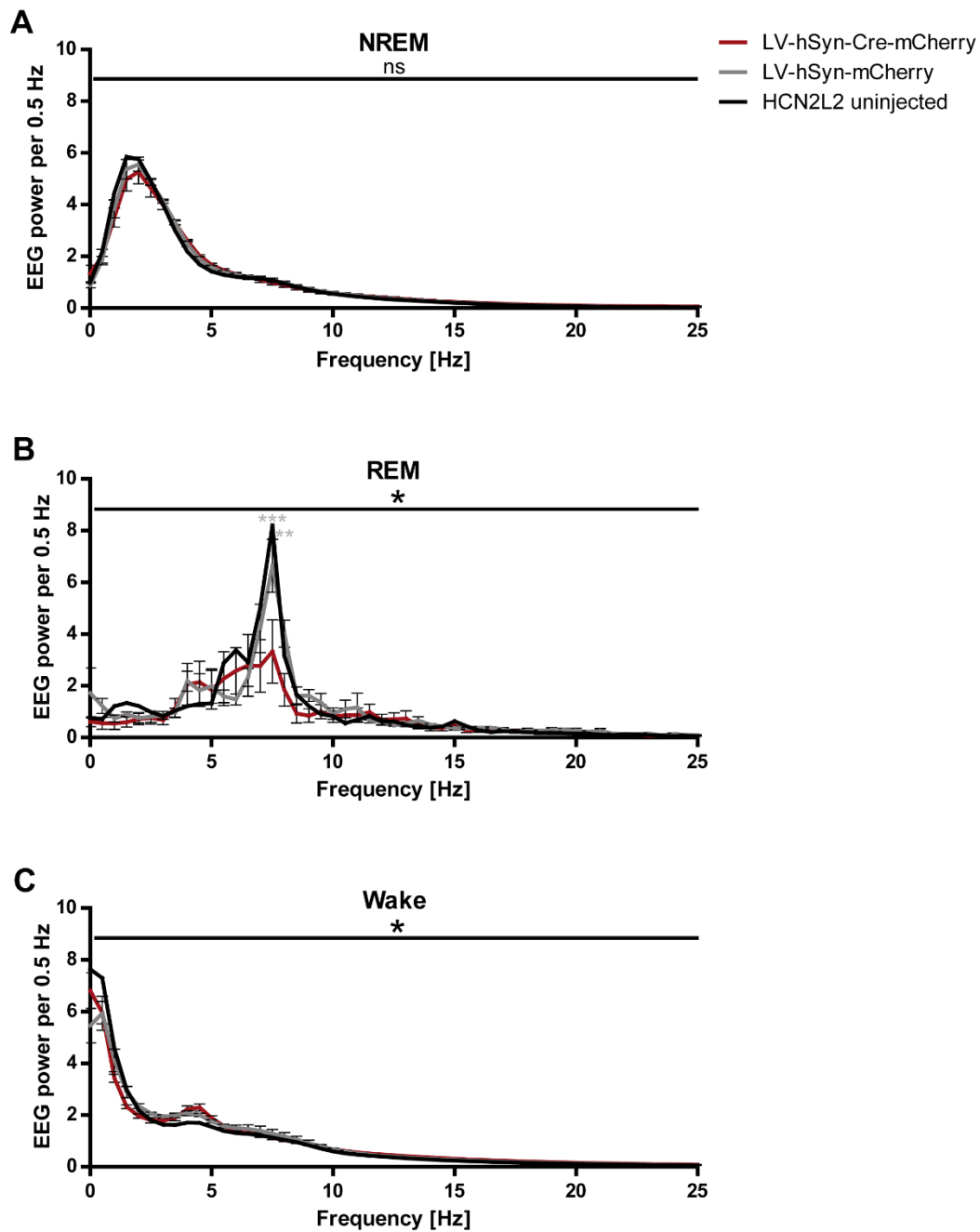
Figure 4.20: Hippocampal EEG measurements of Syn-Cre-mCherry and Syn-mCherry injected animals. (**A**) EEG power spectra of NREM sleep showed no significant differences between Syn-Cre-mCherry injected animals (red, n = 5), Syn-mCherry (grey, n = 5) injected, and uninjected HCN2L2 animals (black, n = 5) in the two-way ANOVA test. (**B**) In REM sleep Cre- and control-group differ significantly in two-way ANOVA test (black stars, *p = 0.0257). In Bonferroni's post hoc test (grey stars) there was a significant difference calculated at frequency 7.5 Hz (***p < 0.001) and 8 Hz (**p < 0.01) between Syn-injected animals. Between Cre-injected animals and uninjected HCN2L2 there was also a significant difference in REM sleep in the Bonferroni's post hoc test at frequency 7 Hz (**p < 0.01) and 7.5 Hz (***p < 0.001) (not indicated in data). (**C**) In wake state there was also a significant difference in the two-way ANOVA test (*p = 0.0205) and in the Bonferroni's post hoc test at frequency 0 Hz (***p < 0.001) and 1 Hz (*p < 0.05) between Syn-injected animals (not indicated in data). Between Cre-injected animals and uninjected HCN2L2 there was a significant difference in wake the Bonferroni's post hoc test at frequency 0 Hz (**p < 0.01), 0.5 and 1 Hz (***p < 0.001) (not indicated in data).

In Figure 4.21A-D further investigations on REM sleep parameters like number, time, duration, and mean power were done. All parameters were not significantly different between Cre- and control-animals.
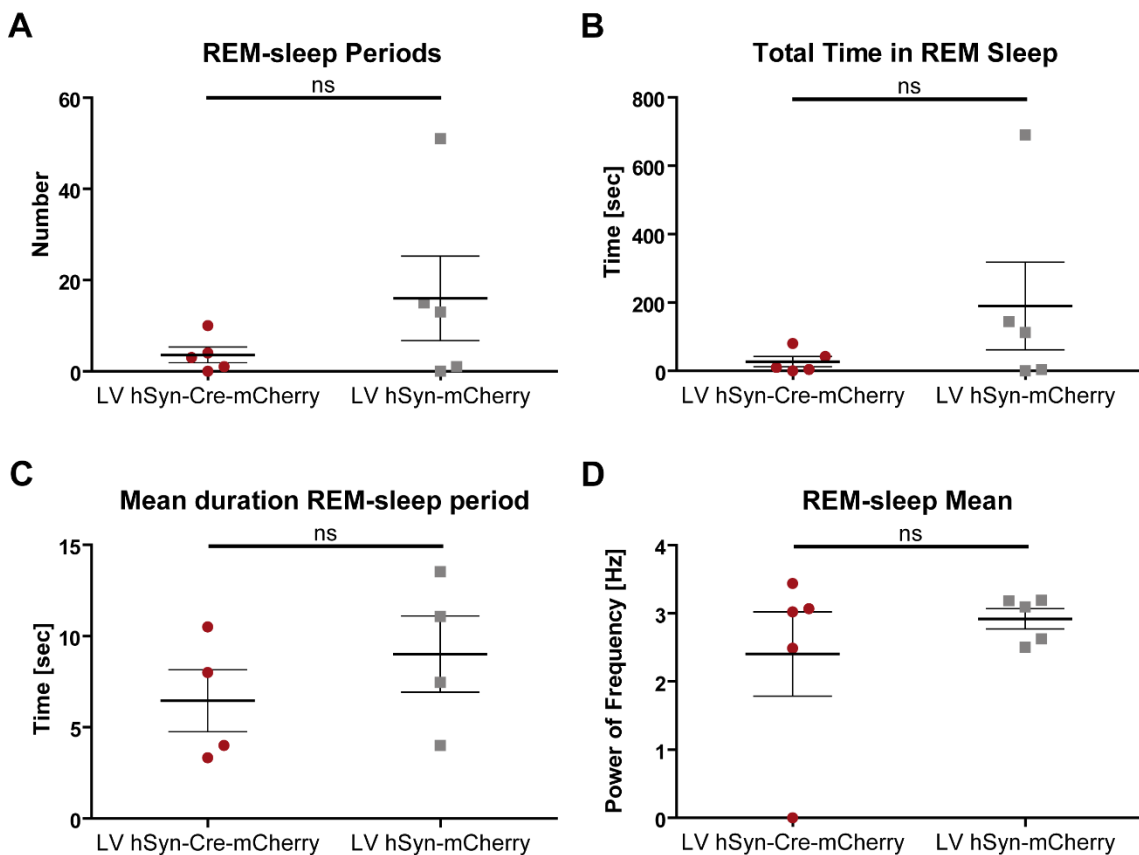
Figure 4.21: REM sleep analysis of Syn-Cre-mCherry and Syn-mCherry injected animals. Sleep analysis of EEG measurements of Syn-mCherry (grey) and Syn-Cre-mCherry-injected animals (red) showed no significantly differences in the number of REM periods (p = 0.2248) (**A**) and in the total time in REM sleep (p = 0.2429) (**B**). The mean duration of REM periods (**C**, p = 0.2248) and the REM mean (**D**, p = 0.4414) were not significantly different between the respective groups. Statistical analyses were done by unpaired t-test.

Further analyses of a representative single REM sleep episode demonstrated the differences of Syn-mCherry and Syn-Cre-mCherry injected animals. This was in line with data presented in Figure 4.20B. The power of theta frequency while REM sleep was reduced in Cre-injected animals compared to control-injected animals. This was shown in the heat map by different colors, while yellow indicated a high power of corresponding frequency. Yellow bars above indicated REM sleep periods (see Figure 4.22A,B).
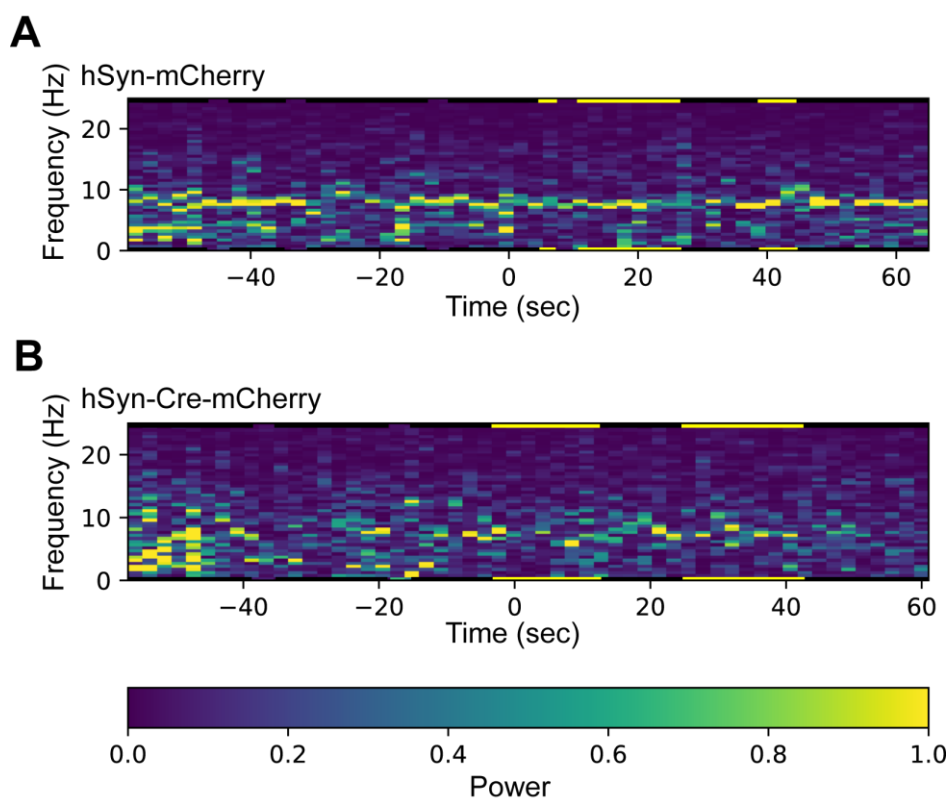
Figure 4.22: Representative REM sleep episodes in Syn-injected animals. A heat map was used to depict REM sleep episodes during NREM sleep. Yellow bars above indicate REM sleep episodes. (**A**) REM sleep in control-injected animals showed a high power (indicated by yellow color) at theta frequency while REM sleep, indicating occurring theta rhythm. (**B**) The power of theta frequency was not as prominent as in the control episode.

4.2.4 Hippocampal-dependent behavior was impaired in hSyn-Cre-injected animals

Following a similar reasoning as in GAD-injected animals, the WCM experiment was performed to clarify the effect of the deletion of HCN2 in neurons in the MS on hippocampal-dependent behavior. The animals used were injected with either LV-hSyn-Cre-mCherry or LV-hSyn-mCherry aged between 10 and 12 weeks. The groups were compared in terms of latency [sec], accuracy [%], wrong platform visits [#], and accurate learners [%]. The behavioral performance of week 1 (day 1-5) and week 2 (day 1r-5r) were analyzed separately.

Both groups showed no significant difference regarding the latency, accuracy, number of wrong platform visits, and number of accurate learners in the first week of the experiment (see Figure 4.23A-D, day1-5). The performance of Cre- and control-injected animals in the latency was almost equal, the time needed to reach the platform decreased in both groups. The accuracy in week one of control and Cre- injected-animals improved from day 1 to day 5. The number of wrong platform visits in the first week decreased from day 1 to day 5. The number of

animals reaching the accurate learners criterion in the first week was increasing in both cohorts.
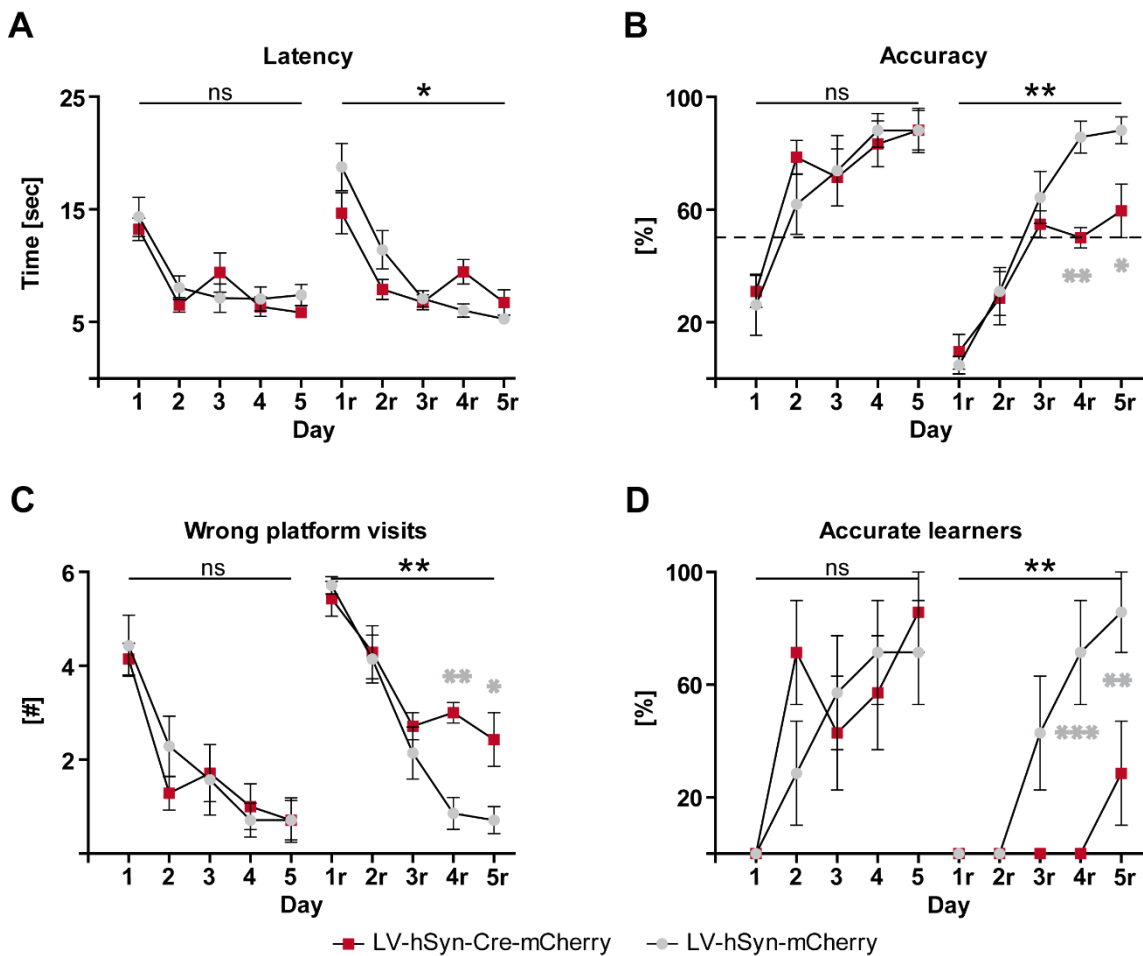
Figure 4.23: WCM of LV-hSyn-injected mice showed deficits in reversal learning in Cre-injected mice. Learning curve of LV-hSyn-mCherry (grey, n = 7) and LV-hSyn-Cre-mCherry (red, n = 7) injected mice. Black stars indicated the results of two-way ANOVA test, while Bonferroni's post hoc test was indicated with grey stars. In the first week (learning week, day 1-5) all animals performed in the spatial learning equally in all four learning parameter ($p_{1-5} > 0.05$). In the second week (relearning, day 1r-5r) the two groups underwent reversal learning. (**A**) The latency performance of Cre- and control-injected animals was similar in week one. In the relearning week the time needed to reach the platform decreased in both groups with a significant difference of *p = 0.0101 by two-way ANOVA. (**B**) The accuracy in week one improved constantly from day 1 to day 5 in both groups, in week two there was a significant difference between the respective groups with **p = 0.0079 by two-way ANOVA. (**C**) The number of wrong platform visits in the second week decreased from day 1 ≈ 4 and day 5 < 1 with **p = 0.0079 by two-way ANOVA. (**D**) The number of accurate learners in the first week of the control group was constantly increasing compared to the Cre group with **p = 0.0055 by two-way ANOVA.

In the second week, the relearning week, the four parameters were determined and compared between control and Cre-injected animals: Cre-injected animals did not reach a steady state for the latency during the second week. The Cre-injected animals show a significantly higher latency compared to control-injected

animals. Similar, the accuracy did not steadily increase in the second week in Cre-injected animals compared to control-injected animals. The values of Cre-injected animals were fluctuating at day 3, 4 and 5 around the value of 50%. Control-injected animals reached accuracy level of the same value in the first and second week, whereas Cre-injected animals did significantly not reach the same accuracy levels in the second week compared to the first week. Especially on day 4r and day 5r the differences between Cre- and control-injected animals were significant. The number of platform visits decreased continuously in control-injected animals in the second week while the number of wrong platform visits of Cre-injected animals again stagnated around value 3. This behavior is significantly different between the respective groups. The number of animals reaching the accurate learners criterion was significantly lower in the second week compared to the first week and increased in control-injected animals beginning with day 3r, while Cre-injected animals showed an increase at day 5r.

4.2.5 Object and social recognition tests were not influenced by hSyn-Cre-injection

To examine a possible connection between the HCN2 expression in the MS neurons and the object and social recognition test was performed.

For the ORT, the groups were compared in terms of the number of visits at the two objects (see Figure 4.24). The control group showed a significant higher number of visits of the novel object 2 compared to the already known object 1, indicating a correct test setup and implementation of the ORT.
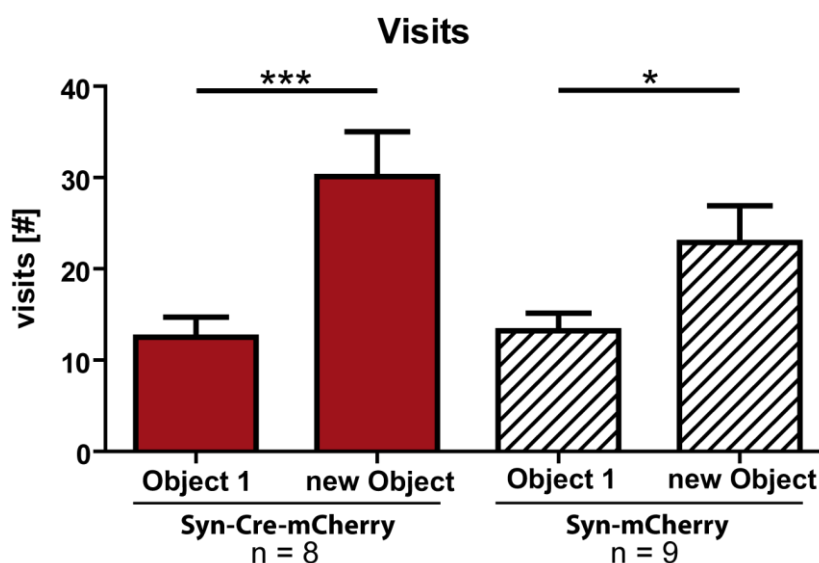
Figure 4.24: Object recognition test with LV-Syn injected mice showed significant differences in Cre-injected animals. LV-Syn injected animals and LV-Syn-Cre injected animals did show a significant differences between the number of visits of object 1 and object 2 (***p = 0.008, *p = 0.0230). Statistical analyses were done by unpaired t-test.

The significant difference of the number of visits at object 1 compared to object 2 of the LV-Syn-Cre injected animals indicates an unimpaired object recognition memory in hSyn-Cre-mCherry injected animals.

With the data of the ORT a reanalysis was possible with the TSE Software to investigate the fear condition of Syn-injected animals. There was no significant difference in the speed while exploring time, the percentage of time spent at the border of the environment, and time spent in the center of the environment be-tween the two groups of animals (see Figure 4.25A-C).
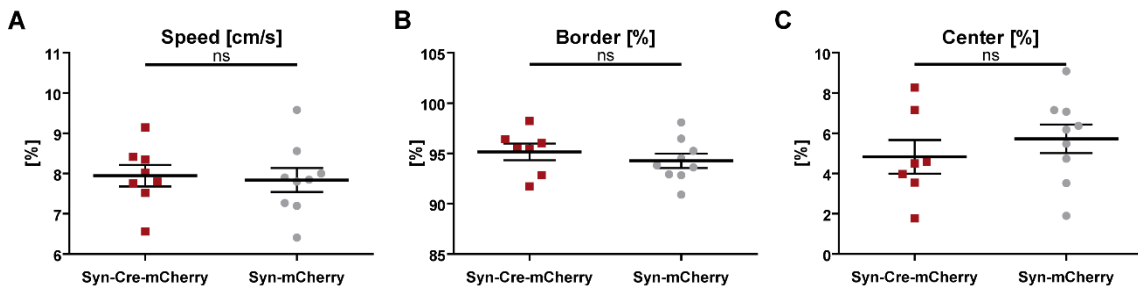
Figure 4.25: Center-border-ratio in Syn-injected animals showed no differences. (**A**) The speed of Syn-injected animals while object recognition test was not significant different. (**B**) The percentage of time spent at the border or (**C**) center area of the environment indicating the amount of fear was not significantly different. Statistical analyses were done by unpaired t-test.

The third behavior experiment performed was the SRT. The animals got in con-tact with either an already known juvenile animal (same social partner) or an un-known juvenile animal (different social partner) with the age of 5 to 8 weeks for training phase, short-term memory (stm), and long-term memory (ltm). The groups were compared in the time of contact. Control-injected animals interacted with different social partners (see Figure 4.26A) for a similar or even longer time period as they did during the training phase. Cre-injected animals instead showed a successively decreasing time of interaction. The difference between the two groups in the ltm experiment was also not significantly different. Control- and Cre-injected animals were spending the same amount of time with the same social partner at all three time points (see Figure 4.26B).
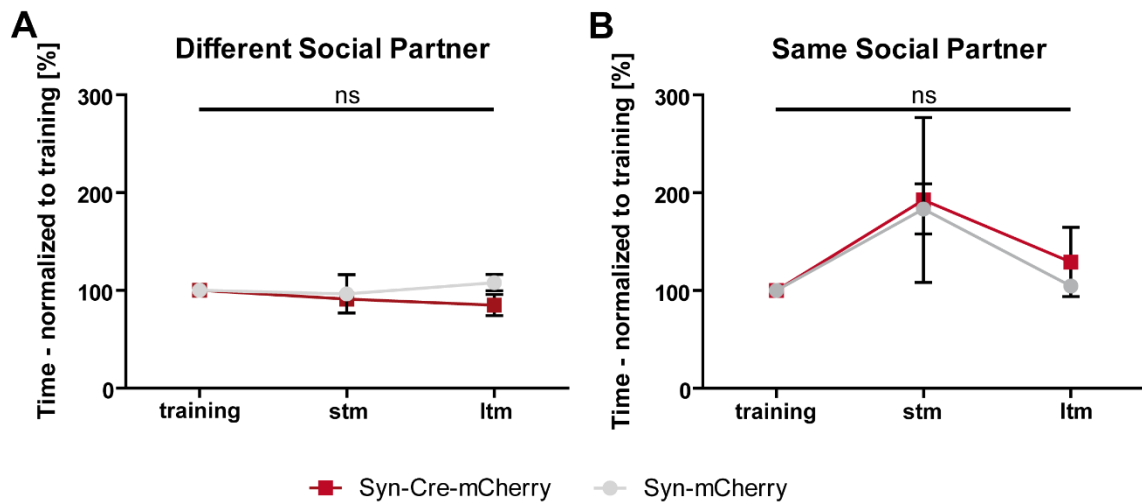
Figure 4.26: Social recognition test with LV-Syn-injected mice showed no significant differences between Cre- and control-injected animals. (**A**) The normalized time of social contacts with different social interaction partner was not significant different between Cre- (n = 3) and control-injected (n = 2) animals. (**B**) The normalized time of social contacts with the same social interaction partner was not significant different between Cre- (n = 3) and control-injected (n = 5). Statistical analyses were done by unpaired t-test (p = 0.400).

5 Discussion

In the first part of my thesis, the role of HCN2 in different types of neurons of the MS was investigated on the cellular, network, and behavioral level. To investigate this question, I had to meet several challenges: Firstly, the approach needed to be selective for the MS. Secondly, the MS is composed of different cell types with different firing properties. Most of these cells can be grouped into three main populations: GABAergic, cholinergic, and glutamatergic neurons. These three populations give raise to three septo-hippocampal subcircuits. Thirdly, not all neurons of a given subtype contain HCN channels and additionally express different HCN channel subtypes. In order to be able to analyze the circuit-specific role of HCN2 for MS function, the approach needs to be I) HCN specific, II) MS specific, III) the approach should allow for identification of the cell in question of a fluorescence marker protein, and IV) the approach should be cell type and circuit specific. Given these requirements, pharmacological approaches like ZD7288 cannot be used, because it is a non-selective blocker of HCN channels. Additionally, there is evidence that ZD7288 also blocks sodium and calcium channels in neurons (Felix, Sandoval et al. 2003, Wu, Liao et al. 2012). In order to meet the requirements outlined above, I chose to use a genetic approach involving a floxed HCN2 mouse line and LV particles. By applying these selective LV particles stereotactically into the MS, a knockdown specifically in the MS because of the low distribution level of LV particles is achieved. The promoter dependent expression of the Cre recombinase is selective for specific neuron types and resulted from carefully selected promoters which are selectively active in distinct neuronal subtypes. Therefore, this approach achieved HCN2 specificity and MS specificity. The LV-driven Cre-expression can be identified by the mCherry fluorescence protein. Red fluorescing neurons show HCN2 knockdown. Finally, by using neuron specific promoters also circuit selectivity is achieved.
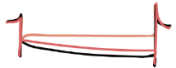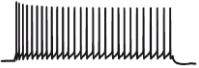
The expression of HCN2 in GABAergic neurons in the MS and the indicated important influence of GABAergic neurons in the MS on the hippocampus substantiate the educated guess that these neurons play the main role in influencing the hippocampus (Smythe, Colom et al. 1992, Toth, Freund et al. 1997, Buzsaki 2002, Bender, Gorbati et al. 2015, Boyce, Glasgow et al. 2016, Gangadharan, Shin et al. 2016, Unal, Crump et al. 2018). Therefore, the investigations started with the GABAergic neuronal subpopulation and was followed by a pan-neuronal approach.

The IHC analyses confirmed the validity of both approaches. Additionally, by investigating the neuronal expression of HCN channels in the MS a strong expression of HCN2 and a weaker expression of HCN1 and HCN4 in control-injected

animals is seen in accordance with literature (Morris, Fyffe et al. 2004, Notomi and Shigemoto 2004, Varga, Hangya et al. 2008, Spahn 2015, Muller and Remy 2018). In Cre-injected animals the absence of HCN2 in mCherry expressing cells is confirmed as well. Additionally, the specificity of the used GAD67 promoter was confirmed by IHC experiments by the co-localization of the mCherry signal with a GAD67-specific signal. These results confirm that the approach is HCN2 specific, MS specific, circuit selective, and therefore is appropriated and valid.
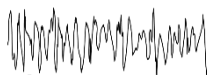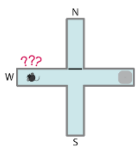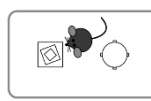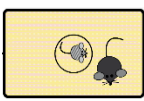
In addition, electrophysiological experiments in acute brain slice preparations additionally confirm the validity of the approach. The overall outcome on electrophysiological level of the two different approaches are given in Table 11. It is evident that for both approaches electrophysiological properties were changed in the same way. Therefore, I will discuss these changes for both approaches side by side in the next section.

Table 11: Overview of the electrophysiology results. The main findings of electrophysiological experiments of the MS project. The different groups of injected LV particles are listed. Symbols mean: (↓) reduced, (-) no change, (↑) increased in comparison to control-injected animals.

	Electrophysiology				
	RMP	Rebound spikes	I_h amplitude	Sag	Firing properties
GAD-Cre-mCherry	-	↓	↓	fast ↓	burst ↑↑ fast ↓↓
Syn-Cre-mCherry	-	↓	↓↓	-	burst, fast ↑ slow ↓↓

A brief inspection of the results obtained from the *in vivo* experiments (EEG, polysomnography, and behavioral experiments) in Table 12 revealed that there are differences between the results obtained by the two approaches. Therefore, these data will be discussed separately.

Table 12: Overview of the EEG and behavior results. The main findings of EEG and behavioral experiments of the MS project. The different groups of injected LV particles are listed. Symbols mean: (↓) reduced, (-) no change, (↑) increased in comparison to control-injected animals.

| | EEG | Behavior | | |
	Theta power in REM sleep	WCM	ORT	SRT
GAD-Cre-mCherry	↓	-	↓	-
Syn-Cre-mCherry	↓↓	↓↓	-	-

Electrophysiological experiments confirmed that in line with the literature the MS contains distinct types of neurons, such as GABAergic, glutamatergic, and cholinergic neurons (Muller and Remy 2018). Most of the neurons in general but also specifically GABAergic neurons are fast-firing cells. In GAD-Cre-injected animals the HCN2 knockdown implied a reduction of the number of fast-firing cells and an increase of burst-firing cells. On the other hand, in Syn-Cre-injected animals the number of fast- and burst-firing neurons was increased and number of slow-firing cells was decreased. The I_h amplitude was reduced in GAD-Cre-injected animals to 27.3 % (from 35.2 pA to 9.6 pA) and in Syn-Cre-injected animals to 52.8 % (from 42.6 pA to 22.5 pA) compared to control-injected mice (data not shown). The reduced I_h, however, did not impair the RMP although it is strongly influenced by HCN channel properties. In summary, there was a mild change in firing properties and a strong reduction of I_h current and rebound spikes due to HCN2 knockdown. Moreover, the number of cells exhibiting I_h was strongly reduced compared to control-injected animals, indicating that HCN2 is a major component of I_h in these cells. Given that the I_h-current was not completely abolished suggests that there are HCN channels other than HCN2 expressed, which contribute to I_h-currents in these cells. Considering these results obtained in IHC experiments, it is most likely that HCN1 and HCN4 make up these additional components of I_h in these cells. Interestingly, the reduced I_h however, did not change the RMP. This finding is surprising, as in a mouse line with global deletion of HCN2 (HCN2KO), the RMP of thalamocortical neurons was shifted to more hyperpolarized potential. As a consequence, Cav3.1 T-type calcium channels got activated and fired low-threshold bursts in response to incoming depolarizing inputs (Ludwig, Budde et al. 2003). A similar shift of the RMP in thalamocortical neurons was observed in

another knock-in mouse model, in which cAMP dependent regulation of HCN2 was ablated leading to a reduced HCN2-dependent current (Hammelmann, Stieglitz et al. 2019). The unchanged RMP in HCN2KO neurons of the MS could result from very high baseline conductance at the RMP carried by other HCN channels or other ion channels which could clamp the membrane potential to the observed ≈-56 mV, even in the absence of HCN2. These ion channels could dominate the conductance at the RMP and therefore the effect of HCN2 at the RMP cannot be seen.

In contrast to the situation at the RMP, where the activity of HCN channels may be masked by the activity of other HCN channels or other ion channels, at more hyperpolarized potentials the presence of HCN2 can be clearly seen in control injected animals. In line with this notion, hyperpolarizing current injections induce a pronounced voltage sag in the control-injected animals but not in GABAergic HCN2 knockdown neurons (see Figure 4.6). While in GABAergic neurons this effect is clearly present, in the pan-neuronal approach this effect is not significant. The hSyn-Cre-injected animals indeed show a consistent low sag in fast-firing neurons but control neurons show a great variance in the data. This could be explained by the assumption that not all neurons express HCN2 and consequently control cells not expressing HCN2 seemed to have the same properties as Cre-expressing cells. Therefore, no significant differences can be calculated.

Most importantly, once HCN2 channels are activated during hyperpolarizing current injections, HCN2 mediated currents induce robust rebound spikes. These findings indicate that robust activation of HCN2 at hyperpolarizing potentials is not sufficient to counteract other non-HCN2 mediated currents present at more depolarized potentials and also likely at the RMP. In contrast, in HCN2 deficient neurons rebound spikes are less efficient induced, especially in slow- and burst-firing neurons. This indicates that HCN2, while not important at RMP, may be a dominant channel after activation at more hyperpolarizing potentials and may be highly relevant for the induction of rebound spikes. Mechanistically GABAergic hyperpolarization via GABA receptors may be the physiological trigger of hyperpolarization of similar amplitude as seen in our sag protocol. A similar activation of rebound spikes is well known for reticular thalamic neurons, which hyperpolarize thalamocortical neurons via $GABA_A$ and $GABA_B$ receptors (McCormick and Bal 1997). Because the properties of rebound spikes are only HCN channel driven, the significant differences show the effect of the HCN2 knockdown in Cre-injected animals. Interestingly, the *in vivo* consequence of HCN2 knockdown in GAD- and Syn-injected animals are not equal and will therefore be discussed in the following chapters.

5.1 The influence of a GABAergic-specific knockdown of HCN2 in the MS

The main functional consequence of HCN2 deletion in GABAergic neurons was the pronounced reduction of I_h in these neurons, the sag reduction, and a decrease in rebound spikes. The rebound spikes are an important physiological characteristic and neuronal event, which effect rhythmic activity in neurons and consequently learning and memory (Tremere, Pinaud et al. 2008). A reduction of rebound spikes could influence rhythmicity and therefore also the theta rhythm formation in the hippocampus. If the theta rhythm is influenced, changes in theta rhythm-dependent physiological processes should be seen for example in REM sleep, learning, and memory (Vertes, Hoover et al. 2004). Additionally, literature data already showed the influence of GABAergic cell expressing HCN channels onto the hippocampal theta rhythm (Varga, Hangya et al. 2008). This influence I confirmed in EEG measurement on GAD-injected animals showing a significant reduction of theta power while REM sleep in Cre-injected animals compared to control and uninjected animals of 24.42% (at frequency 7.5 Hz) while the occurrence of REM sleep was unchanged. This finding was substantiated by Gangadharan et al. (Gangadharan, Shin et al. 2016) showing a decrease of and theta rhythm while inhibiting the septo-hippocampal GABAergic pathway in WT animals. Moreover, the results were supported by Hangya et al., where they reported a reduced theta power during REM sleep in MS HCN2-deficient animals whilst the occurrence of REM sleep was unchanged (Hangya, Borhegyi et al. 2009). In addition, Boyce et al. substantiate these results with their findings about the influence of the activity of GABAergic neurons during REM sleep on memory consolidation. Furthermore, in Cre-injected animals the number of REM sleep periods and the total time in REM sleep are constantly very low. Control animals showed a wide range of values in both parameters, therefore no significant difference was calculated. However, these experiments showed the important role of HCN2 in GABAergic neurons on the theta rhythm generation while REM sleep.

With behavior experiments it was tested if the reduction in I_h, rebound spikes, and theta power in GAD-Cre-injected animals could lead to changes in behavior. The WCM is a common used test to examine hippocampal CA1-dependent spatial learning and spatial flexibility (Kleinknecht, Bedenk et al. 2012). The investigated parameters are not significantly different in the first and second week between Cre- and control-injected animals. These results show that selective HCN2 deletion in GABAergic neurons in the MS did not lead to impaired hippocampal spatial learning and memory. Although, the analyzed parameter of the latency is an unstable parameter, strongly influenced by the individual motivation of the animals,

and their ability to swim. This parameter additionally shows that no motor skill limitations are provoked by stereotactic injection.

The results of the ORT of GAD-injected animals showed a significant difference in the number of visits in the control group, proofing a correct implementation of the ORT. Additionally, Cre-injected animals did not show significant differences in exploring the familiar object compared to the new object, indicating an impaired object recognition memory. However, the WCM did not show any significant differences in the GAD-injected animals although both test are known to be hippocampal dependent. Hereby it is important to distinguish between object recognition with and without a spatial factor influencing the experiment. Most of the ORT performed in literature including spatial or contextual factors, e.g. landmarks in the experimental lab and therefore are hippocampal dependent (Forwood, Winters et al. 2005). The ORT performed in this study was conducted in an environment that was neutralized by black curtains and thus did not include landmarks that could lead to spatial learning. The results of the decreased object recognition is in line with the results shown in the object exploration experiments of Gangadharan et al. (Gangadharan, Shin et al. 2016). They showed a decrease of object exploration (and theta rhythm) while inhibiting the septo-hippocampal GABAergic pathway in WT animals. Conclusively it could be said that HCN2 channels in GABAergic neurons involved in object recognition, but not in hippocampal spatial learning.

The behavior of GAD-injected animals showed immobility during object recognition possibly indicating fear. However, the center-border-ratio did not show significant differences between Cre- and control-injected animals in the percentage of staying longer in the center or border.

The third behavior experiment in this project was the SRT. The role of the hippocampus in the social memory had been shown in various studies, especially with regard to long-term memory (Maaswinkel, Baars et al. 1996, Kogan, Frankland et al. 2000). Different processes are involved and are influencing the behavior and the results, like recognition ability, social learning, individual position in the social association (dominant, subordinated), and consequently their behavior (aggressive, socially interactive) (Tzakis and Holahan 2019). To decrease this variability and external influences, different experimental setups were established to reduce listed influences and to increase the selectivity for more powerful data (Leroy, Brann et al. 2017, McAllister, Wright et al. 2018, Deng, Gu et al. 2019). In the results of the SRT, control-injected animals showed the expected behavior of spending the same amount of time with every new unknown social partner, while Cre-injected animals instead showed a (not significant) decrease of social interaction time in the stm and ltm test. This observation could arise out of fear or a

loss of interest and motivation against the social partner. The second cohort (same social partner) served as control for proving the correct implementation of the test. Control and Cre-injected animals showed a decreasing amount of time interacting with the same social partner. These results show that the deletion of HCN2 in the MS in GABAergic neurons do not have an influence on social memory. This is in accordance with the general knowledge of social memory which seem to be dependent on CA2 region (Hitti and Siegelbaum 2014, Stevenson and Caldwell 2014) and encoded social contact into declarative memory by projecting to ventral CA1. Theta rhythm instead is part of the perforant path, including CA1 and CA3, but not CA2 (Brown, Alexander et al. 2020). Therefore, hippocampal CA2-dependent social memory is not affected by HCN2 deletion in GABAergic neurons, shown by the results of the SRT.

To summarize, it can be concluded that the deletion of HCN2 in GABAergic neurons was indeed efficient to impair electrophysiological and theta properties, but not to impair spatial hippocampal behavior, while the object recognition is impaired. Most likely also other types of neurons of the MS are participating in behavior, just like glutamatergic and cholinergic neurons. Before another neuron type was investigated, it was investigated if a deletion of HCN2 in neurons in general in the MS show an effect on REM sleep, theta rhythm, and learning behavior.

5.2   The influence of a neuron-specific knockdown of HCN2 in the MS

In GABAergic neurons I obtained on the one side a mismatch between a pronounced functional role of HCN2 for the generation of rebound spikes in MS network, theta rhythm *in vivo*, and object recognition. On the other side there is a lack of functional effects for the spatial hippocampal dependent behavior of the animal. A possible explanation for this apparent mismatch could be that the deletion of HCN2 in the GABAergic subcircuit of the MS hippocampal system is sufficient to reduce rebound firing and theta but not sufficient to reach the threshold to induce spatial hippocampal dependent behavioral changes. This could be caused by MS neuron types beside GABAergic, which *in vivo* contribute to HCN2 dependent effects on firing, theta generation, and theta dependent behavior. To test this, I deleted HCN2 in all neurons of the MS using the pan-neuronal approach with a hSyn promoter to investigate the impact on the theta rhythm generation and its influence on learning, memory, and REM sleep.

In Syn-Cre-injected animals electrophysiological experiments showed strongly reduced rebound spikes. As already mentioned, rebound spikes have an influence on the hippocampus, its rhythmic activities, and therefore on behavior

(Vertes, Hoover et al. 2004, Tremere, Pinaud et al. 2008). The reduction of theta power while REM sleep of 49.85% (at frequency 7.5 Hz) was stronger compared to GAD-Cre-injected animals. The number of REM sleep periods and the total time in REM sleep are consistently very low in Cre-injected animals. These results confirm the influence of the MS neurons on the hippocampus, in particular the influence of the HCN2 channel in the MS neurons on the theta rhythm generation during REM sleep.

In the first week of the WCM, the parameters were not significantly different between the respective groups. However, in the second week Cre-injected animals did not improve over 50% chance level in the accuracy and number of wrong platform visits, while WT showed – as expected – steadily increasing accuracy. These results showed that the selective HCN2 deletion in MS neurons led to an impairment in learning the platform's location because of an impaired spatial learning ability. This is in line with the reduced rebound spikes in Syn-Cre-injected neurons observed in patch clamp recordings. Their reduction influenced theta rhythm generation and therefore hippocampal spatial learning and memory was impaired. Differences in hippocampal dependent spatial learning could be explained by septal modulation of hippocampal LTP rather than changing intrinsic hippocampal LTP. Therefore, further experiments on electrophysiological level will investigate the effect of the deleted HCN2 on LTP and LTD formation. It was already shown that HCN2 play an important role in the mechanism underlying synaptic plasticity, demonstrated by enhanced LTP levels in HCN2KO mice (Matt, Michalakis et al. 2011). In contrast to HCN1, HCN2 did not constrain LTP in the perforant path by the modulation of dendritic integration in pyramidal neurons. Moreover, HCN2KO mice exhibit increased LTP levels at the perforant path synapses without LTP modification at the Schaffer collaterals synapses. Additionally, by combining the stereotactic injection of lentiviral particles with the preparation of the intact septo-hippocampal system (Stieglitz 2018) it is possible to examine theta oscillations in the hippocampus that is still innervated by the MS (Khalilov, Esclapez et al. 1997, Amilhon, Huh et al. 2015, Robinson, Manseau et al. 2016). This preparation can be used to study the influence of the MS on the hippocampus alone, without other brain regions that are involved *in vivo*. Therefore, in addition to patch clamp experiments in the MS, depth profile analyses in the hippocampus to examine the direct influence of the MS firing neurons and their relation to the theta cycle will be performed.

In the ORT, the results of the control group showed a correct implementation of the ORT seen in the significant higher number of visits at the unknown object compared to the familiar one. This significant difference is also shown in the group of Cre-injected animals indicating an unimpaired object recognition

memory. As already mentioned, the ability of object recognition is strongly connected to the hippocampus if spatial factors influence the ORT. However, in the ORT performed in this study spatial factors are excluded by the experimental setup (Forwood, Winters et al. 2005), seen in the unimpaired object recognition compared to the impaired spatial learning in the WCM. If the ORT still is influenced by spatial factors, this would have been seen in impaired object (and spatial) object recognition. These results show that the deletion of HCN2 in neurons of the MS does not lead to an impairment of the object recognition memory although the hippocampal spatial learning in the WCM experiment is affected by HCN2 knockdown in the MS.

The third behavior experiment in this project was the SRT. Regarding the results of this test, control-injected animals showed expected and typical behavior by meeting different social partners three times: the interaction time remained the same or increased while Cre-injected animals showed a decreasing time of interaction with different social partners. This observation was similar to the results of GAD-injected animals and could arise out of fear or a loss of interest and motivation against the social partner. By meeting the same social partner both groups showed the same amount of time interacting with the social partner: The time of interaction decreased from stm to ltm, because animals recognized the already known partner and lost interest. Consequently, the deletion of HCN2 in MS neurons did not result in an impaired social memory of Syn-Cre-injected animals. As already mentioned above, this is in accordance with literature and the knowledge of the CA2-dependent social memory (Hitti and Siegelbaum 2014, Stevenson and Caldwell 2014).

Like the GAD-injected animals, the fear of the injected animals was investigated. As expected, in Syn-injected animals there was no significant difference between Cre- and control-injected animals in the percentage of staying more in the center or in the border region. These results indicate that no fear-related bias influenced the results.

5.3   Conclusion and Outlook for investigating the role of HCN2 in the MS

The knockdown of HCN2 in neurons of the MS showed pronounced effects at the cellular, electrophysiological, and behavioral level. Especially the reduced theta power while REM sleep and the impaired learning behavior underlined the important influence of the HCN2 channel in the MS.

The review of Nuñez and Buño showed the interaction between the MS and the hippocampus, the influence in theta rhythm, and its crucial role in cognitive processes (Nunez and Buno 2021). The results of the EEG recordings in this thesis are in accordance with the literature already mentioned and showed a remarkable theta reduction while REM-sleep. Moreover, the behavior experiments in GAD-injected animals did not show impaired spatial learning, while Syn-injected animals showed deficits in hippocampal spatial learning in the WCM experiment. The HCN2 channel in GABAergic neurons seems to influence the theta generation, but the reduced theta power evoked by HCN2 deletion in GABAergic neurons was not strong enough to impair hippocampal spatial learning. In contrast to the results of GAD-injected animals, the larger theta reduction in Syn-injected impaired hippocampal spatial learning, showed in the WCM experiment. Interestingly, the ORT test showed an impaired object recognition memory in GAD-injected animals, while Syn-injected animals did not show impaired object recognition. More in detail, in Syn-Cre-injected animals a downregulation of activating and inhibiting HCN2-containing neurons in an equal manner was evoked. Therefore no imbalance between activation and inhibition occurred and neither an arising activation nor an arising inhibition influenced hippocampal activity or other brain areas in a greater extend. In contrast to GAD-Cre-injected animals, GABAergic neurons and their inhibiting properties were downregulated due to HCN2 knockdown and therefore the activating influence of for example cholinergic and glutamatergic neurons determine the activating influence and cause an impaired object recognition. It should also be mentioned, that there is evidence that the hippocampus has only little if any impact on the ability of object recognition and other brain areas are involved in object recognition (Mumby 2001). Conclusively, the ORT results show an important role of the HCN2 channel in GABAergic neurons on object recognition, either by the influence on the hippocampus or by the influence of other brain areas outside the hippocampus.

Regarding the WCM, another important question at this point is, how changes in theta and behavior are related. Interestingly, there is evidence that there are at least two subtypes of theta rhythms occurring in the hippocampus and are categorized as either an atropine-resistant theta rhythm (theta 1, 7-12 Hz) or an atropine-sensitive theta rhythm (theta 2, 4-9 Hz) (see Figure 5.1) (Kramis, Vanderwolf et al. 1975, Bland 1986, Mikulovic, Restrepo et al. 2018). The atropine-sensitive theta rhythm type 2 was abolished by injection of a muscarinic antagonist, while the latter was nearly unaffected (Bland 1986). A similar categorization was done by Shin et al. categorizing theta rhythm into PLC-β1-dependent and PLC- β2-dependent theta rhythm (Shin, Kim et al. 2005).
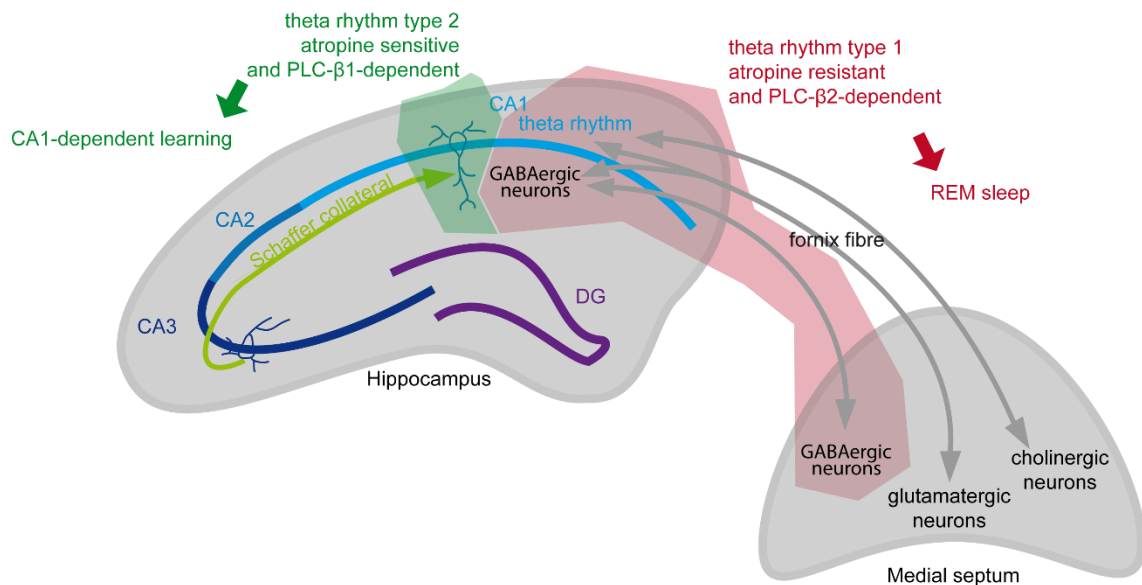
Figure 5.1: Influence of the MS on hippocampal neurons in theta 1 and theta 2 generation. Two different subtypes of theta rhythm occur in the hippocampus. Colored in red is the atropine resistant and PLC-β2-dependent theta rhythm (type 1, 7-12 Hz) and in green the atropine sensitive and PLC-β1-dependent theta rhythm (type 2, 4-9 Hz) (Bland 1986, Shin, Kim et al. 2005). The influence of MS GABAergic neurons on GABAergic neurons of the hippocampus affects REM sleep, while Purkinje cells of the CA1 affect CA1-dependent learning.

They suggested the PLC-β1-dependent pathway in the pyramidal cells of the hippocampus to be involved in the atropine-sensitive component of the theta rhythm. On the other hand, the atropine-resistant theta rhythm type 1 was based on the interaction between GABAergic neurons of the MS and GABAergic interneurons in the hippocampus (Stewart and Fox 1990). Further analyses of REM sleep theta 1 (see Figure 5.2) showed a reduced power. Also the AUC in Syn-Cre-mCherry (AUC of 6.603) was reduced compared to GAD-Cre-mCherry injected animals (AUC of 7.839).
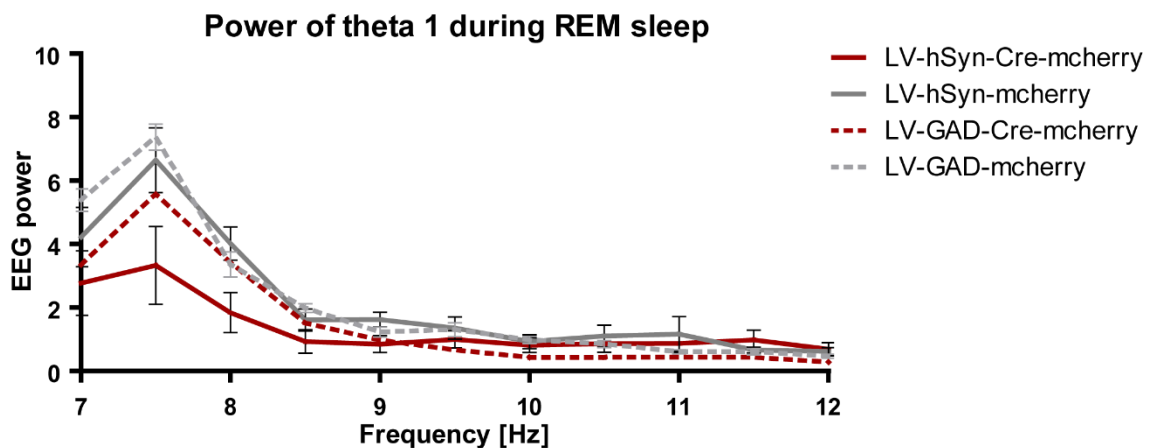
Figure 5.2: The Power of theta 1 during REM sleep in Syn- and GAD-Cre-mCherry injected animals. REM sleep EEG power spectrum of theta 1 from 7 to 12 Hz shows a stronger reduction of power in Syn-Cre-mCherry injected animals compared to GAD-Cre-mCherry injected animals.

The stronger reduced AUC shows the stronger effect of HCN2 knockdown in the respective neuron population in the MS onto theta generation. The stronger effect observed in Syn-Cre-mCherry injected animals on theta 1 during REM sleep could also influence theta 2 because of achieving the necessary threshold resulting in an impairment of hippocampal behavioral.

According to the data in this thesis, the atropine-resistant theta 1 rhythm was impaired by pan-neuronal and GABAergic neuron-specific HCN2 deletion, and as a result the theta power while REM sleep was decreased. The theta rhythm responsible for hippocampal learning theta 2 was instead unimpaired in GAD-Cre-injected animals, while in Syn-Cre-injected animals, theta 2 may also be reduced. Measuring theta 2 while the WCM experiment was not possible because of legal regulations and animal protection. In accordance with literature this data revealed on the one hand, that MS neurons are strongly involved in the generation and entrainment of hippocampal field potential (Bender, Gorbati et al. 2015, Boyce, Glasgow et al. 2016, Gangadharan, Shin et al. 2016). This reveals the fact that GABAergic neurons regulate circuit activity by the rhythmic disinhibition of pyramidal neurons (Smythe, Colom et al. 1992, Toth, Freund et al. 1997, Buzsaki 2002, Unal, Crump et al. 2018) seen in a reduction of theta rhythm during REM sleep. On the other hand, both theta types were impaired in Syn-Cre-injected animals, therefore a reduced theta rhythm while REM sleep plus reduced hippocampal learning was observable.

The effects of injecting hSyn-driven LV particles represent the sum of the interplay of all different neuron types presents in the MS. The deletion of HCN2 in GABAergic neurons did not show significant differences on hippocampal spatial behavior, leading to the assumption that another neuron type influences the septo-hippocampal system to a greater extend. Further work will investigate glutamatergic neurons of the MS by using the LV approach with the glutamatergic neuron-specific promoter CamKIIα. In contrast to GABAergic neurons, not much is known about glutamatergic function during behavior and theta rhythm generation, but they are an important source of synaptic excitation in the septo-hippocampal system (Manseau, Danik et al. 2005, Huh, Goutagny et al. 2010, Leao, Targino et al. 2015) as well as influencing theta oscillations (Fuhrmann, Justus et al. 2015). A recently published paper showed that glutamatergic neurons in the MS exhibited higher activities during wakefulness, mainly through the transition from NREM sleep to wake state (An, Sun et al. 2021). Additionally, the influence of glutamatergic neurons on hippocampal oscillations could also occur due to the projections from glutamatergic neurons of the MS on the GABAergic neurons in the hippocampus, shown in Figure 1.3, Figure 5.1, and Figure 5.3.
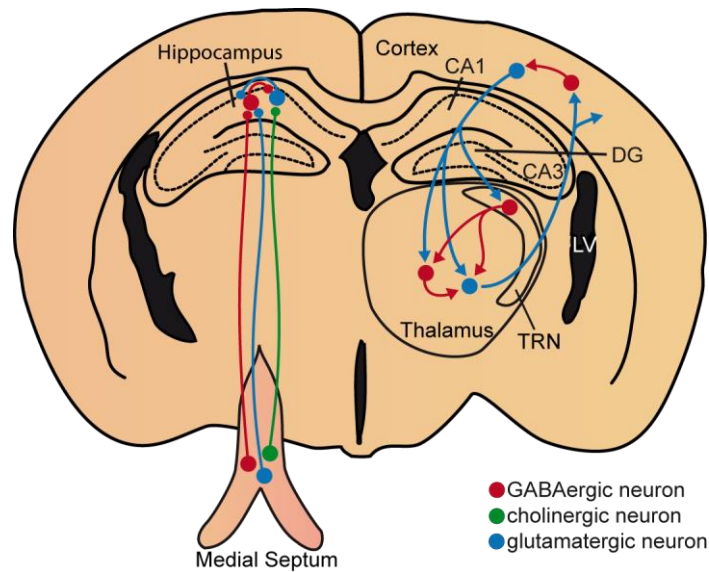
Figure 5.3: Schematic drawing of the connection between thalamus-cortex and MS-hippo-campus. The connection between the thalamus, the thalamic reticular nucleus (TRN), and the cortex is shown in comparison with the MS interconnection with the hippocampus. In both circuits, glutamatergic neurons are innervating GABAergic neurons.

This innervation in the septo-hippocampal system is similar to the innervation of glutamatergic neurons on GABAergic in the thalamus shown in Groh et al. (Groh, Krieger et al. 2018). More in detail, cortical regions project to the thalamus, and the thalamic reticular nucleus (TRN) projects via GABAergic neurons to specific thalamic nuclei for thalamocortical rhythm generation. Thalamic GABAergic neurons influence thalamocortical neurons and therefore change thalamic oscillations. In contrast, in the septo-hippocampal system, glutamatergic neurons project to GABAergic neurons and therefore influence septo-hippocampal oscillations such as the theta rhythm (Pinault 2004, Groh, Krieger et al. 2018, Hammelmann, Stieglitz et al. 2019). However, first it needs to be examined if HCN2 is expressed in glutamatergic neurons. Müller and Remy did not report an HCN expression in glutamatergic neurons of the MS (Muller and Remy 2018).

Another neuron type in the MS, which could be involved in hippocampal modification are cholinergic neurons. They are the least common neuron type with less than 5% of the neurons being cholinergic. Additionally, no co-expression of ChAT together with HCN1 or HCN2 was found by analyzing the MS cholinergic neurons (Varga, Hangya et al. 2008). However, cholinergic neurons increase their activity during hippocampal theta oscillations (Dudar 1977, Simon, Poindessous-Jazat et al. 2006, Zhang, Lin et al. 2010). Additionally, an induction of theta rhythm by acetylcholine, cholinergic agonists, (Alonso and Garcia-Austt 1987, MacVicar and Tse 1989, Bland and Colom 1993), or an increase of theta rhythm by an increased cholinergic activity via blocking acetylcholine hydrolysis (Macadar, Roig et al. 1970, Roig, Budelli et al. 1970, Buno, Garcia-Sanchez et al. 1978,

Gaztelu and Buno 1982) showed the influencing role of cholinergic neurons on the hippocampus. This indicates an important role for learning and memory processes (Kesner 1988, Hasselmo 1999). On the other hand it is already shown, that cholinergic projections to the hippocampus show a spatial role of cholinergic MS neurons but not a role in object recognition (Cai, Gibbs et al. 2012). Moreover, a blockade of theta rhythm was shown by specific cholinergic antagonists (Monmaur and Thomson 1983, Vinogradova 1995, McQuiston 2010). Cholinergic neurons also modulated the excitability of other neurons to induce theta rhythmic firing (Colgin 2013). Behavior experiments with selective optogenetic activation of cholinergic MS DbB neurons showed strong network effects during inactive behavioral states, weak effects during active behavior in rats, and stress related behavior in mice (Mamad, McNamara et al. 2015, Mineur, Mose et al. 2022). Although no expression of HCN2 in cholinergic neurons was found yet, this will be investigated in future IHC experiments. Depending on the results, patch clamp experiments, EEG recordings, and behavioral studies can be implemented with a cholinergic specific promoter.

To summarize the results of this project it becomes apparent that HCN2 channels in GABAergic have an effect on theta generation, electrophysiological properties, and object recognition but not on hippocampal spatial behavior. Whereas HCN2 channels in all types of neurons of the MS are impressive involved in theta generation, electrophysiological properties, and hippocampal spatial behavior. The influence of other neurons types like glutamatergic and cholinergic neurons is the subject of current research.

6 Literature

Akama-Garren, E. H., N. S. Joshi, T. Tammela, G. P. Chang, B. L. Wagner, D. Y. Lee, W. M. Rideout, 3rd, T. Papagiannakopoulos, W. Xue and T. Jacks (2016). "A Modular Assembly Platform for Rapid Generation of DNA Constructs." Sci Rep **6**: 16836.

Alonso, A. and E. Garcia-Austt (1987). "Neuronal sources of theta rhythm in the entorhinal cortex of the rat. II. Phase relations between unit discharges and theta field potentials." Exp Brain Res **67**(3): 502-509.

Amaral, D. G. and M. P. Witter (1989). "The three-dimensional organization of the hippocampal formation: a review of anatomical data." Neuroscience **31**(3): 571-591.

Amilhon, B., C. Y. Huh, F. Manseau, G. Ducharme, H. Nichol, A. Adamantidis and S. Williams (2015). "Parvalbumin Interneurons of Hippocampus Tune Population Activity at Theta Frequency." Neuron **86**(5): 1277-1289.

An, S., H. Sun, M. Wu, D. Xie, S. W. Hu, H. L. Ding and J. L. Cao (2021). "Medial septum glutamatergic neurons control wakefulness through a septo-hypothalamic circuit." Curr Biol **31**(7): 1379-1392 e1374.

Andersen, P. and J. Eccles (1962). "Inhibitory phasing of neuronal discharge." Nature **196**: 645-647.

Antunes, M. and G. Biala (2012). "The novel object recognition memory: neurobiology, test procedure, and its modifications." Cogn Process **13**(2): 93-110.

Ayash, S., U. Schmitt and M. B. Muller (2020). "Chronic social defeat-induced social avoidance as a proxy of stress resilience in mice involves conditioned learning." J Psychiatr Res **120**: 64-71.

Barbizet, J. (1963). "Defect of memorizing of hippocampal-mammillary origin: a review." J Neurol Neurosurg Psychiatry **26**: 127-135.

Bender, F., M. Gorbati, M. C. Cadavieco, N. Denisova, X. Gao, C. Holman, T. Korotkova and A. Ponomarenko (2015). "Theta oscillations regulate the speed of locomotion via a hippocampus to lateral septum pathway." Nat Commun **6**: 8521.

Biel, M., C. Wahl-Schott, S. Michalakis and X. Zong (2009). "Hyperpolarization-activated cation channels: from genes to function." Physiol Rev **89**(3): 847-885.

Bland, B. H. (1986). "The physiology and pharmacology of hippocampal formation theta rhythms." Prog Neurobiol **26**(1): 1-54.

Bland, B. H. and L. V. Colom (1993). "Extrinsic and intrinsic properties underlying oscillation and synchrony in limbic cortex." Prog Neurobiol **41**(2): 157-208.

Boyce, R., S. D. Glasgow, S. Williams and A. Adamantidis (2016). "Causal evidence for the role of REM sleep theta rhythm in contextual memory consolidation." Science **352**(6287): 812-816.

Brown, H. and D. Difrancesco (1980). "Voltage-clamp investigations of membrane currents underlying pace-maker activity in rabbit sino-atrial node." J Physiol **308**: 331-351.

Brown, L. Y., G. M. Alexander, J. Cushman and S. M. Dudek (2020). "Hippocampal CA2 Organizes CA1 Slow and Fast gamma Oscillations during Novel Social and Object Interaction." eNeuro **7**(2).

Buno, W., Jr., J. L. Garcia-Sanchez and E. Garcia-Austt (1978). "Reset of hippocampal rhythmical activities by afferent stimulation." Brain Res Bull **3**(1): 21-28.

Buzsaki, G. (2002). "Theta oscillations in the hippocampus." Neuron **33**(3): 325-340.

Cai, L., R. B. Gibbs and D. A. Johnson (2012). "Recognition of novel objects and their location in rats with selective cholinergic lesion of the medial septum." Neurosci Lett **506**(2): 261-265.

Calandreau, L., R. Jaffard and A. Desmedt (2007). "Dissociated roles for the lateral and medial septum in elemental and contextual fear conditioning." Learn Mem **14**(6): 422-429.

Cheng, J., G. Umschweif, J. Leung, Y. Sagi and P. Greengard (2019). "HCN2 Channels in Cholinergic Interneurons of Nucleus Accumbens Shell Regulate Depressive Behaviors." Neuron **101**(4): 662-672 e665.

Clark, R. E. and S. J. Martin (2005). "Interrogating rodents regarding their object and spatial memory." Curr Opin Neurobiol **15**(5): 593-598.

Colgin, L. L. (2013). "Mechanisms and functions of theta rhythms." Annu Rev Neurosci **36**: 295-312.

Colgin, L. L. (2016). "Rhythms of the hippocampal network." Nat Rev Neurosci **17**(4): 239-249.

Colgin, L. L. and E. I. Moser (2009). "Hippocampal theta rhythms follow the beat of their own drum." Nat Neurosci **12**(12): 1483-1484.

Colom, L. V., M. T. Castaneda, T. Reyna, S. Hernandez and E. Garrido-Sanabria (2005). "Characterization of medial septal glutamatergic neurons and their projection to the hippocampus." Synapse **58**(3): 151-164.

Craven, K. B. and W. N. Zagotta (2006). "CNG and HCN channels: two peas, one pod." Annu Rev Physiol **68**: 375-401.

Dale Purves, G. J. A., David Fitzpatrick, William C. Hall, Anthony-Samule LaMantia, James O. McNamara, S. Mark Williams (2004). Neuroscience, Sinauer Associates.

De Gennaro, L. and M. Ferrara (2003). "Sleep spindles: an overview." Sleep Med Rev **7**(5): 423-440.

Delenda, C. (2004). "Lentiviral vectors: optimization of packaging, transduction and gene expression." J Gene Med **6 Suppl 1**: S125-138.

Deng, X., L. Gu, N. Sui, J. Guo and J. Liang (2019). "Parvalbumin interneuron in the ventral hippocampus functions as a discriminator in social memory." Proc Natl Acad Sci U S A **116**(33): 16583-16592.

Desikan, S., D. E. Koser, A. Neitz and H. Monyer (2018). "Target selectivity of septal cholinergic neurons in the medial and lateral entorhinal cortex." Proc Natl Acad Sci U S A **115**(11): E2644-E2652.

Dittgen, T., A. Nimmerjahn, S. Komai, P. Licznerski, J. Waters, T. W. Margie, F. Helmchen, W. Denk, M. Brecht and P. Osten (2004). "Lentivirus-based genetic manipulations of cortical neurons and their optical and electrophysiological monitoring in vivo." Proc Natl Acad Sci U S A **101**(52): 18206-18211.

Doyle, D. A., J. Morais Cabral, R. A. Pfuetzner, A. Kuo, J. M. Gulbis, S. L. Cohen, B. T. Chait and R. MacKinnon (1998). "The structure of the potassium channel: molecular basis of K+ conduction and selectivity." Science **280**(5360): 69-77.

Dudar, J. D. (1977). "The role of the septal nuclei in the release of acetyl-choline from the rabbit cerebral cortex and dorsal hippocampus and the effect of atropine." Brain Res **129**(2): 237-246.

El-Kholy, W., P. E. MacDonald, J. M. Fox, A. Bhattacharjee, T. Xue, X. Gao, Y. Zhang, J. Stieber, R. A. Li, R. G. Tsushima and M. B. Wheeler (2007). "Hyperpolarization-activated cyclic nucleotide-gated channels in pancreatic beta-cells." Mol Endocrinol **21**(3): 753-764.

Emery, E. C., G. T. Young, E. M. Berrocoso, L. Chen and P. A. McNaughton (2011). "HCN2 ion channels play a central role in inflammatory and neuropathic pain." Science **333**(6048): 1462-1466.

Eric R. Kandel, J. H. S., Thomas M. Jessell, Steven A. Siegelbaum, A.J. Hudspeth (2013). Principles of Neural Science, The McGraw-Hill Companies.

Felix, R., A. Sandoval, D. Sanchez, J. C. Gomora, J. L. De la Vega-Beltran, C. L. Trevino and A. Darszon (2003). "ZD7288 inhibits low-threshold Ca(2+) channel activity and regulates sperm function." Biochem Biophys Res Commun **311**(1): 187-192.

Forwood, S. E., B. D. Winters and T. J. Bussey (2005). "Hippocampal lesions that abolish spatial maze performance spare object recognition memory at delays of up to 48 hours." Hippocampus **15**(3): 347-355.

Freund, T. F. (1989). "GABAergic septohippocampal neurons contain parvalbumin." Brain Res **478**(2): 375-381.

Freund, T. F. and M. Antal (1988). "GABA-containing neurons in the septum control inhibitory interneurons in the hippocampus." Nature **336**(6195): 170-173.

Frotscher, M. and C. Leranth (1985). "Cholinergic innervation of the rat hippocampus as revealed by choline acetyltransferase immunocytochemistry: a combined light and electron microscopic study." J Comp Neurol **239**(2): 237-246.

Fuhrmann, F., D. Justus, L. Sosulina, H. Kaneko, T. Beutel, D. Friedrichs, S. Schoch, M. K. Schwarz, M. Fuhrmann and S. Remy (2015). "Locomotion, Theta Oscillations, and the Speed-Correlated Firing of Hippocampal Neurons Are Controlled by a Medial Septal Glutamatergic Circuit." Neuron **86**(5): 1253-1264.

Gangadharan, G., J. Shin, S. W. Kim, A. Kim, A. Paydar, D. S. Kim, T. Miyazaki, M. Watanabe, Y. Yanagawa, J. Kim, Y. S. Kim, D. Kim and H. S. Shin (2016). "Medial septal GABAergic projection neurons promote object exploration behavior and type 2 theta rhythm." Proc Natl Acad Sci U S A **113**(23): 6550-6555.

Gaztelu, J. M. and W. Buno, Jr. (1982). "Septo-hippocampal relationships during EEG theta rhythm." Electroencephalogr Clin Neurophysiol **54**(4): 375-387.

Golden, S. A., H. E. Covington, 3rd, O. Berton and S. J. Russo (2011). "A standardized protocol for repeated social defeat stress in mice." Nat Protoc **6**(8): 1183-1191.

Green, J. D. and A. A. Arduini (1954). "Hippocampal electrical activity in arousal." J Neurophysiol **17**(6): 533-557.

Green, M. E., G. Edwards, A. J. Kirkup, M. Miller and A. H. Weston (1996). "Pharmacological characterization of the inwardly-rectifying current in the smooth muscle cells of the rat bladder." Br J Pharmacol **119**(8): 1509-1518.

Groh, A., P. Krieger, R. A. Mease and L. Henderson (2018). "Acute and Chronic Pain Processing in the Thalamocortical System of Humans and Animal Models." Neuroscience **387**: 58-71.

Gu, H., J. D. Marth, P. C. Orban, H. Mossmann and K. Rajewsky (1994). "Deletion of a DNA polymerase beta gene segment in T cells using cell type-specific gene targeting." Science **265**(5168): 103-106.

Hajszan, T., M. Alreja and C. Leranth (2004). "Intrinsic vesicular glutamate transporter 2-immunoreactive input to septohippocampal parvalbumin-containing neurons: novel glutamatergic local circuit cells." Hippocampus **14**(4): 499-509.

Halliwell, J. V. and P. R. Adams (1982). "Voltage-clamp analysis of muscarinic excitation in hippocampal neurons." Brain Res **250**(1): 71-92.

Hammelmann, V., M. S. Stieglitz, H. Hulle, K. Le Meur, J. Kass, M. Brummer, C. Gruner, R. D. Rotzer, S. Fenske, J. Hartmann, B. Zott, A. Luthi, S. Spahn, M. Moser, D. Isbrandt, A. Ludwig, A. Konnerth, C. Wahl-Schott and M. Biel (2019). "Abolishing cAMP sensitivity in HCN2 pacemaker channels induces generalized seizures." JCI Insight **4**(9).

Hangya, B., Z. Borhegyi, N. Szilagyi, T. F. Freund and V. Varga (2009). "GABAergic neurons of the medial septum lead the hippocampal network during theta activity." J Neurosci **29**(25): 8094-8102.

Hasselmo, M. E. (1999). "Neuromodulation: acetylcholine and memory consolidation." Trends Cogn Sci **3**(9): 351-359.

Hasselmo, M. E., E. Fransen, C. Dickson and A. A. Alonso (2000). "Computational modeling of entorhinal cortex." Ann N Y Acad Sci **911**: 418-446.

Hitti, F. L. and S. A. Siegelbaum (2014). "The hippocampal CA2 region is essential for social memory." Nature **508**(7494): 88-92.

Hobson, J. A. and E. F. Pace-Schott (2002). "The cognitive neuroscience of sleep: neuronal systems, consciousness and learning." Nat Rev Neurosci **3**(9): 679-693.

Huh, C. Y., R. Goutagny and S. Williams (2010). "Glutamatergic neurons of the mouse medial septum and diagonal band of Broca synaptically drive hippocampal pyramidal cells: relevance for hippocampal theta rhythm." J Neurosci **30**(47): 15951-15961.

Ishii, T. M., M. Takano, L. H. Xie, A. Noma and H. Ohmori (1999). "Molecular characterization of the hyperpolarization-activated cation channel in rabbit heart sinoatrial node." J Biol Chem **274**(18): 12835-12839.

Jensen, O. and J. E. Lisman (1996). "Theta/gamma networks with slow NMDA channels learn sequences and encode episodic memory: role of NMDA channels in recall." Learn Mem **3**(2-3): 264-278.

Joshi, A., M. Salib, T. J. Viney, D. Dupret and P. Somogyi (2017). "Behavior-Dependent Activity and Synaptic Organization of Septo-hippocampal GABAergic Neurons Selectively Targeting the Hippocampal CA3 Area." Neuron **96**(6): 1342-1357 e1345.

Kesner, R. P. (1988). "Reevaluation of the contribution of the basal forebrain cholinergic system to memory." Neurobiol Aging **9**(5-6): 609-616.

Khalilov, I., M. Esclapez, I. Medina, D. Aggoun, K. Lamsa, X. Leinekugel, R. Khazipov and Y. Ben-Ari (1997). "A novel in vitro preparation: the intact hippocampal formation." Neuron **19**(4): 743-749.

Kiss, J., A. J. Patel, K. G. Baimbridge and T. F. Freund (1990). "Topographical localization of neurons containing parvalbumin and choline acetyltransferase in the medial septum-diagonal band region of the rat." Neuroscience **36**(1): 61-72.

Kleinknecht, K. R., B. T. Bedenk, S. F. Kaltwasser, B. Grunecker, Y. C. Yen, M. Czisch and C. T. Wotjak (2012). "Hippocampus-dependent place learning enables spatial flexibility in C57BL6/N mice." Front Behav Neurosci **6**: 87.

Knapp, J. A., N. P. Morris, Z. Henderson and R. T. Matthews (2000). "Electrophysiological characteristics of non-bursting, glutamate decarboxylase messenger RNA-positive neurons of the medial septum/diagonal band nuclei of guinea-pig and rat." Neuroscience **98**(4): 661-668.

Kocsis, B. and S. Li (2004). "In vivo contribution of h-channels in the septal pacemaker to theta rhythm generation." Eur J Neurosci **20**(8): 2149-2158.

Kogan, J. H., P. W. Frankland and A. J. Silva (2000). "Long-term memory underlying hippocampus-dependent social recognition in mice." Hippocampus **10**(1): 47-56.

Kohler, C., V. Chan-Palay and J. Y. Wu (1984). "Septal neurons containing glutamic acid decarboxylase immunoreactivity project to the hippocampal region in the rat brain." Anat Embryol (Berl) **169**(1): 41-44.

Kopell, N. and G. LeMasson (1994). "Rhythmogenesis, amplitude modulation, and multiplexing in a cortical architecture." Proc Natl Acad Sci U S A **91**(22): 10586-10590.

Kramis, R., C. H. Vanderwolf and B. H. Bland (1975). "Two types of hippocampal rhythmical slow activity in both the rabbit and the rat: relations to behavior and effects of atropine, diethyl ether, urethane, and pentobarbital." Exp Neurol **49**(1 Pt 1): 58-85.

Kuisle, M., N. Wanaverbecq, A. L. Brewster, S. G. Frere, D. Pinault, T. Z. Baram and A. Luthi (2006). "Functional stabilization of weakened thalamic pacemaker channel regulation in rat absence epilepsy." J Physiol **575**(Pt 1): 83-100.

Landfield, P. W., J. L. McGaugh and R. J. Tusa (1972). "Theta rhythm: a temporal correlate of memory storage processes in the rat." Science **175**(4017): 87-89.

Larson, J. and G. Lynch (1986). "Induction of synaptic potentiation in hippocampus by patterned stimulation involves two events." Science **232**(4753): 985-988.

Leao, R. N., Z. H. Targino, L. V. Colom and A. Fisahn (2015). "Interconnection and synchronization of neuronal populations in the mouse medial septum/diagonal band of Broca." J Neurophysiol **113**(3): 971-980.

Lee, C. H. and R. MacKinnon (2017). "Structures of the Human HCN1 Hyperpolarization-Activated Channel." Cell **168**(1-2): 111-120 e111.

Lee, I. and R. P. Kesner (2004). "Differential contributions of dorsal hippocampal subregions to memory acquisition and retrieval in contextual fear-conditioning." Hippocampus **14**(3): 301-310.

Lee, I. and R. P. Kesner (2004). "Encoding versus retrieval of spatial memory: double dissociation between the dentate gyrus and the perforant path inputs into CA3 in the dorsal hippocampus." Hippocampus **14**(1): 66-76.

Leger, M., A. Quiedeville, V. Bouet, B. Haelewyn, M. Boulouard, P. Schumann-Bard and T. Freret (2013). "Object recognition test in mice." Nat Protoc **8**(12): 2531-2537.

Leroy, F., D. H. Brann, T. Meira and S. A. Siegelbaum (2017). "Input-Timing-Dependent Plasticity in the Hippocampal CA2 Region and Its Potential Role in Social Memory." Neuron **95**(5): 1089-1102 e1085.

Lewis, A. S., E. Schwartz, C. S. Chan, Y. Noam, M. Shin, W. J. Wadman, D. J. Surmeier, T. Z. Baram, R. L. Macdonald and D. M. Chetkovich (2009). "Alternatively spliced isoforms of TRIP8b differentially control h channel trafficking and function." J Neurosci **29**(19): 6250-6265.

Li, M., X. Zhou, S. Wang, I. Michailidis, Y. Gong, D. Su, H. Li, X. Li and J. Yang (2017). "Structure of a eukaryotic cyclic-nucleotide-gated channel." Nature **542**(7639): 60-65.

Liebe, S., G. M. Hoerzer, N. K. Logothetis and G. Rainer (2012). "Theta coupling between V4 and prefrontal cortex predicts visual short-term memory performance." Nat Neurosci **15**(3): 456-462, S451-452.

Lopez-Gonzalez, Z., C. Ayala-Aguilera, F. Martinez-Morales, O. Galicia-Cruz, C. Salvador-Hernandez, J. Pedraza-Chaverri, M. Medeiros, A. M. Hernandez and L. I. Escobar (2016). "Immunolocalization of hyperpolarization-activated cationic HCN1 and HCN3 channels in the rat nephron: regulation of HCN3 by potassium diets." Histochem Cell Biol **145**(1): 25-40.

Ludwig, A., T. Budde, J. Stieber, S. Moosmang, C. Wahl, K. Holthoff, A. Langebartels, C. Wotjak, T. Munsch, X. Zong, S. Feil, R. Feil, M. Lancel, K. R. Chien, A. Konnerth, H. C. Pape, M. Biel and F. Hofmann (2003). "Absence epilepsy and sinus dysrhythmia in mice lacking the pacemaker channel HCN2." EMBO J **22**(2): 216-224.

Ludwig, A., X. Zong, M. Jeglitsch, F. Hofmann and M. Biel (1998). "A family of hyperpolarization-activated mammalian cation channels." Nature **393**(6685): 587-591.

Ludwig, A., X. Zong, J. Stieber, R. Hullin, F. Hofmann and M. Biel (1999). "Two pacemaker channels from human heart with profoundly different activation kinetics." EMBO J **18**(9): 2323-2329.

Luthi, A. and D. A. McCormick (1998). "H-current: properties of a neuronal and network pacemaker." Neuron **21**(1): 9-12.

M. F. Bear, B. W. C., M. A. Paradiso (2016). Neuroscience - Exploring the Brain, Wolters Kluwer.

Maaswinkel, H., A. M. Baars, W. H. Gispen and B. M. Spruijt (1996). "Roles of the basolateral amygdala and hippocampus in social recognition in rats." Physiol Behav **60**(1): 55-63.

Macadar, O., J. A. Roig, J. M. Monti and R. Budelli (1970). "The functional relationship between septal and hippocampal unit activity and hippocampal theta rhythm." Physiol Behav **5**(12): 1443-1449.

MacVicar, B. A. and F. W. Tse (1989). "Local neuronal circuitry underlying cholinergic rhythmical slow activity in CA3 area of rat hippocampal slices." J Physiol **417**: 197-212.

Mamad, O., H. M. McNamara, R. B. Reilly and M. Tsanov (2015). "Medial septum regulates the hippocampal spatial representation." Front Behav Neurosci **9**: 166.

Manseau, F., M. Danik and S. Williams (2005). "A functional glutamatergic neurone network in the medial septum and diagonal band area." J Physiol **566**(Pt 3): 865-884.

Matt, L., S. Michalakis, F. Hofmann, V. Hammelmann, A. Ludwig, M. Biel and T. Kleppisch (2011). "HCN2 channels in local inhibitory interneurons constrain LTP in the hippocampal direct perforant path." Cell Mol Life Sci **68**(1): 125-137.

McAllister, B. B., D. K. Wright, R. C. Wortman, S. R. Shultz and R. H. Dyck (2018). "Elimination of vesicular zinc alters the behavioural and neuroanatomical effects of social defeat stress in mice." Neurobiol Stress **9**: 199-213.

McCormick, D. A. and T. Bal (1997). "Sleep and arousal: thalamocortical mechanisms." Annu Rev Neurosci **20**: 185-215.

McQuiston, A. R. (2010). "Cholinergic modulation of excitatory synaptic input integration in hippocampal CA1." J Physiol **588**(Pt 19): 3727-3742.

Mikulovic, S., C. E. Restrepo, S. Siwani, P. Bauer, S. Pupe, A. B. L. Tort, K. Kullander and R. N. Leao (2018). "Ventral hippocampal OLM cells control type 2 theta oscillations and response to predator odor." Nat Commun **9**(1): 3638.

Mineur, Y. S., T. N. Mose, L. Vanopdenbosch, I. M. Etherington, C. Ogbejesi, A. Islam, C. M. Pineda, R. B. Crouse, W. Zhou, D. C. Thompson, M. P. Bentham and M. R. Picciotto (2022). "Hippocampal acetylcholine modulates stress-related behaviors independent of specific cholinergic inputs." Mol Psychiatry.

Mitchell, S. J., J. N. Rawlins, O. Steward and D. S. Olton (1982). "Medial septal area lesions disrupt theta rhythm and cholinergic staining in medial entorhinal cortex and produce impaired radial arm maze behavior in rats." J Neurosci **2**(3): 292-302.

Mizumori, S. J., C. A. Barnes and B. L. McNaughton (1990). "Behavioral correlates of theta-on and theta-off cells recorded from hippocampal formation of mature young and aged rats." Exp Brain Res **80**(2): 365-373.

Monmaur, P. and M. A. Thomson (1983). "Topographic organization of septal cells innervating the dorsal hippocampal formation of the rat: special reference to both the CA1 and dentate theta generators." Exp Neurol **82**(2): 366-378.

Moosmang, S., M. Biel, F. Hofmann and A. Ludwig (1999). "Differential distribution of four hyperpolarization-activated cation channels in mouse brain." Biol Chem **380**(7-8): 975-980.

Morris, N. P., R. E. Fyffe and B. Robertson (2004). "Characterisation of hyperpolarization-activated currents (I(h)) in the medial septum/diagonal band complex in the mouse." Brain Res **1006**(1): 74-86.

Much, B., C. Wahl-Schott, X. Zong, A. Schneider, L. Baumann, S. Moosmang, A. Ludwig and M. Biel (2003). "Role of subunit heteromerization and N-linked glycosylation in the formation of functional hyperpolarization-activated cyclic nucleotide-gated channels." J Biol Chem **278**(44): 43781-43786.

Muller, C. and S. Remy (2018). "Septo-hippocampal interaction." Cell Tissue Res **373**(3): 565-575.

Mumby, D. G. (2001). "Perspectives on object-recognition memory following hippocampal damage: lessons from studies in rats." Behav Brain Res **127**(1-2): 159-181.

Neunuebel, J. P. and J. J. Knierim (2014). "CA3 retrieves coherent representations from degraded input: direct evidence for CA3 pattern completion and dentate gyrus pattern separation." Neuron **81**(2): 416-427.

Nolan, M. F., G. Malleret, J. T. Dudman, D. L. Buhl, B. Santoro, E. Gibbs, S. Vronskaya, G. Buzsaki, S. A. Siegelbaum, E. R. Kandel and A. Morozov (2004). "A behavioral role for dendritic integration: HCN1 channels constrain spatial memory and plasticity at inputs to distal dendrites of CA1 pyramidal neurons." Cell **119**(5): 719-732.

Noma, A. and H. Irisawa (1976). "Membrane currents in the rabbit sinoatrial node cell as studied by the double microelectrode method." Pflugers Arch **364**(1): 45-52.

Noma, A. and H. Irisawa (1976). "A time- and voltage-dependent potassium current in the rabbit sinoatrial node cell." Pflugers Arch **366**(2-3): 251-258.

Notomi, T. and R. Shigemoto (2004). "Immunohistochemical localization of Ih channel subunits, HCN1-4, in the rat brain." J Comp Neurol **471**(3): 241-276.

Nunez, A. and W. Buno (2021). "The Theta Rhythm of the Hippocampus: From Neuronal and Circuit Mechanisms to Behavior." Front Cell Neurosci **15**: 649262.

Paxinos, G. a. K. B. F. (2004). "The mouse brain in stereotaxic coordinates." Gulf professional publishing.

Payandeh, J., T. Scheuer, N. Zheng and W. A. Catterall (2011). "The crystal structure of a voltage-gated sodium channel." Nature **475**(7356): 353-358.

Petsche, H. and C. Stumpf (1962). "[The origin of theta-rhytm in the rabbit hippocampus]." Wien Klin Wochenschr **74**: 696-700.

Pignatelli, M., A. Beyeler and X. Leinekugel (2012). "Neural circuits underlying the generation of theta oscillations." J Physiol Paris **106**(3-4): 81-92.

Pinault, D. (2004). "The thalamic reticular nucleus: structure, function and concept." Brain Res Brain Res Rev **46**(1): 1-31.

Richard Jung, A. E. K. (1938). "Eine methodik der ableitung lokalisierter potentialschwankungen aus subcoritcalen Hirngebieten." Archiv f. Psychiatrie und Nervenkrankheiten: 1-30.

Robinson, J., F. Manseau, G. Ducharme, B. Amilhon, E. Vigneault, S. El Mestikawy and S. Williams (2016). "Optogenetic Activation of Septal Glutamatergic Neurons Drive Hippocampal Theta Rhythms." J Neurosci **36**(10): 3016-3023.

Robinson, R. B. and S. A. Siegelbaum (2003). "Hyperpolarization-activated cation currents: from molecules to physiological function." Annu Rev Physiol **65**: 453-480.

Roig, J. A., R. Budelli, O. Macadar and J. M. Monti (1970). "Hippocampal theta rhythm in relation with unit discharges in septum and hippocampus." Electroencephalogr Clin Neurophysiol **28**(5): 520.

Rotstein, H. G., D. D. Pervouchine, C. D. Acker, M. J. Gillies, J. A. White, E. H. Buhl, M. A. Whittington and N. Kopell (2005). "Slow and fast inhibition and an H-current interact to create a theta rhythm in a model of CA1 interneuron network." J Neurophysiol **94**(2): 1509-1518.

Santoro, B., S. Chen, A. Luthi, P. Pavlidis, G. P. Shumyatsky, G. R. Tibbs and S. A. Siegelbaum (2000). "Molecular and functional heterogeneity of hyperpolarization-activated pacemaker channels in the mouse CNS." J Neurosci **20**(14): 5264-5275.

Santoro, B., D. T. Liu, H. Yao, D. Bartsch, E. R. Kandel, S. A. Siegelbaum and G. R. Tibbs (1998). "Identification of a gene encoding a hyperpolarization-activated pacemaker channel of brain." Cell **93**(5): 717-729.

Santoro, B., R. A. Piskorowski, P. Pian, L. Hu, H. Liu and S. A. Siegelbaum (2009). "TRIP8b splice variants form a family of auxiliary subunits that regulate gating and trafficking of HCN channels in the brain." Neuron **62**(6): 802-813.

Seifert, R., A. Scholten, R. Gauss, A. Mincheva, P. Lichter and U. B. Kaupp (1999). "Molecular characterization of a slowly gating human hyperpolarization-activated channel predominantly expressed in thalamus, heart, and testis." Proc Natl Acad Sci U S A **96**(16): 9391-9396.

Shin, J., D. Kim, R. Bianchi, R. K. Wong and H. S. Shin (2005). "Genetic dissection of theta rhythm heterogeneity in mice." Proc Natl Acad Sci U S A **102**(50): 18165-18170.

Simon, A. P., F. Poindessous-Jazat, P. Dutar, J. Epelbaum and M. H. Bassant (2006). "Firing properties of anatomically identified neurons in the medial septum of anesthetized and unanesthetized restrained rats." J Neurosci **26**(35): 9038-9046.

Smythe, J. W., L. V. Colom and B. H. Bland (1992). "The extrinsic modulation of hippocampal theta depends on the coactivation of cholinergic and GABA-ergic medial septal inputs." Neurosci Biobehav Rev **16**(3): 289-308.

Sotty, F., M. Danik, F. Manseau, F. Laplante, R. Quirion and S. Williams (2003). "Distinct electrophysiological properties of glutamatergic, cholinergic and GABAergic rat septohippocampal neurons: novel implications for hippocampal rhythmicity." J Physiol **551**(Pt 3): 927-943.

Spahn, S. (2015). Functional characterization of HCN2 channels in the septo-hippocampal system.

Stephanie A. Jacobs, F. H., Joe Z. Tsien and Wei Wei (2016). "Social Recognition Memory Test in Rodents." bio-protocol **6**(9).

Stevenson, E. L. and H. K. Caldwell (2014). "Lesions to the CA2 region of the hippocampus impair social memory in mice." Eur J Neurosci **40**(9): 3294-3301.

Stewart, M. and S. E. Fox (1990). "Do Septal Neurons Pace the Hippocampal Theta Rhythm?" TINS **13**(5).

Stieber, J., G. Stockl, S. Herrmann, B. Hassfurth and F. Hofmann (2005). "Functional expression of the human HCN3 channel." J Biol Chem **280**(41): 34635-34643.

Stieglitz, M. S. (2018). The control of neuronal activity and behavior by members of the HCN and TPC family.

Stieglitz, M. S., S. Fenske, V. Hammelmann, E. Becirovic, V. Schottle, J. E. Delorme, M. Scholl-Weidinger, R. Mader, J. Deussing, D. P. Wolfer, M. W. Seeliger, U. Albrecht, C. T. Wotjak, M. Biel, S. Michalakis and C. Wahl-Schott (2017). "Disturbed Processing of Contextual Information in HCN3 Channel Deficient Mice." Front Mol Neurosci **10**: 436.

Stumpf, C., H. Petsche and G. Gogolak (1962). "The significance of the rabbit's septum as a relay station between the midbrain and the hippocampus. II. The differential influence of drugs upon both the septal cell firing pattern and the hippocampus theta activity." Electroencephalogr Clin Neurophysiol **14**: 212-219.

Sun, J. and R. MacKinnon (2017). "Cryo-EM Structure of a KCNQ1/CaM Complex Reveals Insights into Congenital Long QT Syndrome." Cell **169**(6): 1042-1050 e1049.

Sun, Y., A. Q. Nguyen, J. P. Nguyen, L. Le, D. Saur, J. Choi, E. M. Callaway and X. Xu (2014). "Cell-type-specific circuit connectivity of hippocampal CA1 revealed through Cre-dependent rabies tracing." Cell Rep **7**(1): 269-280.

Swanson, L. W. and W. M. Cowan (1979). "The connections of the septal region in the rat." J Comp Neurol **186**(4): 621-655.

Takeuchi, Y., A. J. Nagy, L. Barcsai, Q. Li, M. Ohsawa, K. Mizuseki and A. Berenyi (2021). "The Medial Septum as a Potential Target for Treating Brain Disorders Associated With Oscillopathies." Front Neural Circuits **15**: 701080.

Tao, X. and R. MacKinnon (2019). "Cryo-EM structure of the KvAP channel reveals a non-domain-swapped voltage sensor topology." Elife **8**.

Tiscornia, G., O. Singer and I. M. Verma (2006). "Production and purification of lentiviral vectors." Nat Protoc **1**(1): 241-245.

Toth, K., T. F. Freund and R. Miles (1997). "Disinhibition of rat hippocampal pyramidal cells by GABAergic afferents from the septum." J Physiol **500 (Pt 2)**: 463-474.

Tremere, L. A., R. Pinaud, R. P. Irwin and C. N. Allen (2008). "Postinhibitory rebound spikes are modulated by the history of membrane hyperpolarization in the SCN." Eur J Neurosci **28**(6): 1127-1135.

Tzakis, N. and M. R. Holahan (2019). "Social Memory and the Role of the Hippocampal CA2 Region." Front Behav Neurosci **13**: 233.

Unal, G., M. G. Crump, T. J. Viney, T. Eltes, L. Katona, T. Klausberger and P. Somogyi (2018). "Spatio-temporal specialization of GABAergic septo-hippocampal neurons for rhythmic network activity." Brain Struct Funct **223**(5): 2409-2432.

Vanderwolf, C. H. (1969). "Hippocampal electrical activity and voluntary movement in the rat." Electroencephalogr Clin Neurophysiol **26**(4): 407-418.

Varga, V., B. Hangya, K. Kranitz, A. Ludanyi, R. Zemankovics, I. Katona, R. Shigemoto, T. F. Freund and Z. Borhegyi (2008). "The presence of pacemaker HCN channels identifies theta rhythmic GABAergic neurons in the medial septum." J Physiol **586**(16): 3893-3915.

Vega-Flores, G., A. Gruart and J. M. Delgado-Garcia (2014). "Involvement of the GABAergic septo-hippocampal pathway in brain stimulation reward." PLoS One **9**(11): e113787.

Verma, I. M. and M. D. Weitzman (2005). "GENE THERAPY: Twenty-First Century Medicine." Annual Review of Biochemistry **74**(1): 711-738.

Vertes, R. P. (2005). "Hippocampal theta rhythm: a tag for short-term memory." Hippocampus **15**(7): 923-935.

Vertes, R. P., W. B. Hoover and G. Viana Di Prisco (2004). "Theta rhythm of the hippocampus: subcortical control and functional significance." Behav Cogn Neurosci Rev **3**(3): 173-200.

Vertes, R. P. and B. Kocsis (1997). "Brainstem-diencephalo-septohippocampal systems controlling the theta rhythm of the hippocampus." Neuroscience **81**(4): 893-926.

Vinogradova, O. S. (1995). "Expression, control, and probable functional significance of the neuronal theta-rhythm." Prog Neurobiol **45**(6): 523-583.

Wahl-Schott, C., S. Fenske and M. Biel (2014). "HCN channels: new roles in sinoatrial node function." Curr Opin Pharmacol **15**: 83-90.

Winson, J. (1978). "Loss of hippocampal theta rhythm results in spatial memory deficit in the rat." Science **201**: 160-163.

Witter, M. P. (2007). "The perforant path: projections from the entorhinal cortex to the dentate gyrus." Prog Brain Res **163**: 43-61.

Wu, X., L. Liao, X. Liu, F. Luo, T. Yang and C. Li (2012). "Is ZD7288 a selective blocker of hyperpolarization-activated cyclic nucleotide-gated channel currents?" Channels (Austin) **6**(6): 438-442.

Wu, X., R. Ramentol, M. E. Perez, S. Y. Noskov and H. P. Larsson (2021). "A second S4 movement opens hyperpolarization-activated HCN channels." Proc Natl Acad Sci U S A **118**(37).

Xu, C., S. Datta, M. Wu and M. Alreja (2004). "Hippocampal theta rhythm is reduced by suppression of the H-current in septohippocampal GABAergic neurons." Eur J Neurosci **19**(8): 2299-2309.

Ying, S. W. and P. A. Goldstein (2005). "Propofol-block of SK channels in reticular thalamic neurons enhances GABAergic inhibition in relay neurons." J Neurophysiol **93**(4): 1935-1948.

Ying, S. W., G. R. Tibbs, A. Picollo, S. Y. Abbas, R. L. Sanford, A. Accardi, F. Hofmann, A. Ludwig and P. A. Goldstein (2011). "PIP2-mediated HCN3 channel gating is crucial for rhythmic burst firing in thalamic intergeniculate leaflet neurons." J Neurosci **31**(28): 10412-10423.

Zagotta, W. N., N. B. Olivier, K. D. Black, E. C. Young, R. Olson and E. Gouaux (2003). "Structural basis for modulation and agonist specificity of HCN pacemaker channels." Nature **425**(6954): 200-205.

Zhang, H., S. C. Lin and M. A. Nicolelis (2010). "Spatiotemporal coupling between hippocampal acetylcholine release and theta oscillations in vivo." J Neurosci **30**(40): 13431-13440.

Zola, S. M. and L. R. Squire (2001). "Relationship between magnitude of damage to the hippocampus and impaired recognition memory in monkeys." Hippocampus **11**(2): 92-98.

Zolles, G., D. Wenzel, W. Bildl, U. Schulte, A. Hofmann, C. S. Muller, J. O. Thumfart, A. Vlachos, T. Deller, A. Pfeifer, B. K. Fleischmann, J. Roeper, B. Fakler and N. Klocker (2009). "Association with the auxiliary subunit PEX5R/Trip8b controls responsiveness of HCN channels to cAMP and adrenergic stimulation." Neuron **62**(6): 814-825.

7   List of abbreviations

αms	Anti-mouse
αrb	Anti-rabbit
µg	Microgram
µm	Micrometer
µl	Microliter
AMPA	α-amino-3-hydroxy-5-methyl-4-isoxazolepropionic acid
ATP-Na	Adenosine 5'-triphosphate disodium salt hydrate
AUC	Area under the curve
BBS	BES buffered solution
bp	Base pairs
CA	Cornu Ammonis
$CaCl_2$	Calcium chloride
CamKIIα	Calmodulin-dependent protein Kinase IIα
cAMP	Cyclic adenosine monophosphate
CB	ChemiBlocker
cGMP	Cyclic guanosine monophosphate
ChAT	Choline acetyltransferase
cm	centimeter
CMV	Cytomegalovirus
CNBD	Cyclic nucleotide-binding domain
CO_2	Carbon dioxide
Ctrl	control
DAPI	4′,6-diamidino-2-phenylindole, DNA stain
DbB	Diagonal band of Broca
DG	Dentate gyrus
DMEM	Dulbecco's Modified Eagle's Medium
DNA	Deoxyribonucleic acid
DV	Distal-ventral

EDTA	Ethylenediaminetetraacetic acid
EEG	Electroencephalography
ELISA	Enzyme-linked immunosorbent assay
EMG	Electromyography
FBS	Fetal bovine serum
GABA	Gamma aminobutyric acid
GAD	Glutamate decarboxylase
GTP-Na	Guanosine 5'-triphosphate sodium salt hydrate
GYG motif	Glycine-tyrosine-glycine motif
H_2O	Water
H_2O_2	Hydrogen peroxide
HBSS	Hank's Buffered Salt Solution
HCN channel	Hyperpolarization-activated cyclic nucleotide-gated channel
HEK293T	Human embryonal kidney 293 cell line expressing SV40 large T antigen
HIV	Human immunodeficiency viruses
HRP	Horse radish peroxidase
hSyn	Human synapsin promoter
Hz	Hertz
IHC	Immunohistochemistry
I_h	Current of HCN channels
kb	Kilobase
KCL	Potassium chloride
KH_2PO_4	Potassium phosphate monobasic
kHz	Kilohertz
KO	Knockout
LB	Luria-Bertani positive/negative medium
LS	Lateral septum
LTD	Long-term depression
ltm	Long-term memory

LTP	Long-term potentiation
LTR	Long terminal repeats
LV	Lateral ventricle
LV	Lentivirus/Lentiviral
M	Molar
MCS	Multiple cloning sites
$MgCl_2$	Magnesium chloride
ml	Milliliter
mM	Millimolar
mm	Millimeter
MS	Medial septum
mV	Millivolt
MΩ	Mega Ohm
Na_2HPO_4	Disodium hydrogen phosphate
NaCl	Sodium chloride
$NaHCO_3$	Sodium bicarbonate
NaOH	Sodium hydroxide
nm	Nanometer
NREM	Non rapid eye movement
O_2	Oxygen
ORT	Object recognition test
pA	Pico ampere
PBS	Phosphate buffered saline
PCR	Polymerase chain reaction
PFA	Paraformaldehyde
PFU	Plaque forming units
pH	Potential/power of hydrogen
pMD.2G	Helper plasmid for lentiviral particle production
pMDL	Helper plasmid for lentiviral particle production

pRSV-Rev	Helper plasmid for lentiviral particle production
qPCR	Quantitative polymerase chain reaction
REM	Rapid eye movement
RNA	Ribonucleic acid
RMP	Resting membrane potential
rpm	Rounds per minutes
RT	Room temperature
S1-6	6 transmembrane α-helices of HCN channels
sec	Second
SRT	Social recognition test
stm	Short-term memory
TBE	Tris/Borate/EDTA
Trip8b	Tetratricopeptide repeat-containing Rab8b-interacting protein
Tris-HCL	Tris(hydroxymethyl)aminomethane hydrochloride
TritonX-100	4-(1,1,3,3-tetramethylbutyl)-phenyl-polyethyleneglycol
TRN	Thalamic reticular nucleus
TVGYG	threonine-valine-glycine-tyrosine-glycine
UV	Ultraviolet
V	Volt
$V_{0.5}$	Half-maximal activation potential
VSV.G	Vesicular stomatitis virus g-protein
WCM	Water Cross Maze
WPRE	Woodchuck hepatitis virus posttranscriptional regulatory element
WT	Wild type
ZD7288	HCN channel blocker
°C	Degree Celsius

8 Appendix

8.1 Primers used for PCR-dependent experiments

Table 13: Primers for genotyping HCN2L2 mice.

Primer name	Sequence 5'-3'
HCN2 14F	GGTCCCAGGCACTTCCATCCTTT
HCN2 15R	GGAAAAATGGCTGCTGAGCTGTCTC
HCN2 16F	CAGCTCCCATTTGCCCTTGTGC

Table 14: Primers for amplification of LV plasmid fragments.

Primer name	Sequence 5'-3'
mCherry fw	TCA ATA CTA GTG TGA GCA AAG GGC GAG GAG G
mCherry rv	TAC GGC CGT TAG TTG TAC AGC TCG TCC ATG
hSyn fw	CCA GCT AGC ATC GGA AAT CGC CCT TAA GC
hSyn rv	GGG CAT GGT GAT CCA ATC TAT TGC TCA CCA TGG TGG C
GAD67 fw	ATA ACG CGT CGT GGA TTT TGC TAA AGC CCT AGG
GAD67 rv	TAT GGT ACC CTC CCG CGT TCG AGG AGG TTG
CamKIIα fw	TGC ACG CGT CAT TAT GGC CTT AGG TCA CTT CAT C
CamKIIα rv	TAG GTA CCG CTG CCC CCA GAA CTG GGG
Cassette fw	ACG ATT AGA TCT GCT GTG CGA TCG TTT ACC ATG C
Cassette rv	TGA GTC GAC CCT CTA GAT GCA TGC TCG AG

8.2   Antibodies used

Table 15: Primary antibodies used in IHC experiments.

Name	Producer/antibody name	Dilution
rb anti-HCN1	Alomone APC056	1:1000
rb anti-HCN2	Alomone APC030	1:1000
rb anti-HCN4	Alomone APC0	1:1000
ms anti-mCherry	Living Colors 632543	1:500
ms anti-GAD67	Emd Milipore MAB5406	1:500

Table 16: Secondary antibodies used in IHC.

Name	Producer/antibody name	Dilution
gt anti-ms Alexa 488	Invitrogen A-11001	1:800
gt anti-rb Alexa 488	Invitrogen A-11034	1:800
Peroxidase anti-rb	Jackson 711-035-152	1:1000
dk anti-ms Cy3	Jackson 715-165-150	1:400
dk anit-rb Cy3	Jackson 711-165-152	1:400

8.3   Publications

Hammelmann, V., M. S. Stieglitz, H. Hülle, K. Le Meur, J. Kass, M. Brümmer, C. Gruner, R. D. Rötzer, S. Fenske, J. Hartmann, B. Zott, A. Luthi, S. Spahn, M. Moser, D. Isbrandt, A. Ludwig, A. Konnerth, C. Wahl-Schott and M. Biel (2019). "Abolishing cAMP sensitivity in HCN2 pacemaker channels induces generalized seizures." JCI Insight **4**(9).

Acknowledgements

First of all, I deeply thank my family for their support, help, and love at any time during these demanding years – it is so valuable to me knowing that I have you by my side and that I can always count on you.

I especially thank Prof. Dr. Christian Wahl-Schott for offering me to work on this fascinating PhD project. His scientific guidance, help, and support during this time was always highly appreciated and motivating. Thank you for all scientific discussions and inspiring wine sessions.

Additionally, I am very grateful to Prof. Dr. Martin Biel for the opportunity to join his lab. I appreciate your scientific advice and your help advancing my research projects. I thank you for being a supportive supervisor and valuable TAC member.

A big thank you to PD Dr. Conny Kopp-Scheinpflug for being my third TAC member. With your excellent expert knowledge and helpful scientific ideas you contributed much to the success of my projects.

Thank you to all the collaborators: First, thanks to Dr. Hristo Varbanov for patching red fluorescent cells forever and a day to substantiate and complement my data. I am looking forward to an ongoing and successful cooperation and I am always happy working with you. Another thanks goes to Niklas Wetzel for his help with programming, the research assistants Antonia, Mara, and Jasmin, Bachelor student Melanie, and worthy successor Eda for their excellent laboratory work.

I especially thank the GSN for their warm welcome into their excellent program. The GSN community is unique and I appreciate being part of it. The GSN gave me the opportunity to develop and strengthen my skills on a scientific and personal level. An additional thanks is for the financial support without which I would not have been able to make that many exciting experiences during my PhD studies.

I am extremely grateful to my two supervisors – the best in the universe. Marc – without you I would not have had such a funny, motivated, and structured start in this lab. Your kind way of telling me what to do but also how not to do things let me develop and grow to follow in your footsteps. Incredible how funny the hours in the animal facility have been trying to implement injections by trial and error again and again. I will never forget this time in the lab with you; it was unique. Verena – you should know there could not have been any better supervisor for me than you: Always available for all kinds of questions, always ready to help with every possible problem, always motivating me and appreciating my work and ideas. You are the best at explaining the world and introducing one into new experiments. I will never forget all these hours we had together in the lab

Affidavit/Eidesstattliche Versicherung

I hereby confirm that the dissertation "The role of the HCN2 channel in the mouse septo-hippocampal circuit" is the result of my own work and that I have only used sources or materials listed and specified in the dissertation.

Hiermit versichere ich an Eides statt, dass ich die vorliegende Dissertation „The role of the HCN2 channel in the mouse septo-hippocampal circuit" selbstständig angefertigt habe, mich außer der angegebenen keiner weiteren Hilfsmittel bedient und alle Erkenntnisse, die aus dem Schrifttum ganz oder annähernd übernommen sind, als solche kenntlich gemacht und nach ihrer Herkunft unter Bezeichnung der Fundstelle einzeln nachgewiesen habe.

Munich, 20.06.2022

Place,   date   Manuela Brümmer

Declaration of author contributions

HCN2L2 injected animals

Patch clamp measurements of Syn-injected animals were performed together with Dr. Marc Stieglitz (Wahl-Schott group, LMU Munich). Patch clamp measurements of GAD-injected animals were performed by Dr. Hristo Varbanov (Wahl-Schott group, Hannover Medical School, Germany).

Munich, 22.06.2022

Place, date	Supervisor	Manuela Brümmer
	(Prof. Dr. Martin Biel)	